

UNIVERSITÀ DEGLI STUDI DI MILANO BICOCCA
Facoltà di Scienze Matematiche, Fisiche e Naturali
Dipartimento di Biotecnologie

PhD
Industrial Biotechnology - XXVII CYCLE

PhD THESIS



GLYCOSAMINOGLYCANS IN AUTOSOMAL GENETIC DISORDERS:
Investigation on Multiple Hereditary Exostoses and Cystic Fibrosis

NOEMI VERALDI
Matr. 072893

Tutor: Prof. GIANNI FRASCOTTI
Co-tutor: Dr. ANTONELLA BISIO

Course coordinator:
Prof. MARCO ERCOLE VANONI

ACADEMIC YEAR 2013/2014

Be famished for knowledge

To my family

ABBREVIATIONS

1D	Mono-dimensional
2D	Two-dimensional
C	Chondrosarcoma
ChABC	Chondroitinase ABC
CF	Cystic Fibrosis
CS	Chondroitin sulfate
DBA	Dibutylamine
ECM	Extracellular matrix
ER	Endoplasmic reticulum
ESI-Q-TOF-MS	Electrospray ionization - quadrupole - time-of-flight mass spectrometry
EXT1	Exostosin-1
EXT2	Exostosin-2
GAG(s)	Glycosaminoglycan(s)
Gal	Galactose
GlcA (or G)	D-glucuronic acid
GlcN (or A)	D-glucosamine
GlcN,3,6S (or A*)	N,3-O,6-O-trisulfated D-glucosamine
GlcN,6S	N,6-O-disulfated-D-glucosamine
GlcNAc	N-acetyl-D-glucosamine
GlcNS	N-sulfated-D-glucosamine
HA	Hyaluronic acid
HEP	Heparin
HPLC-MS	High Performance Liquid Chromatography-Mass Spectrometry
HS	Heparan sulfate
HSPGs	Heparan sulfate proteoglycans
HSQC	Heteronuclear Single Quantum Coherence
IdoA (or I)	L-iduronic acid
IdoA2S	L-iduronic acid 2-O-sulfate
IL-8	Interleukin-8
KS	Keratan sulfate
LR	Linkage region
MO	Multiple Osteochondromas
NMR	Nuclear Magnetic Resonance
NRE	Non-reducing end
RE	Reducing end
Ser	Serine of the LR
SerOx	Oxidized serine residue of the LR
TNF- α	Tumor necrosis factor- α
U	Uronic acid
Δ U	4,5-unsaturated uronic acid
Xyl	Xylose

Contents

INTRODUCTION	1
CHAPTER I: SCIENTIFIC BACKGROUND	4
I.1 What are GAGs?	4
I.2 Biosynthesis and structure of heparan sulfate	5
I.3 Heparan sulfate v. heparin	10
I.4 Heparan sulfate proteoglycans (HSPGs)	12
I.5 Interaction with proteins	14
<i>I.5.1 Fibroblast Growth Factors</i>	14
<i>I.5.2 Chemokines</i>	15
<i>I.5.3 Lipid- or membrane-binding proteins</i>	16
<i>I.5.4 Adhesion proteins</i>	17
<i>I.5.5 Pathogens</i>	18
I.6 HS and HEP degrading enzymes	18
CHAPTER II: CHARACTERIZATION OF HEPARAN SULFATE IN MULTIPLE HEREDITARY EXOSTOSES	21
II.1 Introduction	21
<i>II.1.1 HME and EXT genes</i>	21
<i>II.1.2 Discovery of the correlation between HS and EXT genes</i>	25
<i>II.1.3 Physiology of cartilage</i>	26
<i>II.1.4 Objectives of the work</i>	28
II.2 Characterization of HS from healthy cartilage	30
<i>II.2.1 NMR of GAGs from healthy cartilage</i>	31
<i>II.2.2 Interpretation of mass spectra and identification of oligosaccharides from prepubescent and adult HS</i>	35
<i>II.2.3 Interpretation of mass spectra and identification of oligosaccharides from fetal HS</i>	44
II.3 Characterization of HS from pathological cartilage	47
<i>II.3.1 NMR of GAGs from pathological cartilage</i>	48

II.3.2 Interpretation of mass spectra and identification of oligosaccharides from pathological HS	49
II.4 Overview of similarities and differences between healthy and pathological heparan sulfate	53
II.5 Discussion and future perspectives	53
II.6 Experimental section	57
CHAPTER III: GLYCOSAMINOGLYCANS IN CYSTIC FIBROSIS	61
III.1 Introduction and objectives of the work	61
III.1.1 Cystic Fibrosis	61
III.1.2 Linkage between CF and GAGs	64
III.1.3 Heparin as an anti-inflammatory drug	65
III.1.4 Objectives of the work	67
III.2 Preparation of heparin derivatives as possible anti- inflammatory agents	69
III.2.1 Structural characterization of compounds	70
III.2.2 Inhibition of Elastase activity	70
III.2.3 Interaction with IL8	72
III.2.4 Interaction with TNF-alpha	74
III.2.5 Anticoagulant activity	75
III.2.6 Neutrophil chemotaxis	77
III.2.7 Ability of PS to reduce inflammation and tissue damage <i>in vivo</i>	78
III.3 Evaluation of GAGs level in a murine model of <i>P.aeruginosa</i> infection	80
III.4 Discussion and future perspectives	85
III.5 Experimental section	88
RIASSUNTO IN ITALIANO	96
ACKNOWLEDGEMENTS	100
REFERENCES	101
ANNEX	107

INTRODUCTION

Owing to their biological functions in both physiological and pathological conditions, glycosaminoglycans (GAGs) are considered important biomarkers as well as potential pharmacological targets. Their involvement in cell signaling and cancer progression and some structure-biological activity relationships have been reviewed recently [1].

The results presented in this thesis lend additional credence to the importance of GAGs in regulating the equilibrium between healthy and pathological conditions, particularly with regard to two profoundly different autosomal diseases. In Multiple Hereditary Exostoses, HME, the defect is directly correlated to malfunctions in the biosynthesis of the GAG polysaccharide heparan sulfate, HS, which regulates morphogen gradients and growth-factor signaling reactions during the process of axial bone growth. In consequence of its role in developmental processes, alterations to HS structure are frequently involved in pathophysiology of the skeletal diseases [2][3][4] determining a broad spectrum of clinical manifestations. It is probable that the formation of exostoses relates to the decreased number of growth factors bound to truncated HS chains in growth plate chondrocytes. No information is available on the structure of HS extracted either from patients affected by multiple exostoses, or healthy subjects of different ages; hence, this lack of knowledge will be partially satisfied by this study.

Concerning Cystic Fibrosis (CF), no direct linkage with GAGs is evident, but a correlation has been observed between GAGs of the pulmonary tissue and the inflammatory state of CF patients. Some data suggest a relationship between the presence of chondroitin sulfate (CS) proteoglycans in sputum and severe tracheobronchial infection in CF [5]; moreover, an ongoing inflammatory state is associated with an increased turnover of hyaluronic acid, HA, in the affected tissue compartment [6]. Furthermore, exogenous GAGs could act as inhibitory agents by targeting inflammatory proteins as

heparanase, elastase and several cytokines. The present project is focused on understanding the role of GAGs in inflammation, particularly in CF. Towards meeting this objective, two series of potential anti-inflammatory heparin derivatives were generated and their activities were investigated *in vitro* and *in vivo*. Moreover, a chronic model of *P. aeruginosa* infection was established and GAGs were isolated from lung homogenates and characterized to identify changes in the level of GAGs expressed and their structure.

In **Chapter I** a general introduction to GAGs, specifically heparan sulfate and heparin, and their biological role is reported. The two pathologies are treated separately in the specific chapters which are **Chapter II** for HME and **Chapter III** for CF.

The present study was carried out principally at the Institute for Chemical and Biochemical Research "Ronzoni", but also at the Department of Biochemistry, Institute of Integrative Biology of the University of Liverpool (UK) and at the Institute of Biomedical and Biomolecular Sciences of the University of Portsmouth (UK), where I spent several months. The project relating to CF was financially supported by the Italian Cystic Fibrosis Foundation (FFC) (Project#20/2011: Identification of agents with multiple favourable activities as potential treatments for cystic fibrosis and Project#14/2013: Pathophysiological relevance of glycosaminoglycans in *Pseudomonas aeruginosa* chronic lung infections and validation of new therapeutic approaches to modulate inflammation and tissue remodeling.). I would like to thank the Rizzoli Orthopaedic Institute, Bologna, and especially Dr. Alessandro Parra, for the cartilage samples, the group of Dr. Cigana at San Raffaele Hospital, Milan, for the *in vivo* experiments and Diamond Light Source Ltd., Harwell Innovation Campus, in Didcot (UK) for access to beamline B23 - Circular Dichroism (project SM8027).

Some of the results have been published in:

- Noemi Veraldi, Ashley J. Hughes, Timothy R. Rudd, Huw B. Thomas, Steven W. Edwards, Lynsay Hadfield, Mark A. Skidmore, Giuliano Siligardi, Cesare Cosentino, Janis K. Shute, Annamaria Naggi, Edwin A. Yates. Heparin derivatives for the targeting of multiple activities in the inflammatory response. *Carbohydrate Polymers*, **2015**, 117, 400-407.

Other papers published during the PhD not related to the thesis:

-Marcelo A. Lima, Ashley J. Hughes, Noemi Veraldi, Timothy R. Rudd, Rohanah Hussain, Adriana S. Brito, Suely F. Chavante, Ivarne I. Tersariol, Giuliano Siligardi, Helena B. Nader and Edwin A. Yates, Antithrombin stabilisation by sulfated carbohydrates correlates with anticoagulant activity, *Med Chem Commun*, **2013**, *4*, 870-873.

Part of results has been presented in:

-XII Convention of Investigators in Cystic Fibrosis, Garda (27-29/11/14), poster: Cigana C., Naggi A., Colombo C., Bragonzi A., Lorè N.L., Riva C., Spagnuolo L., De Fino I., Sipione B., Veraldi N., Cariani L., Biffi A., Pathophysiological relevance of glycosaminoglycans in *Pseudomonas aeruginosa* chronic lung infections and validation of new therapeutic approaches to modulate inflammation and tissue remodeling.

-Sigma-Aldrich Young Chemists Symposium (SAYCS), Riccione (27-29/10/14), oral communication: Veraldi N., Parra A., Sangiorgi L., Bisio A., Heparan sulfate from healthy and pathologic human cartilage.

- XV Convegno Scuola di Chimica dei Carboidrati (CSCC), Certosa di Pontignano, Siena (22-25/06/14), poster: Veraldi N., Parra A., Sangiorgi L., Bisio A., Heparan sulfate from healthy and pathologic human cartilage.

-21st Symposium on Glycosaminoglycans, Villa Vigoni, Como (19-21/09/13), oral communication: Veraldi N., Parra A., Sangiorgi L., Bisio A., Heparan sulfate from human cartilage.

-X Convention of Investigators in Cystic Fibrosis, Palazzo Erbisti, Verona (29/11-1/12/12), oral communication: Veraldi N., Shute J.K., Naggi A., Yates E.A., Identification of agents with multiple favourable activities as potential treatments for cystic fibrosis.

-20th Symposium on Glycosaminoglycans, Villa Vigoni, Como (20-22/09/12), oral communication: Veraldi N., Parra A., Sangiorgi L., Bisio A., Heparan sulfate from human cartilage.

-XIII Convegno Scuola di Chimica dei Carboidrati (CSCC), Certosa di Pontignano, Siena (24-27/06/2012), oral communication: Veraldi N., Structural analysis of human cartilaginous heparan sulfate; poster: Veraldi N., Naggi A., Shute J., Yates E. Heparin derivatives as potential anti-inflammatory treatment for cystic fibrosis.

CHAPTER 1: SCIENTIFIC BACKGROUND

I.1 What are GAGs?

GAGs are unbranched and anionic polysaccharides made up of repeating disaccharide units of an amino sugar (N-acetyl-D-glucosamine or N-acetyl-D-galactosamine) and an uronic acid (either D-glucuronic acid or its epimer, L-iduronic acid) or, in the case of KS, galactose.

On the basis of the aminosugar present in their chains, GAGs can be classified as:

- **glucosaminoglycans**, characterized by D-glucosamine (GlcN), including heparin (HEP) and heparan sulfate (HS), as well as hyaluronic acid (HA) and keratan sulfate (KS);
- **galactosaminoglycans**, characterized by D-galactosamine (GalN), including chondroitin sulfate (CS) and dermatan sulfate (DS).

Each member of the GAG family is commonly described in terms of its prevalent disaccharide sequence (**Table I.1**). However, each single chain generally contains differently sulfated and acetylated glucosamines or galactosamines as well as distinct uronic acids (i.e. D-glucuronic acid (GlcA), L-iduronic acid (IdoA) and 2-O-sulfated-L- iduronic acid (IdoA2S)).

Different combinations of GlcN/GalN and uronic acids lead to tremendous structural variation of glycosaminoglycans first, and proteoglycans, second, and given that glycosaminoglycan chains are much larger than other types of glycans, they strongly influence the chemical properties of proteoglycans [7].

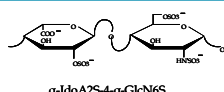
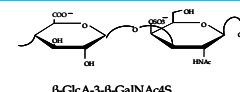
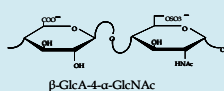
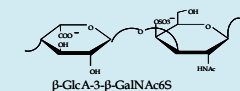
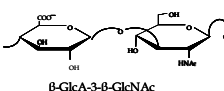
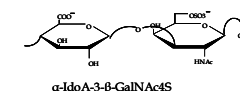
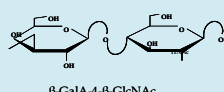
GLUCOSAMINOGLYCANS		GALACTOSAMINOGLYCANS	
NAME	MAIN REPEATING DISACCHARIDE	NAME	MAIN REPEATING DISACCHARIDE
Heparin (HEP)	 $\alpha\text{-IdoA}2\text{S-4-}\alpha\text{-GlcN}6\text{S}$	Chondroitin 4-sulfate (Ch4S)	 $\beta\text{-GlcA-3-}\beta\text{-GalNAc}4\text{S}$
Heparan sulfate (HS)	 $\beta\text{-GlcA-4-}\alpha\text{-GlcNAc}$	Chondroitin 6-sulfate (Ch6S)	 $\beta\text{-GlcA-3-}\beta\text{-GalNAc}6\text{S}$
Hyaluronic acid (HA)	 $\beta\text{-GlcA-3-}\beta\text{-GlcNAc}$	Dermatan sulfate (DS)	 $\alpha\text{-IdoA-3-}\beta\text{-GalNAc}4\text{S}$
Keratan sulfate (KS)	 $\beta\text{-GalA-4-}\beta\text{-GlcNAc}$		

Table I.1. Main repeating disaccharides characterizing gluco- and galactosaminoglycans.

The structural heterogeneity of GAGs and their high negative charge density allow these compounds to easily interact with proteins. In fact, most of the biological and pharmacological activities of GAGs are mediated by interactions with proteins, such as growth factors, enzymes, morphogens, cell adhesion molecules and cytokines. Owing to their physiological functions, GAGs constitute a class of compounds with considerable potential for therapeutic applications.

I.2 Biosynthesis and structure of heparan sulfate

Independently from their linear sequence, GAG chains are biosynthesized in the Golgi apparatus by glycosyltransferases, sulfotransferases and epimerases. The process starts with the transfer of xylose by a xylosyltransferase (XT) from UDP-xylose to a specific serine residue (with the exception of KS) within the core protein. Two galactose residues are then linked by galactosyltransferase I and II (GalT-I and GalT-II); finally glucuronic acid (GlcA) is attached by glucuronyltransferase I (GlcAT-I) completing the tetrasaccharide sequence GlcA- β 1, 3-Gal- β 1, 3-Gal- β 1, 4-Xyl,

named linkage region (LR). The attachment of xylose is thought to take place in the ER while the further assembling of the linkage region and the rest of the chain is made in the Golgi apparatus.

The LR can undergo phosphorylation in C2 of xylose and/or sulfation of galactose residues; phosphorylation can be transient and can modulate the activity of transferases, while sulfation of galactose usually leads to the synthesis to chondroitin sulfate [8]. In fact, the biosynthesis diverges after this common step: the next enzyme, N-acetylglucosamine transferase I (GlcNAc T-I) or N-acetylgalactosamine transferase I (GalNAc T-I), channels the biosynthesis toward HEP/HS or CS/DS, respectively.

The initiating GlcNAc transferase recognizes amino acid determinants proximal to the linkage tetrasaccharide and has a domain that interacts with the core protein to guide the addition to sites destined to contain HS. After the attachment of the first GlcNAc (or GalNAc) residue, polymer formation proceeds by the stepwise, alternating addition of GlcA and GlcNAc (or GalNAc) units from their respective UDP-sugars [7].

Heparan sulfate and heparin are synthesized from a common unsulfated precursor known as heparosan (**Figure I.1**). In heparosan, N-acetylglucosamine is α linked to C4 of the GlcA in the linkage region, and a specific copolymerase catalyzes the formation of the actual $[\beta\text{-GlcA-(1}\rightarrow\text{4)-}\alpha\text{-GlcNAc-(1}\rightarrow\text{4)}]_n$ HEP/HS precursor.

Two glycosyltransferases encoded by the genes EXT1 and EXT2 and forming a heterodimeric complex [9][10][11] are responsible for the transfer of GlcNAc and GlcA on the elongating HS chain [12][13][14][15].

After the polymerization, a series of modifications are introduced by four classes of sulfotransferases and epimerases. The availability of the unique sulfate donor, PAPS (3-phosphoadenosine-5-phosphosulfate) is crucial for the activity of sulfotransferases.

The first modification is the N-deacetylation/N-sulfation of glucuronic acid to give GlcNS and is operated by one or more members of a family of four

N-acetylglucosamine-N-deacetylase/N-sulfotransferases (NDSTs) [16] whose level of expression is tissue dependent and each isoform catalyzes different ratio of deacetylation/sulfation [17]. This step determines the occurrence of the subsequent enzymatic modifications and it is critical for the further processing of HS chains [18]. In some cases, glucosamine residues with a free NH₂ group resulting from the apparent decoupling of the two activities have been found, although the process is not fully understood.

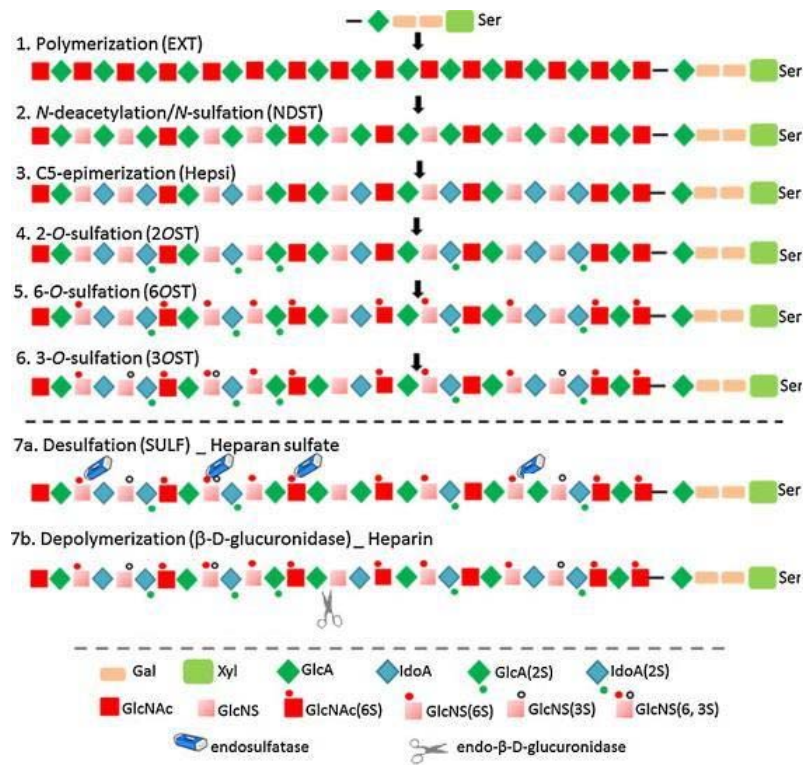


Figure I.1. Biosynthesis of HS and HEP from the precursor heparosan. The first 6 steps occur in the Golgi apparatus while steps 7a/b take place on the cell surface. In mammals, as many as 26 enzymes participate in the formation of HS chains. Adapted from [19]

Conversion of the (GlcA-GlcNAc)_n precursor into the products recognized as HEP/HS occurs through the following modification steps (**Figure I.1**):

- N-deacetylation and N-sulfation of glucosamine residues (this polymer modification appears to be initiated while the chain is still undergoing elongation [20]);
- C5 epimerization of β -D-GlcA to α -L-IdoA residues by a specific epimerase (Hsepi); only the GlcA residues present in GlcNS-GlcA-GlcNS and GlcNS-GlcA-GlcNAc sequences can be converted into IdoA [21]
- 2-O-sulfation of uronic acid units and 6-O- and 3-O-sulfation of GlcN residues by sulfotransferases (OST): 2-OST, active toward both IdoA and GlcA, but prefers the former under most conditions, and several 3-OST and 6-OST enzymes, which transfer O-sulfate groups, following the specificity of each isoform [22].

In addition to the regulation during HS biosynthesis, endo-6-O-sulfatases (Sulf) that selectively release 6-O-sulfates, regulate HS structure post-biosynthetically. Targeted disruption of Sulf-1 and Sulf-2 resulted in increased levels of -IdoA2S-GlcNS6S- and reduced levels of -IdoA2S-GlcNS- units, hence affecting several different signaling pathways [23][24].

A model for the biosynthesis of GAGs was proposed [22] implying that the enzymes are organized and tightly packed in a complex, the so called "GAGosome". Thus, variations in concentration of enzymes/isoforms and their ability to associate with other components of the GAGosome will be very important for their activity.

However, this biosynthetic pathway in which a number of enzymes act consecutively in the Golgi, irreversibly and in a fixed order cannot account for the synthesis of all the substitution patterns of the basic disaccharide unit that are observed in HS. Another recently proposed scheme is based on the disaccharide as the fundamental unit of recognition and modification [25][23]. A tree structure emerged from this scheme in which all commonly occurring HS disaccharides could be synthesized through a common route,

the major branch, while the least common disaccharides occurred on a separate common branch, termed the minor branch. The relative abundance of these two sets of structures would be the result of the specificity of a single enzyme (Hsepi) acting at an early point in the scheme, to convert GlcA-GlcNS to IdoA-GlcNS in preference to converting GlcA-GlcNAc to IdoA-GlcNAc. The biosynthetic route is highly efficient; only 5 enzymes are required to make 6 common disaccharide structures (major structures red trunk in **Figure I.2**) but 15 are required if all 16 structures are included.

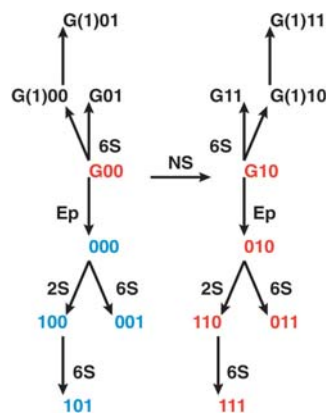


Figure I.2 Proposed highly symmetric tree structure for the biosynthesis of heparan sulfate and heparin. Red (major branch) signifies the common disaccharides, blue the uncommon, IdoA containing structures, emanating from 000. Other structures are in black. The unmodified disaccharide GlcA-GlcNAc is referred to as G00, the epimerized form, IdoA-GlcNAc, as 000 and the subsequent modifications (sulfations) (IdoA2S-GlcNAc) as 100 or (IdoA-GlcNS) 010 and (for IdoA-GlcNAc6S) as 001 and so on for any combination. For example, 2-O-sulfation of GlcA is therefore represented as G(1)00, while the disaccharide GlcA-2S-GlcNS is represented as G(1)10, or IdoA-GlcNS,6S as 011. Taken from [25].

Moreover, instead of applying restrictions to the steps based on the suitability of a single disaccharide unit to undergo the next modification (like in the previous model), enzymes can act on the disaccharide residue adjacent to the disaccharide that has been modified by the previous step.

Following its synthesis and modification processes, HS presents three domains starting from the linkage region towards the non-reducing end. The non-sulfated domain (**NA**) made of GlcA-GlcNAc repeats is the predominant one, the intermediate domain (**NA/NS**) is more sulfated than NA and composed of GlcNAc and GlcNS in combination with GlcA, and the other domain contains the highly sulfated GlcNS residues (**NS**) [21][26]. The different ratios of NA, NS, and NA/NS domains appear to be determined by the cell-type in which the synthesis occurs [22]. The length of the sulfated and non-sulfated segments varies. Outside the cell, two endosulfatases catalyze the removal of specific 6-O-sulfate groups, and secreted heparanase (**section I.6**) can fragment the chains.

Almost at the end of NS domain some chains present a pentasaccharide sequence N-acetyl-D-glucosamine 6-O-sulfate, (α 1 \rightarrow 4) D-glucuronic acid, (β 1 \rightarrow 4) D-glucosamine-N,3-O,6-O-trisulfate, (α 1 \rightarrow 4) L-iduronic acid 2-O-sulfate, (α 1 \rightarrow 4) D-glucosamine-N,6-O-disulfate (ANAc,6S-G-ANS,3S,6S-I2S-ANS,6S) designated AGA*IA, characterized by the trisulfated glucosamine GlcN, 3,6S (or A*). This pentasaccharide is typical of heparin (present in about 1/3rd of chains) although it has been also found in endothelial HS [27], it is the minimal sequence required to bind the protein Antithrombin III with high affinity and plays a pivotal role in heparin anticoagulant/antithrombotic activity.

I.3 Heparan sulfate v. heparin

Heparan sulfate and heparin biosynthesis follows the same cascade of enzymatic steps; nevertheless, the participation of different enzyme isoforms results in distinct structures; for example, NDST2 is required for the synthesis of heparin in mast cells [28], while NDST1 seems to be critical for the synthesis of heparan sulfate [29].

Heparin is often referred to as the more completely modified version of HS. Indeed, it is known to be more *N*- and *O*-sulfated than HS, and,

granules as serglycin proteoglycan and chains are randomly cleaved by endo- β -D-glucuronidase at the GlcA residues at the end of the synthetic process to generate free chains (3-20 kDa) [19][21][32].

I.4 Heparan sulfate proteoglycans (HSPGs)

Among the 30 different proteoglycan protein cores [33], three major subfamilies of proteoglycans have been reported (**Table I.2**). Membrane-spanning syndecans [1] and the glycosylphosphatidylinositol-linked glypicans [3][34] together with other minor HSPGs (such as β -glycan and the third isoform of CD44), constitute the HSPG cell surface family; perlecan, collagen XVIII and agrin constitute the basement membrane proteoglycans [22] (**Figure I.4**). Heparan sulfate can be found with different core proteins which are cell-type specific, but they are not specific for a defined heparan sulfate structure. Indeed, the same core protein can be found with different heparan sulfate structures [26] and some HSPGs also carry different GAG chains (CS/DS).

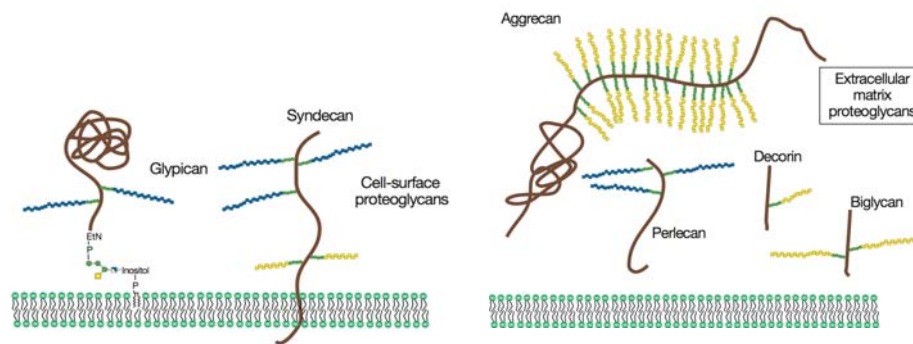


Figure I.4. Representation of the major HSPGs, membrane-spanning (left) and basement membrane (right). Adapted from [7].

High-molecular-weight HSPGs, characteristic of basement membranes, take part in crucial functions such as cell contact inhibition, cell adhesion, tissue compartmentalization and homing processes [4]. Moreover, during developmental processes, HSPGs are involved in hormone and growth

factors diffusion and interaction with receptors, and in morphogen diffusion, gradient formation and stabilization [35][36].

Table I.2. Examples of heparan sulfate proteoglycans. Adapted from[7].

Proteoglycan	Core protein (kD)	Number of glycosaminoglycan chains	Tissue distribution
Perlecan	400	1-3 HS CS/KS	secreted; basement membranes; cartilage
Agrin	200	1-3 HS	secreted; neuromuscular junctions
Collagen type XVIII	147	2-3 HS	secreted; basement membranes
Syndecans 1-4	31-45	1-2 CS 1-3 HS	membrane bound; epithelial cells and fibroblasts
Betaglycan	110	1 HS 1 CS	membrane bound; fibroblasts
Glypicans 1-6	~60	1-3 HS	membrane bound; epithelial cells and fibroblasts
Serglycin	10-19	10-15 heparin/CS	intracellular granules; mast cells

The list of HEP/HS-binding proteins is extensive and continuously growing. The emerging view is that HEP/HS-protein interactions involve specific oligosaccharide sequences. However, the oligosaccharide structure (in term of residue sequence, length and sulfation pattern) and conformation required for a specific binding has been elucidated only for few HEP/HS-protein complexes to date.

I.5 Interaction with proteins

The entirety of HS-protein interactions termed “HS-interactome” [37] is thought to be largely responsible for regulating key biochemical and developmental processes in multicellular organisms.

I.5.1 Fibroblast Growth factors

Although HS regulates the activities of a number of different morphogens, this ability is best understood for the FGFs [38]. It is well established that HS chains are involved in the regulation of FGF/FGF-receptor affinity and stability and, indeed, a competent HS or HS analogue is required for signaling. The known FGFs regulate a multitude of developmental processes including development of the limb, lung, heart, and brain [39]. The main targets of the FGFs are two classes of receptors: the tyrosine kinase receptor family and their co-receptors, the heparan sulfate proteoglycans.

Studies using cells deficient in HS first demonstrated a requirement of HS in the formation of a high affinity FGF-FGF receptor (FGFr) complex [40], whereas studies using chemical inhibitors of HS synthesis demonstrated a requirement for HS in FGF signaling [41].

FGFs exert their effects by binding with high affinity to four distinct but highly related transmembrane tyrosin kinase receptors (FGFr1 - 4). Cell membrane heparan sulfate protects FGFs from denaturation and proteolytic degradation and increases FGF affinity for their receptors facilitating and stabilizing the formation of properly oriented FGF oligomers.

Ternary complex formation occurs only when an HS domain contains the sulfation pattern necessary for both FGF and FGFr recognition [42] (**Figure I.5**).

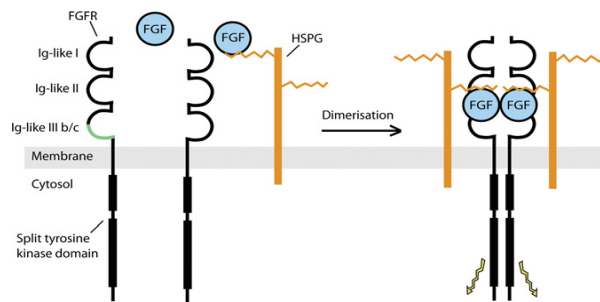


Figure 1.5. Schematic representation of the formation of the ternary complex between FGF, FGFR and HS. Taken from [43].

Acidic FGF (aFGF, or FGF1) and basic FGF (bFGF, or FGF2) were the first members of the family to be discovered and their interactions with HS are the most extensively studied [44].

Besides FGFs, several different growth factors have the ability to bind heparin and heparan sulfate, such as vascular endothelial growth factors (VEGFs), hepatocyte growth factors (HGFs), transforming growth factor- β 1 (TGF- β 1), platelet derived growth factors (PDGFs) and heparin binding epidermal growth factors (HB-EGFs).

These growth factors play different roles in cell proliferation, migration and morphogenesis. Similar to what has been described for FGFs, HS localizes these growth factors at the cell surface or in the ECM and promotes their biological activities.

1.5.2 Chemokines

Chemokines can bind HEP and cell surface GAGs at the vascular endothelium or in the ECM. Chemokines are a superfamily of 8–11kDa secreted chemotactic cytokines involved in a variety of biological functions including selective recruitment and activation of cells during inflammation, leukocyte degranulation, angiogenesis and angiostasis [45].

Cell surface HS was observed to promote the activity of different chemokines, such as interleukin 8 (IL-8), platelet-derived factor 4 (PF4) and stromal cell derived factor-1 α (SDF-1 α or CXCL12), by sequestering these molecules at the cell surface, thereby increasing their effective concentration in the vicinity of their receptor sites.

For example, IL-8-HS /CS interactions determine the location at which IL-8 binds in lung tissue and provides a site for the dimerization of IL-8. Chemokine immobilization is necessary because soluble chemokines could haphazardly bind and activate leucocytes prior to selectin-mediated adhesion, subsequent arrest and firm adhesion, and therefore transmigration of the leukocyte would not occur. Without such a mechanism, chemokine gradients would be disrupted by diffusion, especially in the presence of shear forces in the blood vessels and draining lymph nodes. The interaction is mediated by quite extensive GAG sequences (12-20 saccharide moieties), as a result of chemokine oligomerization. Conversely, soluble GAGs can complex with chemokines in solution and prevent their binding with receptors, inhibiting their activities.

1.5.3 Lipid- or membrane-binding proteins

While there is extensive literature on the interaction of GAGs with various families of proteins, less is known about interactions of GAGs with lipid- or membrane-binding proteins.

Annexin V has a role in the entry of and infection by influenza and hepatitis B viruses; it also exhibits potent anticoagulant activity due to its ability to bind phosphatidylserine on cell membrane surfaces, self-assemble and form a shield that prevents excessive clot formation. It has been proposed that extracellular annexins can serve as GAG-recognition elements *in vivo* [46]. A model was proposed by which HS proteoglycan wraps around the annexin V molecule, sequestering free annexin in readiness for activation and

assisting in docking of other heparin-binding proteins to the membrane-bound annexin layer [47]. Similarly to annexin V, HS wraps around apolipoprotein E (ApoE), which is an important lipid transport protein in human plasma and brain. In the liver, HSPGs act in concert with LRP (low-density lipoprotein receptor related protein) to complete the interaction of remnant particles with LRP in a process known as the HSPG-LRP pathway, in which apoE initially interacts with HSPG on the cell surface [48] and is then transferred to the LRP for internalization [49]. In addition, the interaction of ApoE with HSPG has been implicated in neuronal growth and repair and, consequently, is involved in the progression of late onset familial Alzheimer's disease [50], in which HSPGs facilitate the formation of insoluble fibrils and stabilize them against proteolytic cleavage.

1.5.4 Adhesion proteins

The interaction of HEP and HS with adhesion proteins has implications in various physiological and pathological processes including inflammation, nerve tissue growth, tumor cell invasion and plaque formation in the brain. L-, E- and P-selectins are a family of transmembrane glycoproteins found on leukocyte endothelium and platelets. They are responsible for mediating the initial adhesive events directing the homing of lymphocytes into lymphoid organs and the interaction of leukocytes with the endothelium in inflammation and reperfusion injury states. Selectin interactions may also be involved in the metastasis of certain epithelium cancers. The putative ligand on the endothelium responsible for the interaction of leukocytes with selectins is the carbohydrate antigen sialyl Lewis X (SLe^x), although HS has also been shown to play a role in this interaction. HS interacts with L-, P-, but not with E-selectins. L-selectin binds highly sulfated, particularly O-sulfated, heparan sulfate chains enriched in glucosamine residues whose amino groups are unsubstituted, whereas the presence of iduronic acid

residues seems to inhibit this interaction [51]. Binding to P-selectin generally occurs with a weaker affinity than for the interaction with L-selectin. Heparin tetrasaccharides specifically block interactions of L- and P-selectins with SLe^x demonstrating anti-inflammatory activity *in vivo* [52]. By interacting with selectins, unfractionated heparins also prevent selectin-mediated adhesive events involved in vascular occlusion as well as in tumoral metastasis.

1.5.5 Pathogens

Many viruses make use of HSPGs as receptors to bind to and gain access into target cells, for example HIV-1, herpes simplex virus (HSV), and dengue virus. *Plasmodium falciparum*, the parasite causing malaria, bears at its surface circumsporozoite protein that shows the ability to interact with liver cell HS proteoglycans, promoting pathogen attachment and subsequent cell invasion [53].

1.6 HS and HEP degrading enzymes

HEP and HS can be degraded by two types of enzymes: prokaryotic polysaccharide lyases, named heparinases, acting through an eliminative mechanism (thus affording unsaturated oligosaccharides), and eukaryotic glucuronyl hydrolases, e.g. heparanase, acting through a hydrolytic mechanism. Three major lyases (heparinase I, II and III), able to cleave HEP and HS with different substrate specificity, were isolated from *Flavobacterium heparinum* [54]. Heparinase II has the broadest substrate requirement; it has two distinct active sites, one of which is believed to act on HEP and the other on HS. Heparinase III shows strong specificity for HS. It has been observed that calcium enhances the activity of heparinase I and III, but inhibits the activity of heparinase II [55]. Heparinases are largely used in the preparation

of defined oligosaccharides from HEP and HS required for the structural characterization of such polymers.

Mammalian heparanase is an endo- β -D-glucuronidases that has been demonstrated to partially depolymerize HS in a variety of cells and tissues. It is involved in the regulation of tissue development, wound healing and tumor metastasis, as potent inhibitor of neovascularization and it is over-expressed in tumor cells. Enzymatic degradation of HS proteoglycan stimulates the growth of cancer cells both by releasing growth factors (angiogenic effect) and by disrupting the basement membrane and ECM, thereby facilitating intrusion of tumor cells into tissues (metastatic effect). For these reasons, heparanase was recently recognized as a new promising target for a novel strategy in cancer therapy [56].

Cells secrete matrix proteoglycans directly into the extracellular environment; however, others are shed from the cell surface through proteolytic cleavage of the core protein (e.g., the syndecans). Cells also internalize a large fraction of cell-surface proteoglycans by endocytosis (Figure I.6).

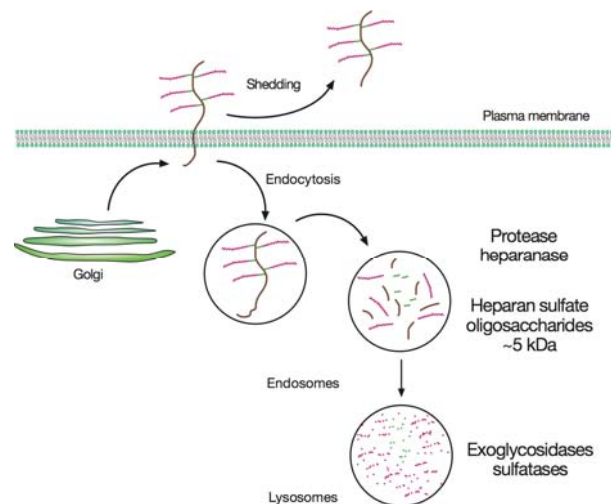


Figure I.6. Heparan sulfate proteoglycan turnover is facilitated by proteolytic shedding from the cell surface and endocytosis, as well as step-wise degradation inside lysosomes. Taken from [7].

Internalized proteoglycans first encounter proteases that cleave the core protein and heparanase that cleaves the HS chains at a limited number of sites, depending on sequence. These smaller fragments eventually appear in the lysosome and undergo complete degradation by way of a series of exoglycosidases and sulfatases. The main purpose of intracellular heparanase may be to increase the number of target sites for exolytic degradative enzymes. CS and DS proteoglycans follow a similar endocytic route, but endoglycosidases that degrade the chains before the lysosome have not been described.

CHAPTER II: CHARACTERIZATION OF HEPARAN SULFATE IN MULTIPLE HEREDITARY EXOSTOSES

II.1 Introduction

II.1.1 HME and EXT genes

Three groups of diseases occur as a consequence of an insufficient HS synthesis and /or impaired metabolism: the first includes thesaurismosis, such as Sanfilippo syndrome [57], another comprises modifications of the consensus sequences on proteoglycan core proteins with impaired post-translational modification of HSPGs (e.g. Glypican 3 defects occur in Simpson Golabi Behmel syndrome [58]). The third group arises from alterations of the enzymes involved in the synthesis of HS chains, contains the EXT1/EXT2 gene mutation (**Figure II.1**) and results in a disease that is known as hereditary multiple exostoses or -this is the currently used name, multiple osteochondromas (MO) [59][60][61]. Hereditary Multiple Exostoses (HME; MIM 133700 and 133701) is an autosomal dominant disorder with an incidence of 1/50,000 characterized by the occurrence of multiple benign cartilage-capped tumors that are typically located at the juxta-epiphyseal regions of long bones and associated with disproportionately short stature [62]. In addition, exostoses (EXT) may occur at other sites, such as the ribs, the shoulder blade (scapula), and pelvis. Osteochondromas appear and develop gradually in childhood and increase in size until the end of puberty. However, existing exostoses can grow slowly over the years. Before birth, HME can be diagnosed by testing DNA taken from the fetus. This can be obtained in one of the following ways:

- By amniocentesis after the 15th week of pregnancy
- By chorionic villus sampling (CVS) between the 11th and 14th week of pregnancy

These methods are used for high-risk pregnancies, for instance if the parents have another child diagnosed with HME or one of the parents has HME. To

be eligible for this testing, the mutations in the gene responsible for causing HME in the family must be known. This means that genetic testing (a blood test) must be done on the person of the family with HME. After birth, the diagnosis of HME is based on X-ray findings. A diagnosis of HME can be confirmed by DNA testing of the EXT1 and EXT2 genes (a blood test).

HME is a genetically heterogeneous disorder, and two different loci, designated EXT1, EXT2, have been mapped to chromosomes 8q24.1 [59] and 11p11-p12 [63], respectively. Also a third locus has been suspected to be responsible of some cases of MO but its presence is not clearly confirmed: it deals about EXT3 probably found at chromosome 19p by a French staff of researchers [64].

Symptoms are more likely to be severe if the mutation is on the EXT1 gene rather than EXT2; EXT1 is also the most commonly affected gene in patients of this disorder [65].

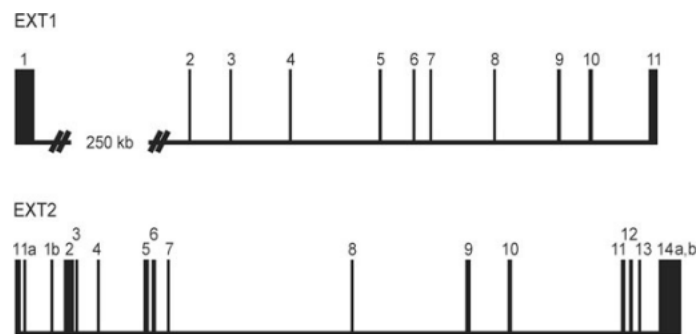


Figure II.1. The EXT1 and EXT2 genes. The EXT1 gene is localized on the chromosome 8q24.11, comprises 11 exons and spans approximately 350 kb of genomic DNA. The majority of mutations is predicted to result in a truncated or non-functional protein. The EXT2 gene is localized on the chromosome 11p11.2, comprises 16 exons two of which alternatively spliced and spans approximately 108 kb of genomic DNA.

Since exostoses appear to represent a benign outgrowth from the growth plate, it would appear that subtle changes in HS expression in this location could have profound effects on chondrocyte growth and/or differentiation. HSPGs affect signaling by hedgehog proteins (including Indian hedgehog,

Ihh), bone morphogenetic proteins (BMPs) and members of the Wnt family of growth factors in an yet undefined manner [66]; moreover, HS is a potent inhibitor of remodeling activities present in bone and cartilage [67]. All these observations have suggested that reduction or lack of HSPGs in HME may alter proper growth factor signaling leading to the aberrant bony growths, i.e. a local perturbation in the Ihh diffusion and release from negative feedback control could cause premature chondrocyte differentiation, apoptosis and ossification in the neighboring population [15].

Heterozygous EXT1 or EXT2 mutations are the only event in more than 90% of the exostoses evaluated [68]. Loss of heterozygosity involving these EXT loci has rarely been observed and has been reported in chondrosarcomas associated with exostoses [69]; EXT1 epigenetic inactivation has been found in other sporadic cancers [70], suggesting that the EXT genes may also have roles as tumor suppressors. Mutations in EXT1 occur throughout the entire length of the gene, while mutations in EXT2 concentrate towards its N-terminus, implying specific functions for this part of the protein.

EXT2 does not harbor significant glycosyltransferase activity in the absence of EXT1; nevertheless, it does not play a redundant role to EXT1 in HS polymerization, in fact transfection of EXT1-deficient cell lines with EXT2 does not restore HS synthesis [69]. Instead, it appears that EXT1 and EXT2 form a hetero-oligomeric complex in vivo that leads to the accumulation of both proteins in the Golgi apparatus. Experimental data suggest that the HS copolymerase may be a complex containing EXT1 and EXT2, in which both subunits are essential for activity and which possesses substantially higher glycosyltransferase activity than EXT1 or EXT2 alone. The stoichiometry of dimerization that must occur for the formation of the active enzymatic complex could be disturbed and result in diminished HS biosynthesis and HS proteoglycan expression [71].

Although EXT1 and EXT2 are ubiquitously expressed, mutations in these genes only affect chondrocytes, suggesting that a chondrocyte-specific

function requires two fully functional EXT1 and EXT2 genes (and that one functional copy of either gene is enough for other cell types) [72]. The expression of EXT1 and EXT2 proteins has been found to be significantly reduced in HME-derived chondrocytes. In addition, due to impaired EXT1/EXT2 function the HSPGs appear to be retained in the Golgi apparatus and cytoplasm of the tumor cell, instead of being transported to the cell surface and/or extra cellular matrix where they normally exert their function. Moreover, EXT mutations were described to induce cytoskeletal abnormalities (altered actin distribution) in osteochondroma chondrocytes [73].

Degeneration to malignant tumor, i.e. chondrosarcoma, can occur both in the presence or absence of mutations in EXT genes [69]. The cause is not clear; however people with certain conditions, e.g. MHE, Ollier's disease (people with multiple enchondromatosis), Maffucci's syndrome (multiple enchondromas and hemangiomas), are more prone to the development of this type of tumor. Also, different degrees of severity can be found. Most chondrosarcomas do not respond to chemotherapy or radiation therapy thus making surgical management crucial in the treatment of chondrosarcoma.

The biological effect of EXT1/2 mutations is not clearly elucidated due to the absence of a complete structural and molecular analysis of HS chains, whose polymerization is catalyzed by EXT genes. To this, the absence of any therapeutic option (except for corrective surgery) as well as the lack of any prognostic marker, represents major problems for MO management.

Many hypothesis are present in literature on the enzymatic efficiency of EXT mutated proteins with production of HSs chain that differ from the wild-type synthesized ones [74].

A paper by Hameetman *et al.* [75] showed absence of HS in cartilage affected by osteochondroma or chondrosarcoma by immunohistochemistry (**Figure II.2**).

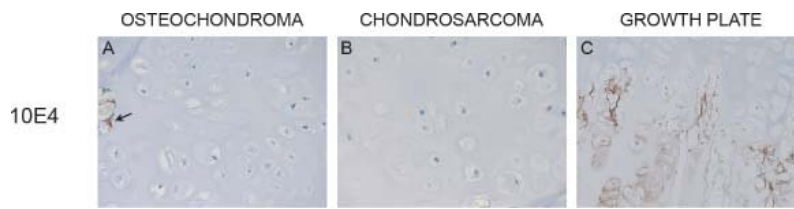


Figure II.2. Expression of heparan sulfate and HSPG core proteins. Absence of expression of native HS chains in osteochondroma (A) and chondrosarcoma (B), while growth plate (C) demonstrates extracellular expression in the late hypertrophic and calcifying zones. The 10E4 antibody reacts with an epitope that occurs in native HS chains. Taken from [75].

However, a real assessment of the biochemical status in MO cartilages-essential for new therapeutic strategies, as well as in human healthy cartilage, has never been performed.

II.1.2 Discovery of the correlation between HS and EXT genes

The correlation between the EXT loci and HS came from studies of Herpes simplex virus (HSV). In 1994, Shieh and Spear [76] demonstrated that HSV-1 utilized cell surface HS for viral attachment, mediated by specific viral glycoproteins present on the viral envelope. Chinese hamster ovary cell mutants defective in HS synthesis were resistant to viral attachment and invasion and exogenous heparin blocked attachment of virions to a variety of cell types [77]. Tufaro *et al.* [78] took advantage of these findings and identified mouse fibroblast cell lines resistant to HSV infection, which also turned out to be deficient in HS synthesis. McCormick *et al.* [79] discovered a gene with complementing activity that also restored HS synthesis; this gene turned out to be EXT1, which had been previously identified as the gene mutated in HME [59]. Prior studies had demonstrated that a single protein catalyzed the transfer of both GlcNAc and GlcA units to nascent HS chains [80], suggesting that both activities were encoded by EXT1. EXT2 was discovered by Lind *et al.* [81] and it was also able to catalyze both the transfer of GlcA and GlcNAc.

II.1.3 Physiology of cartilage

The articular ends of bones are covered with cartilage, an avascular, non-innervated extracellular matrix tissue that is maintained in its functional state by the balanced anabolic and catabolic activities of a sparse number of chondrocytes. The load-bearing properties of cartilage depend on both the composition and macromolecular organization of the ECM [82] in which type II, IX and X collagen molecules are assembled in high concentration of proteoglycan aggregates. The large proteoglycan aggrecan is a major component of cartilage and consists of a 200-kDa protein core to which ~100 chondroitin sulfate chains, and in many cases a similar number of keratan sulfate chains, are attached. These negatively charged glycosaminoglycans create a large osmotic pressure that draws water into the tissue and expands the collagen network [83].

Articular cartilage is the permanent smooth tissue that covers the end of bones at a joint, allowing a fluid movement thanks to the distribution of loads and the decrease of friction. The growth of bones is regulated by areas of developing cartilage tissue called growth plates.

During bone growth, the cartilaginous precursors are divided from the surrounding mesenchymal environment by a thin layer of perichondrial cells that will give rise first to the perichondrium and then to the periosteum. Inside the cartilage anlagen (the term is used to indicate the part that will become the future bone), the proliferation and differentiation processes take place and subsequently the cartilage undergoes ossification through vascular invasion of its hypertrophic part. Therefore the central part of the anlagen starts to become ossified (the future diaphysis of the bone) and the population of chondrocytes is divided into two distinct zones that will give rise to the two growth plates that will guarantee the elongation of the bone for many years until the onset of puberty when the proliferating power of metaphyseal chondrocytes is almost completely consumed and the growth plate completely ossified. Briefly, chondrocytes first produce hyaline

cartilage at the epiphyseal plate, or growth plate, which is located between the epiphysis and metaphysis and pushes the ends of bones upward. In the meanwhile, the population of epiphyseal chondrocytes is regulated by different morphogens and growth factors (principally the Wnt family of growth factors) and undergoes a divergent differentiation process that does not include the vascular invasion and the ossification but will give rise to the articular cartilage which is mostly made of collagen and water.

When ossification of the epiphyses is completed, the growth plate cartilage becomes replaced by bone, but the articular cartilage still remains. Therefore, growing cartilage is only found during the process on bone growth while in adults, when final length has been achieved, it is present as a thin epiphyseal scar. In normal long-bone growth plates, chondrocytes are arranged into zones of resting, proliferating and maturing (hypertrophic) cells [84] (**Figure II.3**).

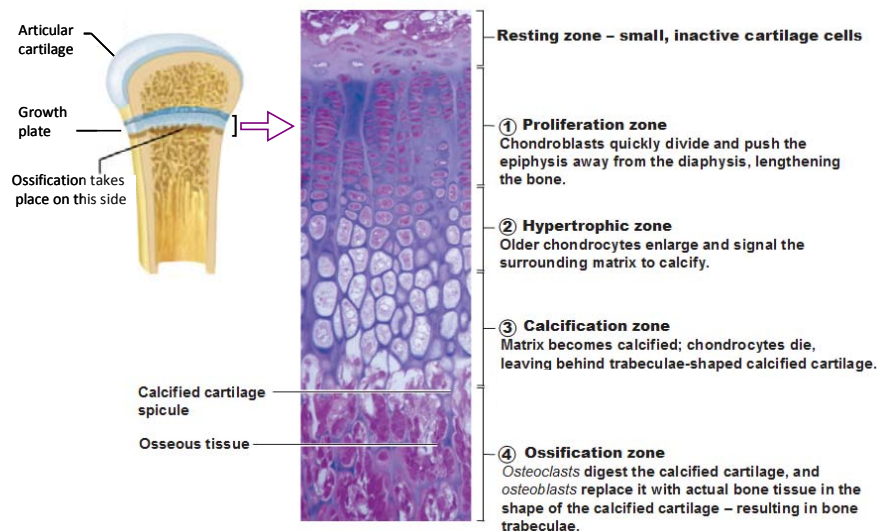


Figure II.3. Zonal organization of growth plate cartilage.

Resting/stem-like chondrocytes divide and give rise to proliferative chondrocytes which enlarge to become hypertrophic chondrocytes that ultimately undergo apoptotic cell death and are replaced by bones.

II.1.4 Objectives of the work

MO is known to be caused by mutations in the HS synthesis genes EXT1 and EXT2 but the real pathogenic mechanism is still unclear, as well as the process of malignant transformation. Moreover, potential prognostic/therapeutic targets are strongly needed since MO is the most frequent skeletal dysplasia in the pediatric/adolescent age and severely affects the quality of life during patients' lifespan.

The project is focused on the structural characterization of HS from pathologic excisions, in order to determine if compositional changes in HS occur or a reduced amount of HS is present in comparison to healthy cartilage. Therefore, the first part of the work dealt with the characterization of HS from healthy cartilage on which no structural information is available in literature, while in the second part a similar procedure was applied to pathologic cartilage.

The approach proposed could be of broad-spectrum relevance and applied to other growth plate related skeletal dysplasias; being HS chains critical regulators of several developmental processes, the clarification of the molecular pathways altered in MO disease will permit to better understand molecular controls in cartilaginous growth and could be used to evaluate and prevent other cartilaginous problems.

To achieve the goal of the study the following objectives have been defined:

1. *To characterize HS from healthy cartilage*

For this purpose, excisions from three types of human cartilage from healthy subjects were collected:

- Articular cartilage
- Growth plate cartilage
- Fetal cartilage

Samples were subjected to extensive enzymatic digestions to remove all GAGs except for HS. NMR and HPLC-MS were used to identify and characterize HS.

2. *To characterize HS from pathologic cartilage*

For this purpose, excisions from patients affected by mutations in the EXT1/EXT2 genes or by chondrosarcoma (C) were collected and processed. Small variations of the method adopted for healthy samples were introduced to characterize HS.

II.3 Characterization of HS from healthy cartilage

The great challenge of this project turned out to be the availability of a reference compositional panel of healthy cartilaginous tissue. The Orthopaedic Institute Rizzoli has access to a broad assortment of cartilaginous samples; nevertheless, the ones used in this project have to be considered 'healthy' only with regard to the pathology under examination (MO). In fact, excisions of cartilage were from patients with malformations or other pathologies which are supposed not to alter directly or indirectly HS composition.

Several analytical approaches have been developed to identify and quantify GAGs isolated from biological samples and are of primary importance to evaluate the purity of the single glycosaminoglycan species used in therapy. Classical procedures involve precipitation, gradient centrifugation, anionic exchange chromatography and electrophoresis. In this work, the procedure adopted is based on a published method [85] that consists in the digestion of all cellular and extracellular components and removal of fragments- thus avoiding extraction procedures, and therefore retaining only the GAG component. Information on cartilage samples is reported in **Table II.1**, where the dry amount of isolated GAGs is also reported.

Table II.1. Summary of the known information on samples. The table contains the wet weight of the excision, the dry weight of isolated GAGs and information on the patient. #From the same patient. *Weighted after the first digestion with ChABC. **Weighted after the first digestion with Hyaluronidase lyase.

<i>Sample</i>	<i>Wet Weight (mg)</i>	<i>GAGs (mg)</i>	<i>Area of excision</i>	<i>Gender</i>	<i>Age</i>
GRP 1	500	18	Femur	F	10
GRP 2#	115	6.7	Femur	M	10
GRP 3	105	4.2	Femur	F	7
ART 1	500	8.5	Humerus head	F	55
ART 2	500	9.9	Femur head	M	8

ART 3#	212	12.2	Femur	M	10
ART 4	180	7.9	-	-	-
F1	150-200	7.3 *	-	M	19 weeks
F2	150-200	12.2 *	-	---	35 weeks
F3	150-200	11.2 *	-	M	17 weeks
F4	150-200	8.9 *	-	M	17 weeks
F5	150-200	3.6 **	-	F	29 weeks
F6	150-200	3.9 **	-	M	20 weeks

Growth plate cartilage can only be found in prepubescent patients, before the ossification process is completed, therefore only one type of cartilage is available in the adult patient (ART1) while mainly growth plate can be found in fetal cartilage, since the ossification process starts from the 2/3 month on. Excisions were taken from amputations or surgeries, while fetal samples were from abortions. In this case, although the physiology of cartilage was perfectly distinguishable from other tissues, due to the mechanical procedure adopted for the pregnancies interruption it was not possible to identify the origin of excision, which usually is long bones or pelvis.

II.2.1 NMR of GAGs from healthy cartilage

The major GAGs present in cartilage are CS and type II KS linked to the proteoglycan Aggrecan (see **Annex Figure A.II.1** for an HSQC of isolated GAGs from commercial Aggrecan), as clearly observable from the 2D-NMR spectra of GAGs from GRP2 reported in **Figure II.4**.

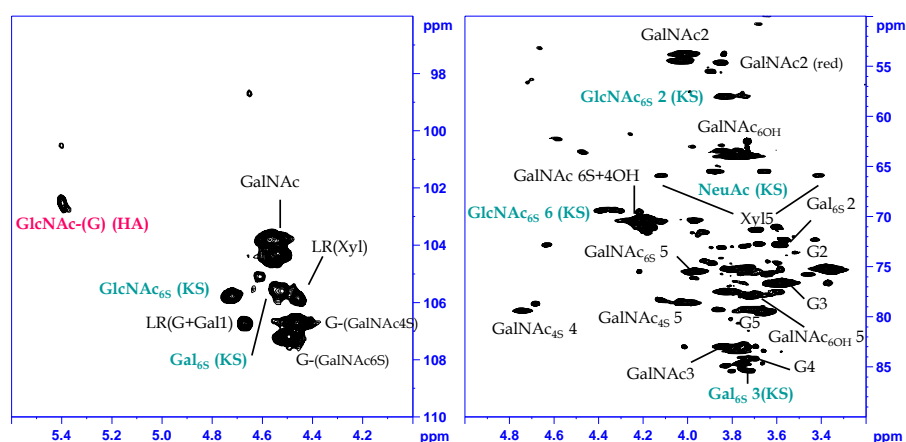


Figure II.4. HSQC-NMR spectra of GAGs from GRP2. Signals of the anomeric region are shown on the left while signals from the backbone are shown on the right. Signals specific to KS are indicated in green, while signals attributable to HA are indicated in red. Signals of residues from the linkage region (LR) were also detected. The signal attributable to the C₂ of GlcA of HA overlaps with CS. NeuAc is neuraminic acid and Xyl is xylose.

2D-NMR spectra of GAGs from healthy cartilage are similar for both ART and GRP samples (see **Annex Figure A.II.2** and **A.II.3** for 2D and ¹H spectra of GAGs from articular cartilage) and were recorded after each passage to verify the disappearance of undesired species and to detect signals from HS. GAGs were divided into two fractions by ultrafiltration in order to have an estimation of the dimension: A >10 kDa, B <10 kDa and >3 kDa. Each fraction was subjected to further digestion with chondroitinase ABC (ChABC) and hyaluronate lyase. No GAGs were detected in fractions lower than 3 kDa. As reported in **Figure II.5**, 1D-NMR profiles changed after enzymatic digestions but did not reveal any presence of HS, nor did the 2D-NMR analysis (not shown), which usually is more informative.

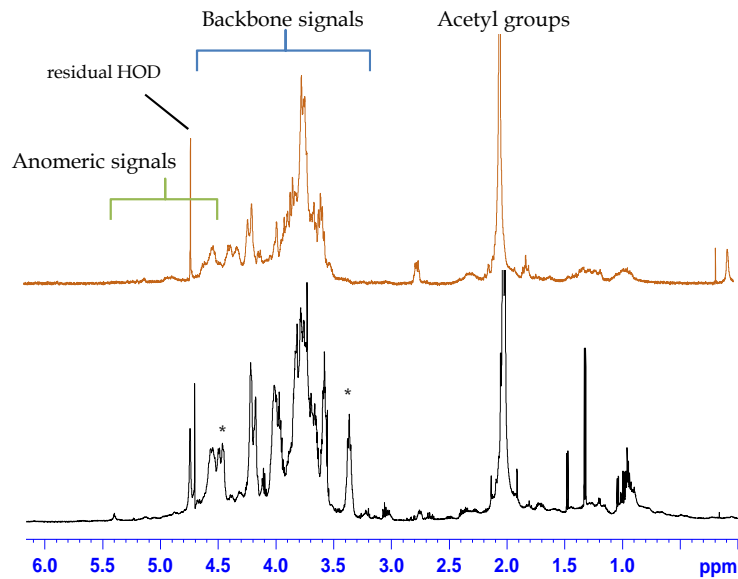


Figure II.5. $^1\text{H-NMR}$ spectra of GAGs from GRP2-A (>10 kDa) before (black) and after (orange) the digestion with ChABC and hyaluronate lyase. * indicates GlcA signals that disappear after the enzymatic digestion.

Moreover, the peculiar structural features of type II keratan sulfate prevented its degradation by enzymatic digestion methods. In fact, type II KS is characterized by fucosylation of GlcNAc6S and sialic acid capping of non-reducing terminal Gal or Gal6S (Figure II.6).

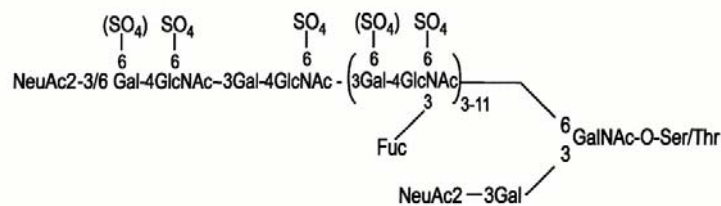


Figure II.6. Structure of articular cartilage type II KS. Sulfates in parentheses indicate partial or incomplete sulfation of monomers at this site.

Two enzymes known to act specifically on KS chains, both employed to try to digest KS, turned out to be ineffective: a) keratanase, an endo- β -

galactosidase which is inhibited both by Gal6S and when either neighboring fucose or sialic acid residues are present [86], and b) keratanase II, which cleaves between a GlcNAc6S residue and Gal or Gal6S.

A possible way to degrade KS is represented by hydrazinolysis which causes deacetylation of GlcNAc residues, followed by nitrous acid treatment [87]. Nevertheless, the procedure, besides being technically difficult to perform, can degrade also HS.

Six fetal samples have been characterized by following a similar procedure. The first four samples were not fractionated by ultrafiltration and were subjected to extensive digestion with ChABC and kyaluronate lyase followed by keratanase in an attempt to degrade KS. Instead, two samples were fractionated by ultrafiltration and 2D-NMR analysis showed in both the fractions the same composition in KS and CS then prepubescent/adult cartilage and no signals from HS were detected (**Figure II.7**) after enzymatic digestions.

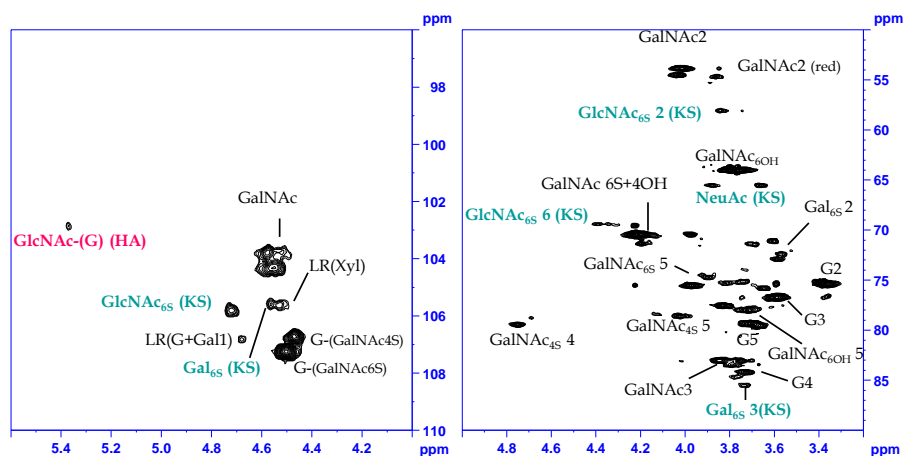


Figure II.7. HSQC NMR spectra of GAGs from F5-A after digestions with ChABC and hyaluronidase lyase. The profile of fraction F5-B (not shown) is identical.

In an attempt to isolate HS, the bigger fractions (A, >10 kDa) were loaded onto a QAE-sephadex A-25 column and eluted with increasing NaCl

concentration (0M, 0.25M, 0.5M, 1M, 2.5M). Each fraction was desalted by 3 kDa ultrafiltration and checked by NMR. Only fractions eluted at 0.5M and 1M NaCl (and 2.5M to a lower extent) contained GAGs (see **Annex Figure A.II.4**). This type of strong anion exchange chromatography has been used by others for fractionation of heparin based on charge and dimension [88] but it was not possible to separate HS from CS or KS with this method; therefore, the two fractions containing GAGs were mixed together prior to the last digestion step.

A common approach for structural analysis of HS is to characterize the disaccharide structures following its complete enzymatic depolymerization [89]. All healthy samples have been subjected to digestion of HS with a cocktail of heparinases (I, II, III) and 1/3rd of the desalted digestion products were analyzed by HPLC-MS.

II.2.2 Mass spectra interpretation and identification of oligosaccharides from prepubescent and adult HS

At the beginning of the project several attempts to gain as much information as possible of HS were made, by trying different enzymatic digestion approaches or changing the chromatographic elution gradient or adding a standard to quantify disaccharides. Therefore, the first GRP and ART samples (500mg of starting material) were treated differently from the others. Particularly, an attempt to gain more structural information was made by sequential digestions of ART2 (8 y.o.) and GRP1 (10 y.o.) with the three heparin lyases (or heparinases) I, II and III, which differ for their specificity of action on different HS sequences. Actually, sequential enzyme action is usually exploited to obtain sequence information, whereas the simultaneous enzymatic action (cocktail) is usually carried out to achieve the exhaustive digestion.

In **Figure II.8** are reported the profiles of fractions A (>10 kDa) of ART2 and GRP1 both after digestion with the cocktail of the three enzymes, while

profiles after sequential digestions are reported in **Annex Figure A.II.5** and **A.II.6**.

Each mass/charge ratio (m/z) value can be attributed to an oligosaccharide; principal mass peaks of interest are reported in **Table II.2**, while other experimental m/z values are reported in **Annex Table A.II.1**.

Table II.2. LC-MS data for several common oligosaccharides from digested cartilaginous HS.
When more interpretations are possible, alternatives are indicated.

<i>Monoisotopic m/z value</i>	<i>Corresponding mass value</i>	<i>Structure hypothesis</i>	<i>Prevalent ion form</i>
416.032	417	$\Delta 2,1,0$	$[M-H]^{-1}$
458.043	459	$\Delta 2,1,1$	$[M-H]^{-1}$
458.042	918	$\Delta 4,2,2$	$[M-2H]^{-2}$
496.002	497	$\Delta 2,2,0$	$[M-H]^{-1}$
504.647	1011	$\Delta 2,0,1-LR$	$[M-2H]^{-2}$
538.022	539	$\Delta 2,2,1$	$[M-H]^{-1}$
544.622	1091	$\Delta 2,1,1-LR$	$[M-2H]^{-2}$
546.077	1094	$\Delta U5,2,2$	$[M-2H]^{-2}$
575.962	577	$\Delta 2,3,0$	$[M-H]^{-1}$
575.962	1154	$\Delta 4,6,0$	$[M-2H-2SO_3]^{-2}$
584.589	1171	$\Delta 2,2,1-LR$ or $\Delta 6,2,0$	$[M-2H]^{-2}$
634.094	635	$\Delta U3,1,1$	$[M-H]^{-1}$
669.059	2009	$\Delta U7,6,2+3DBA$ or $\Delta 6,3,3-LR$	$[M-3H+DBA]^{-3}$
694.189	1390	$\Delta 4,0,2-LR$	$[M-2H]^{-2}$
774.148	1550	$\Delta 8,2,1$ or $\Delta 4,2,2-LR$ or $\Delta U5,5,1+2DBA$	$[M-2H]^{-2}$
775.570	1553	$\Delta U7,3,3$	$[M-2H]^{-2}$

HPLC-MS analyses detected the presence of heterogeneous oligosaccharides, revealing incomplete digestion of HS, although with the heparinase cocktail/HEP ratio of 2mU/0.1 mg usually it is possible to obtain complete depolymerization to mostly disaccharides and few tetrasaccharides and hexasaccharides. Only products analyzed in a single run can be compared each other regarding the intensity of peaks, e.g. the amount of material, while it is always possible to compare the m/z patterns.

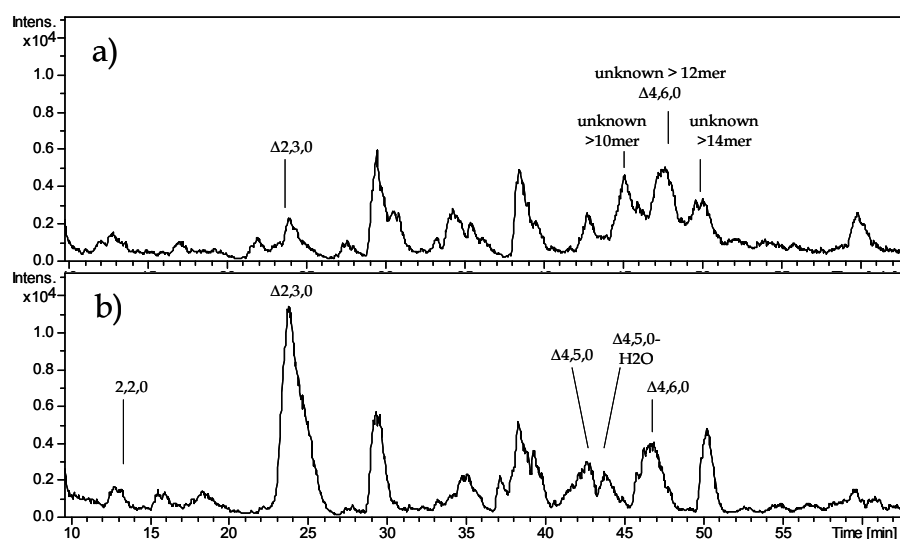


Figure II.8. HPLC profiles of digestion products from heparinase cocktail digestion of prepubescent HS. a) ART2-A (>10 kDa), b) GRP1-A (> 10 kDa). Oligosaccharides were identified by their mass/charge ratio and labeled as follow: the unsaturated bond of the terminal uronic acid is indicated by Δ , and the number of monomers, the number of sulfates and the number of acetyls are reported. Oligosaccharides for which a not precise interpretation is available were labeled as 'unknown'. An estimation of the monosaccharide units is also reported.

An higher degree of heterogeneity was found in fractions B (<10 kDa) that were only subjected to sequential digestions. An example of the HPLC profiles (GRP1-B) is reported in **Annex Figure A.II.7**. A good amount of acetylated oligosaccharides was detected in these fractions, thus balancing the absence of such products in the bigger fractions. Samples were digested with keratanase (endo- β -galactosidase) in an attempt to degrade KS, therefore only oligosaccharides bearing remnants of the linkage region were detected, i.e. $\Delta 2,0,1$ -G-Gal, since the Gal-Xyl-Ser sequence has been split. The procedure of sequential digestions, besides to be particularly involved on consideration of the scarcity of material available, resulted in dispersion of information and results. Moreover, also digestion with heparinase cocktail generated a variety of oligosaccharides, mostly disaccharides in

GRP1 but longer fragments in ART2, suggesting the presence of sequences resistant to digestion. For these reasons only digestion with the cocktail of enzymes was performed on all the other samples both healthy and pathologic. Repeated digestions of ART2-A with the cocktail of heparin lyases originated mostly di-trisulfated disaccharides (data not shown) confirming the presence of HS with a high degree of sulfation in both the A fractions.

In parallel to the sequential digestion procedure, an attempt to quantify the disaccharide species was made by addition of a standard oligosaccharide to the digestion products of ART-1 (55 y.o.) (**Figure II.9**). The standard was the disaccharide 2-O-sulfated-iduronic acid linked to 6-O-sulfated-anhydromannose (IdoA2S-aM6S) with a specific m/z ratio of 499.02 (MW 500Da, for its structure see **Annex Figure A.II.8**). Nevertheless, the chromatographic peak of the standard was not well resolved and overlapped partly with the digestion product $\Delta U_{3,1,1}$. Anyway, it turned out to be worthless since only quantification of disaccharides, which are not the predominant species, can be made with this method.

A high amount of saturated oligosaccharides together with an odd number of residues was observed in fraction B, while fraction A resulted less sulfated than the corresponding fraction of ART2. Further comparison between adult and prepubescent articular HS would require a statistically relevant number of samples.

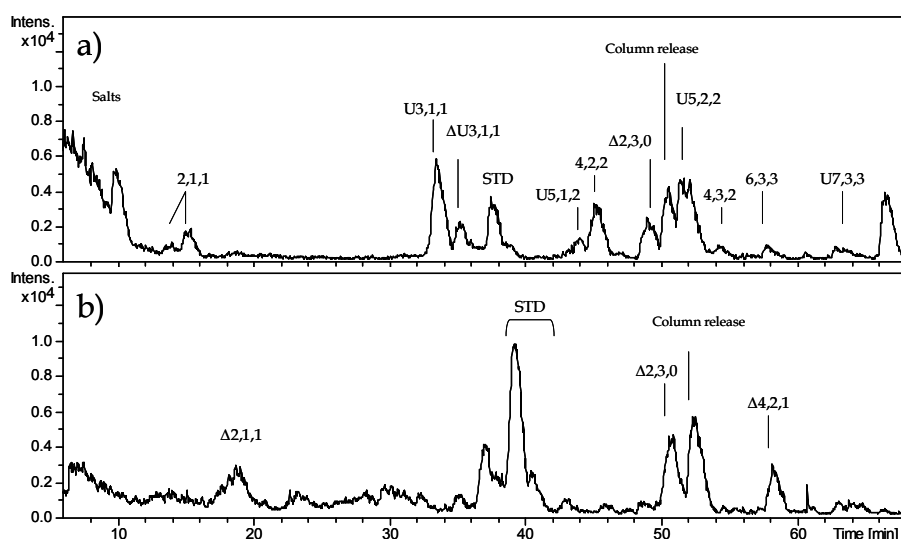


Figure II.9. HPLC profiles of digestion products from heparinase cocktail digestion of prepubescent HS. a) ART1-B (<10 kDa) , b) ART1-A (>10 kDa). STD indicates the IdoA2S-am6S disaccharide used as reference. When an uronic acid is present at both the RE and NRE it is indicated by U.

In **Figure II.10** the HPLC profiles of ART3 and GRP2, which are excisions from the same patient, are reported. The elution gradient adopted was longer for the last four prepubescent samples analyzed, in order to achieve a better chromatographic separation (see also **Annex Figure A.II.9**). Fractions B (< 10kDa) contained more digestion products than the corresponding bigger fractions as deducible by the higher intensities of peaks. Repeated digestions did not affect the final composition, demonstrating the presence in cartilaginous HS of sequences resistant to enzymatic cleavage.

Even if HPLC-MS analysis is not quantitative, comparison among samples is possible under identical conditions. The most representative digestion products found in both fractions are $\Delta U5,2,2$, $\Delta 8,2,1$ (or $\Delta U5,5,1$ or $\Delta 4,2,2$ -LR) and $\Delta 2,3,0$. The presence of saturated oligosaccharides with an odd number of residues, i.e. U5,2,2 and U7,3,3 (see **Figure II.9**) or U5,4,1 (see **Figure II.10**), can be explained as preexisting fragments generated by the endogenous action of an endo-glucuronidase, such as heparanase, which

releases fragments bearing an uronic acid at the RE. The presence of unsaturated odd oligosaccharides, i.e. $\Delta U5,2,2$, can be explained by the action of heparinases on longer fragment generated by a previous heparanase digestion (**Figure II.11**).

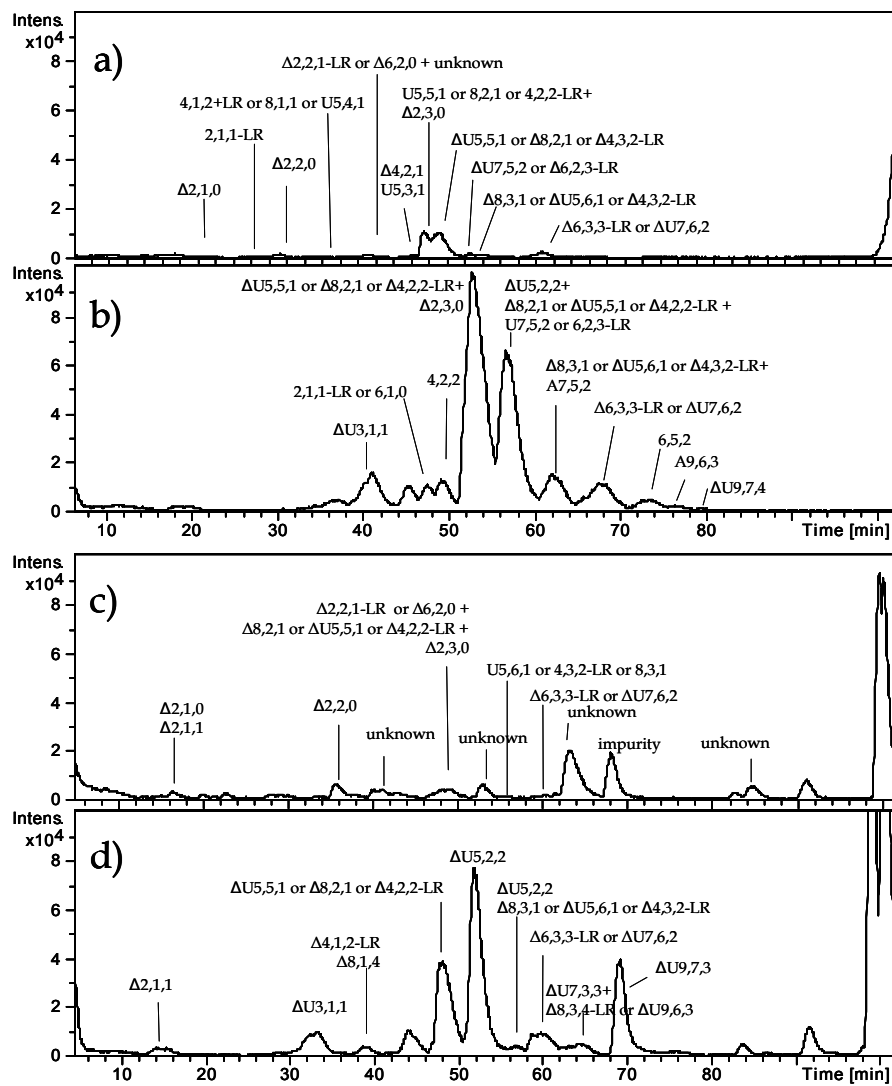


Figure II.10. HPLC profiles of heparinases digestion products from prepubescent HS. a) GRP2-A >10 kDa, b) GRP2-B <10 kDa, c) ART3-A >10 kDa, d) ART3-B <10 kDa. Oligosaccharides were identified by their mass/charge ratio (m/z) and labeled as follow. The unsaturated bond of the terminal uronic acid is indicated by Δ , and the number of monomers,

the number of sulfates and the number of acetyls are reported. For some m/z ratios, more than one oligosaccharide structure is possible. Oligosaccharides for which a not precise interpretation is available were labeled as 'unknown'. When an uronic acid (or a glucosamine) is present at both the RE and NRE it is indicated by U (or A). LR indicates the tetrasaccharide G-Gal₂Xyl of the linkage region.

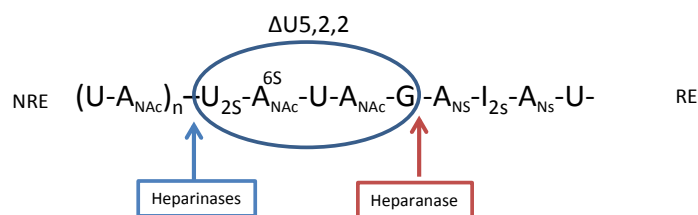


Figure II.11. Scheme of the odd oligosaccharide $\Delta U5,2,2$. Putative cleavage sites for Heparinases, between the glucosamine and the uronic acid, and Heparanase, between the uronic acid and the glucosamine, are indicated by the light-blue and red arrows, respectively.

Moreover, Mao *et al.* [90] discovered a novel peeling reaction that specifically degrades HS oligosaccharides, containing 3-O-sulfated glucosamine residue at the reducing-ends. Unintentional peeling reactions are reported to occur during chemical and/or enzymatic reactions, chromatography and sample storage, and are apparently catalyzed by mildly basic conditions. It has been established that exhaustive depolymerization of 3-O-sulfation containing HS/heparin by heparin lyases will generate lyase-resistant HS tetrasaccharides that have GlcNS3S6S at the reducing-ends. Thus, in the extracted mass spectra of the tetrasaccharide $\Delta U\text{-GlcNAc-GlcA-GlcNS,3S,6S}$ the authors observed the appearance of the ion at m/z 634.06, originated from a peeling reaction.

Accordingly, the presence of unsaturated odd oligosaccharides, e.g. $\Delta U3,1,1$ (m/z 634.09), could be originated both i) from a possible partial peeling reaction of longer digestion products with an even number of residues, and/or ii) from the action of heparin lyases on oligosaccharides endogenously generated by Heparanase.

For many m/z ratios more than one oligosaccharide structure can be assigned since the error between the theoretical and the calculated masses is less than 5 ppm for both the interpretations (limit of the instrument). The choice is often based on the retention time that is proportional mostly to the number of sulfate groups present in the molecule. Nevertheless, the possible interaction with DBA, used as counter-ion to allow a good chromatographic separation, causes shielding of the negative charges and a consequent modulation of the retention time. An example of the interpretation of data is reported in **Table II.3** where are reported the experimental data and the hypothesis of structures of two known oligosaccharides and of two oligosaccharides for whom more than one interpretation is possible.

Table II.3. Experimental data obtained by LC-UV-MS analysis and proposed neutral formula of some unknown compounds found in HS.

EXPERIMENTAL DATA							
m/z experimental [M-2H] ²⁻	546.077	575.962	1068.232		774.148		
Experimental isotope pattern (M)/(M+1)/(M+2)	100/40/27	100/15/17	100/81/65		100/65/44		
HYPOTHESIS of STRUCTURE							
Neutral molecular formula (tolerance <11 ppm)	C ₃₄ H ₄₈ N ₂ O ₃₄ S ₂	C ₁₂ H ₁₈ N ₁ O ₁₉ S ₃	C ₃₀ H ₇₆ N ₄ O ₄₇ S ₂	C ₇₃ H ₁₁₆ N ₄ O ₆₂ S ₃	C ₅₀ H ₇₆ N ₄ O ₄₇ S ₂	C ₄₈ H ₈₄ N ₄ O ₄₂ S ₅	C ₅₁ H ₇₆ N ₂ O ₄₈ S ₂
Structural connections between species	M + 2H	M + H	M + 2H+DBA		M + 2H	M + 2H+2DBA	M + 2H
Monoisotopic neutral mass (theoretical)	1092.152	575.964	2136.536	2136.520	1548.312	1548.316	1548.300
m/z theoretical [M-2H] ²⁻	546.077	575.964	1068.268	1068.261	774.156	774.158	774.150
Theoretical isotope pattern (M)/(M+1)/(M+2)	100/41/24	100/17/19	100/86/75	100/86/63	100/60/36	100/60/49	100/60/37

It is possible to observe a better matching between the theoretical and experimental isotope pattern for the two known oligosaccharides compared to the others. In **Figure II.12** are reported the mass spectra of the digestion products reported in **Table II.3**.

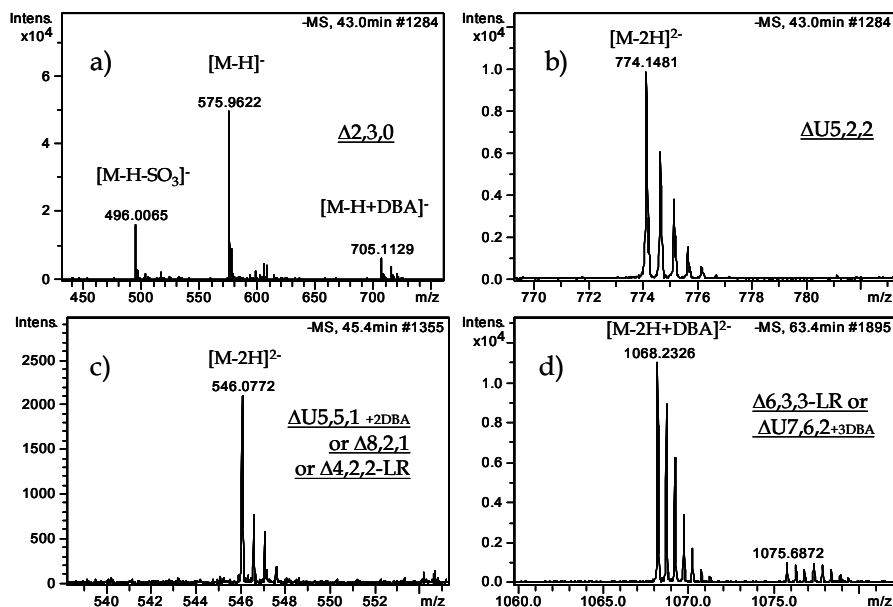


Figure II.12. Mass spectra of selected oligosaccharides observed by IPRP-HPLC/ESI-Q-TOF:) Δ U2,3,0; b) Δ U5,2,2; c) Δ U5,5,1 or Δ 8,2,1 or Δ 4,2,2-LR; d) Δ U7,6,2 or Δ 6,3,3-LR.

Isolation of selected peaks would be desirable to further investigate and possibly distinguish among alternative structures but it would require a much higher amount of material.

Many oligosaccharides bearing the linkage region have been found, like Δ 2,2,1-LR, Δ 4,2,2-LR and Δ 6,3,3-LR, in both the fractions of either ART or GRP HS. In fact, high levels of oligosaccharides bearing the LR should be found in the smaller fractions since shorter length of the starting HS chains is expected. There are no big differences in the global composition of HSs from ART or GRP prepubescent cartilage. Fractions A from ART HSs showed minor presence of digestion products than the corresponding GRP fractions. It is not easy to calculate a precise sulfation degree from HPLC-MS profiles because of the presence of both long and ambiguous oligosaccharides. Nevertheless, it can be estimated to be similar to that of canonic HS (0-1 sulfate/disaccharide), although a high presence of both

sulfated and acetylated glucosamines, typical for the NA/NS domain of HS, was observed.

Some oligosaccharides with unsubstituted amino groups have been detected, i.e. $\Delta 8,2,1$, in agreement with previous data reported in literature [29]. Unsubstituted amino groups [91] are supposed to play a role in L-selectin binding [92]. The presence of free amino groups is not an artifact of purification, since N-sulfate groups survive harsher conditions [93] than the mild conditions used for the present HS preparation. Toida *et al.* [91] found different HSs with unsubstituted 1 or 2 amino groups in each chain and suggested that the GlcNH₂ residue may reside in a transition sequence between high and low sulfation sequences.

II.2.3 Mass spectra interpretation and identification of oligosaccharides from fetal heparan sulfate

Products from fetal unfractionated HS were separated with a multistep gradient similar to the one used for the first prepubescent samples ART2 and GRP1. Profiles were very similar for F1, F3 and F4 with the predominance of the U_{5,2,2} oligosaccharide (which is supposed to be generated by endogenous heparanase action), while scarce fragments from HS were found in F2 (**Figure II.13**). As abovementioned in **Section II.2.1**, these samples were digested with keratanase in an attempt to degrade KS, therefore only oligosaccharides bearing remnants of the linkage region were detected, since the Gal-Xyl-Ser sequence has been split.

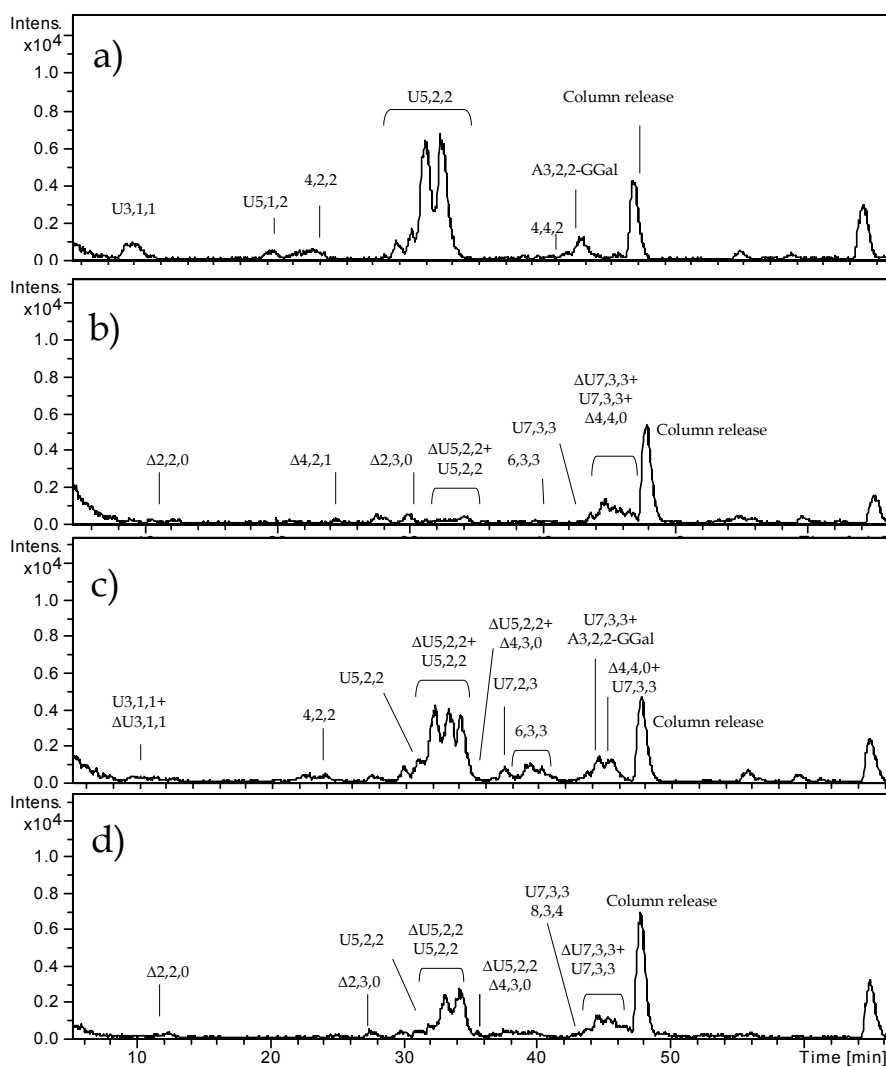


Figure II.13. HPLC-profiles of heparinases digestion products from unfractionated fetal HS. a) F1, b) F2, c) F3, d) F4. The unsaturated bond of the terminal uronic acid is indicated by Δ , and the number of monomers, the number of sulfates and the number of acetyls are reported.

The same elution gradient used for ART3/4 and GRP2/3 was adopted for the HPLC-MS analysis of the two fractionated samples F5 and F6 to permit a better separation of the poorly sulfated disaccharides eventually present, i.e. $\Delta 2,0,1$ and $\Delta 2,1,1$ or $\Delta 2,1,0$, which were in fact detected (**Figure II.14** and **Annex Figure A.II.10**). HPLC-MS profiles showed incomplete digestion of

HS and the presence of very long oligosaccharides up to hexadecasaccharides of ~5000 Da in the bigger fractions.

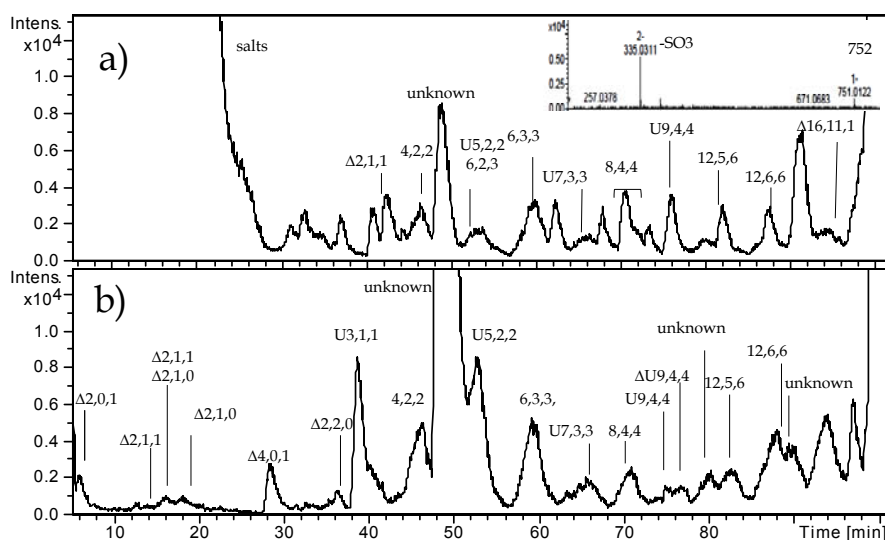


Figure II.14. HPLC profiles of heparinases digestion of fetal HS. The two fractions of sample F6, a) > 10kDa and b) < 10kDa, are reported. Oligosaccharides were identified by their mass/charge ratio and labeled as follow. The unsaturated bond of the terminal uronic acid is indicated by Δ , and the number of monomers, the number of sulfates and the number of acetyls are reported. In the upper right corner is reported the mass spectrum of the unknown peak eluted at 50 min.

The most abundant product in both fractions is an unknown oligosaccharide with mass 752 Da [M-H: 751] and eluted at ~50 minutes that does not correspond to any known HS or GAG structure. It is remarkable the presence of an extremely high number of saturated oligosaccharides deriving from the NRE of HS, especially in the bigger fractions F6-A and F5-A, but also in unfractionated samples, suggesting the existence of short original HS chains. Profiles of the other fractionated fetal HS (F5) are different and show the presence of more digestion products in fraction A than B.

II.3 Characterization of HS from pathologic cartilage

As explained in the introduction (**Section II.1.1**), degeneration to chondrosarcoma can occur both in the presence or absence of mutations in EXT gene; however, people with MO are more prone to the development of this type of tumor. Our data support this evidence, since 3 patients out of 4 showed presence of mutations in the EXT genes. NMR showed the presence of the PIPES buffer used in the first digestion steps with Proteinase K and DNase I, therefore a purification step by anion exchange chromatography onto a QAE-sephadex column was used. GAGs were eluted with 2.5M NaCl molarity while PIPES was eluted with 3M NaCl. In **Table II.4** information on patients, on the type of mutation present and the amount of isolated GAGs are indicated.

Table II.4. List of pathologic samples. Information on patients, type of mutation and amount of recovered GAGs are reported. Amount of starting wet cartilage: 150-200 mg. *MO4 and MO4a are two excisions from the same patient and area. ** Processing of MO6 is undergoing. § C2 and C4 come from different chondrosarcomas of the same patient.

<i>Sample</i>	<i>Type of mutation</i>	<i>Area of excision</i>	<i>Gender</i>	<i>Age</i>	<i>GAGs (mg) after QAE sephadex</i>	<i>GAGs (mg) After ChABC digestion</i>
MO1	EXT1 exon 7, splice site	right distal femur	F	15	7.2	1.5
MO2	EXT1 exon 2, missense	tibia	M	15	7.3	1.5
MO3	EXT2 exon 4, frameshift	femur	M	16	3.5	1.4
MO4	EXT2 exon 8, nonsense	right chest	M	5	4.5	1.2
MO4a*	EXT2 exon 8, nonsense	right chest	M	5	1.6	0.7
MO5	EXT1 exon 2, missense	left proximal fibula	M	11	2.9	0.7
MO6	EXT1 <i>in toto</i> deletion	right proximal homer	M	14	1.9	**
C1	none	right iliac wing	F	22	3.1	2.1
C2§	EXT1 exon 10, nonsense	acetabulum / pubis	F	36	5.5	1.2
C3	EXT2 exon 2, nonsense	right ileum	M	25	3.1	2.1
C4§	EXT1 exon 10, nonsense	pubis	F	36	5	0.8

II.3.1 NMR of GAGs from pathological cartilage

Since for pathologic samples shorter HS chains were possibly expected, GAGs were divided by ultrafiltration into three fractions: A >10 kDa, B <10 kDa and >3 kDa, C <3 kDa and >1 kDa. Each fraction was subjected to further digestion with ChABC and hyaluronate lyase, as reported in **Annex Figure A.II.11**. 1D-NMR profiles changed after enzymatic digestions but did not reveal any presence of HS, nor did the 2D-NMR analysis (not shown), which should be more informative. Due to the scarce amount of KS present in the sample MO2, it was possible to clearly distinguish signals of HS in the fraction B after repeated digestions with chondroitinase ABC. The 1D-NMR recorded before and after the digestion with heparinases (**Figure II.15**) showed that HS was relatively pure and contained little or no protein, non-HS GAGs or nucleic acid contaminants. Although no compositional information on HS can be obtained by 1D-NMR, a low amount of acetyl groups can be observed. Also, a spectrum of murine HS reported by Warda *et al.* [94] showed a similar profile, although with lower IdoA content. This spectrum of HS clearly demonstrated good level of iduronic acid content. This is an important observation complementary to HPLC-MS analysis of di-oligosaccharide components following heparin lyases digestion. Actually, such analysis cannot distinguish definitively between glucuronic and iduronic acid.

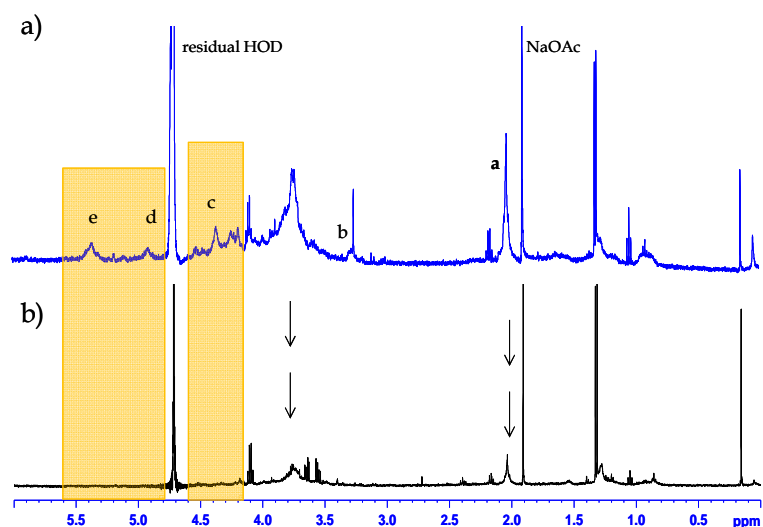


Figure II.15. 1D-NMR spectra of MO2-B (< 10kDa) before, a) and after, b) the digestion with heparinases. Signals of HS are indicated in the spectrum a). Signals correspond to a. N-acetyl (CH₃) GlcNAc (2.0 ppm); b. GlcNS, H-2 (3.2 ppm); c. GlcA, H-1 (4.4 ppm); d. IdoA, H-1 (4.9-5 ppm); and e. GlcN (Ac or S) H-1 (5.4 ppm). Arrows indicate the decrease of acetyl groups (a) and backbone signals (b-h).

II.3.2 Mass spectra interpretation and identification of oligosaccharides from pathological cartilage

Since no information was available in literature on the dimensions of HS from MO cartilage, also the fraction <3 kDa was analyzed for its content in HS. HPLC-MS analysis (not shown) showed absence of mass peaks attributable to HS either deriving from heparinases digestion or originally present in cartilage; therefore, no HS smaller than 3 kDa was detected by our procedure. Like what observed for prepubescent healthy samples, for many m/z ratios more than one oligosaccharide structure can be assigned since the error between the two calculated masses is less than 5 ppm (limit of the instrument).

For each of the first three samples processed (MO1, MO4 or C1), fractions A and B were first analyzed separately (**Annex Figure A.II.12** for MO1 and C1,

A.II.13 for MO4 and MO4*), then combined (A+B), digested a second time and analyzed again. Profiles are reported in **Figure II.16**.

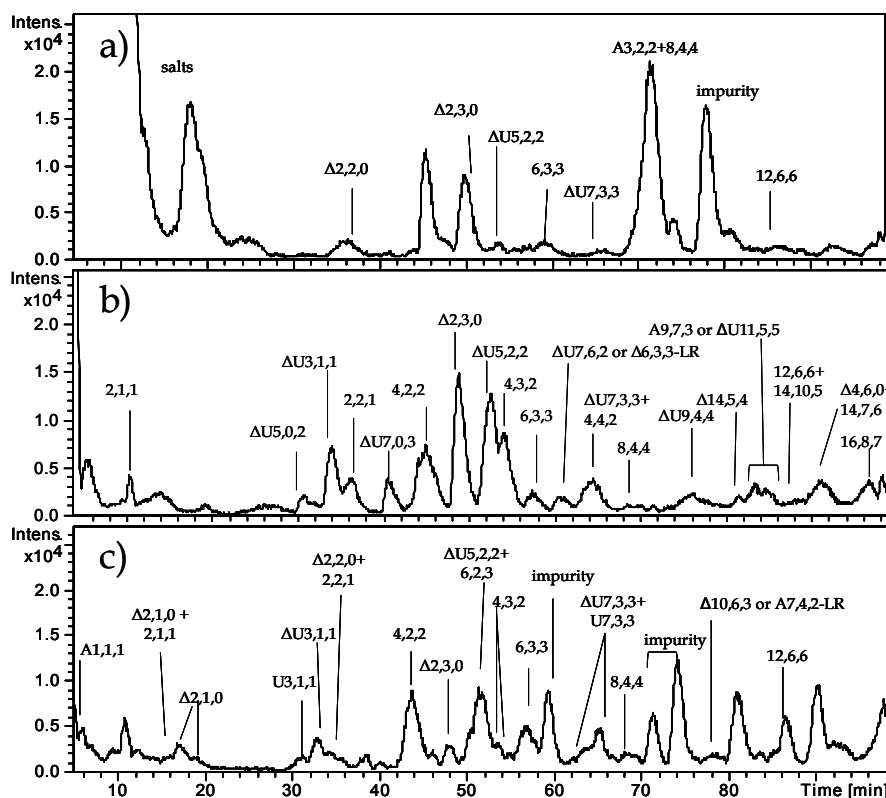


Figure II.16. HPLC profiles of heparinase digestion products of pathologic HS. Mixing of both fractions A and B from a) MO1, b) MO4, c) C1.

HS was detected in both fraction A and B of each pathological sample as shown in MO (**Figure II.17** and **Annex Figure A.II.14**) and C (**Figure II.18** and **Annex Figure A.II.15**).

Fraction B of HS from MO showed the presence of more digestion products than fraction A, like healthy HS. The most representative ones are $\Delta U5,2,2$ in MO3-B and MO2-A and also $\Delta 2,2,1$ which is the most abundant in both MO2-B and MO3-A.

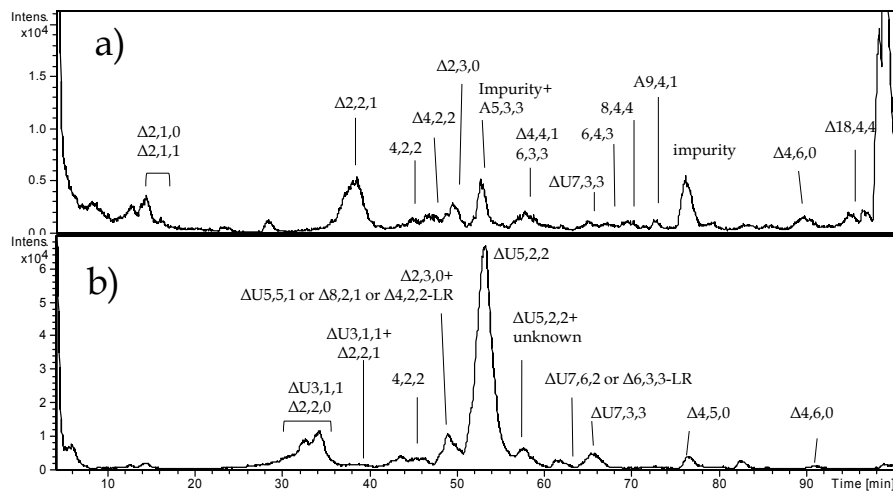


Figure II.17. Example of HPLC profiles of heparinase digestion products of MO HS. a) MO3 fraction A, b) MO3 fraction B.

Fractions A of cartilage from chondrosarcomas showed the presence of more digestion products than the corresponding B fractions; particularly, the most represented species is the trisulfated disaccharide. Therefore, HS from C2 and C3 showed a higher degree of sulfation with respect to HS from exostoses and healthy cartilage HS. In addition, mass peaks identified as fragments bearing a remnant structure of 135Da and indicated by the letter R, i.e. $\Delta 2,3,0\text{-R}$, were identified in C2, C3, C4, but also in MO4* and MO5. The presence of such structures is unusual and was detected in our laboratory only in heparin preparations subjected to chemical treatment that caused opening of the reducing residue leaving a remnant structure. Since no harsh treatments were used during the preparation of these samples, it is probable that either they spontaneously generate during processing because of an internal instability of the starting molecule or they are present in the tissue as longer fragments that are then cut by heparin lyases.

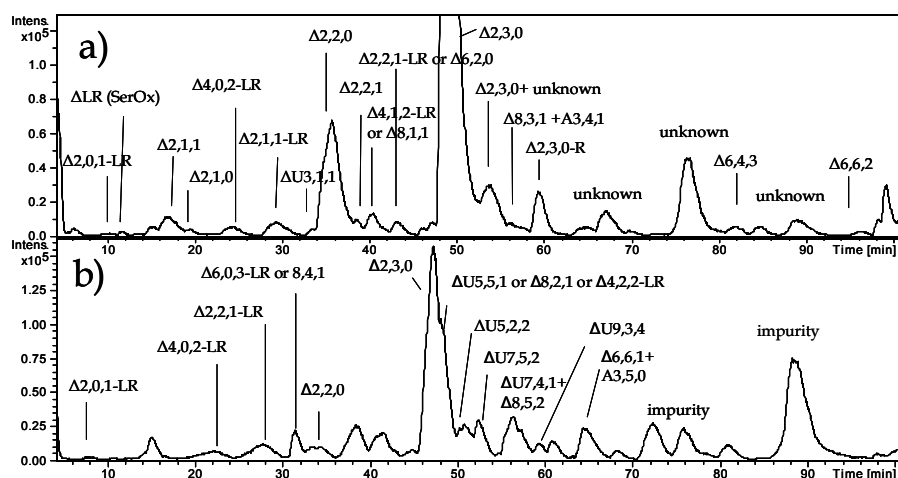


Figure II.18. Example of HPLC profiles of heparinase digestion products from C HS. a) C2-A (>10kDa); (b) the spectrum of C2-B (<10 kDa) in which the trisulfated disaccharide ($\Delta 2,3,0$) reaches an intensity of 3.5×10^5 , has been cut to permit a better visualization of all the other peaks. Fragments bearing the linkage region and the oxidized serine residue of the proteoglycan are indicated by LR(SerOx).

Moreover, unknown oligosaccharides with m/z values very similar to known structures but differing for two protons have been detected, as shown in **Figure II.19**. The isotope pattern and retention time are different and permit to distinguish the two structures although no clear understanding of the mode of generation of the unknown compound is available.

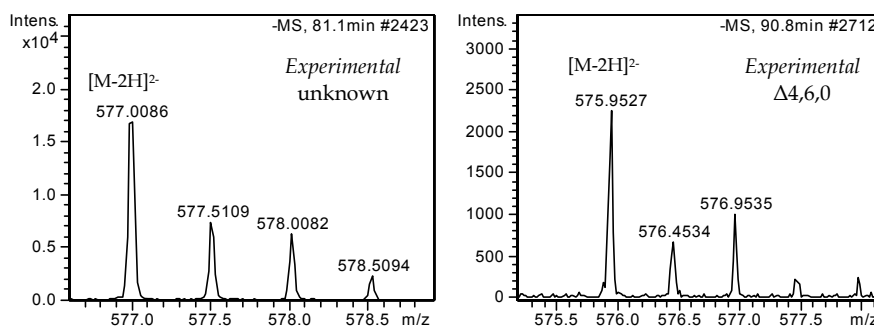


Figure II.19. Isotope pattern of selected compounds with similar m/z observed by IPRP-HPLC/ESI-Q-TOF. On the left is reported the unknown mass eluted at 80-81 min and probably corresponding to $\Delta 4,6,0+2H$, while on the right is reported the $\Delta 4,6,0$ from MO3-A.

One sample from a patient with in toto deletion of EXT1 (MO6) was subjected to cellulose acetate electrophoresis in order to detect the presence of GAGs and HS with an alternative analytical method. By comparison with a mixture of defined GAGs, namely HA, HEP, CS, it was possible to detect the presence of CS and a small amount of probably high molecular weight HA or fragments of proteoglycans which did not migrate in two fractions eluted from QAE sephadex (A, flow through and B eluted with 2M NaCl, see **Annex Figure A.II.16**). In the case of HS, the amount of material was too low to be detected.

II.4 Overview of similarities and differences between healthy and pathologic heparan sulfate

The project is focused on the structural characterization of HS from pathologic excisions, in order to determine if compositional changes in HS occur or a reduced amount of HS, i.e. reduced chain length, is present in comparison to healthy cartilage. The main features pointed out by this study are as follows:

- 1) High degree of sulfation of HS from chondrosarcomas bearing mutations in the EXT genes compared to both healthy and MO HS: the principal component of HS from chondrosarcoma is $\Delta 2,3,0$
- 2) Different structural features between HS chains higher and lower than 10 kDa in all samples
- 3) No great differences in the composition between healthy and MO HS
- 4) Presence of many oligosaccharides with an odd number of residues, indicating a high level of endogenous hydrolysis and/or the presence of original short HS chains

II.5 Discussion and future perspectives

Even if the role of HS chains in cartilaginous growth is well known, their structural alteration in several developmental diseases, as well as functional

consequences, are frequently unclear, often leading to the absence of effective therapies. To tackle this issue, an approach was used which will have the effect of improving molecular and biochemical knowledge of MO pathogenesis and which could be extended to other cartilaginous diseases currently unexplained at molecular level. A complete and refined genetic and biochemical characterization of the HS from cartilage will permit to reach a better knowledge about the human cartilage biology, unravelling the structure of the key players involved in endochondral development.

Many papers demonstrated that there is no unique HS but many HSs with different degrees of sulfation depending on the tissue of extraction.

In agreement, our results showed the presence of high variability among healthy samples. Although comparison between articular and growth plate HS is not essential to the aim of the project, nevertheless the method adopted allowed us to detect differences between the two types of cartilage. It is also possible that not only modulation of growth plate but also of articular HS takes place in young subjects which undergo continuous changes during development. Instead, adult articular cartilage in healthy conditions -not exposed to arthritis or related pathologies- could show less variability in composition, since the endochondral development has reached a stop but, more samples should be investigated to verify this hypothesis. It must be underlined that several factors can contribute to the observed variability:

- 1) Samples are considered healthy for the pathology under examination; nevertheless, other alterations that indirectly could have influenced cartilage cannot completely be excluded
- 2) The area of excision is of great importance. The strict organization of cartilage (**Figure II.3**) depends on a gradient of growth factors which is highly regulated by HSPGs and is specific for the different zones. Hence, excisions of different depth and/or breadth could contain different amounts of HSPGs.

Taking into account these considerations, the real comparison will be between healthy growth plates, of which fetal cartilage is the eligible example, and pathologic cartilage from exostoses and/or chondrosarcomas. In most of the samples, HS degradation did not go to completion possibly due to other GAG species that limited the action of Heparin lyases by aggregation phenomena and to differences in the canonic sequences recognized by the enzymes or both.

As support of what above-written regarding the importance of the excision in the final results, HPLC-MS profiles of HS from two excisions of the same area of cartilage are reported in **Annex Figure II.13** and showed different oligosaccharide composition, although with prevalence of shorter chains (fraction B) in both of them.

A second consideration is that HS is present in both MO and chondrosarcoma samples bearing mutations in the EXT genes. The machinery of the biosynthesis of HS comprises not only the glycosyltransferases encoded by EXT1 and EXT2 but also EXTL genes, which can provide for a small amount of HS sufficient to carry on bone growth but not enough to do it in the proper way.

Moreover, differences can be found in samples C2 and C3 from patients with mutations in the EXT genes and C1 from a patient with no mutations. Particularly, HSs from C2 and C3 showed to be richer in the trisulfated disaccharide than C1, especially in the bigger fractions A, whereas a more homogeneous composition with a mixture of both sulfated and acetylated oligosaccharides was observed in C1. More samples from patients affected by chondrosarcoma not bearing the above-mentioned mutations are necessary to draw a conclusion.

The procedure adopted for the isolation and purification of HS has been refined during the course of the project and enriched in repeated purification steps in an attempt to increase the sensitivity of the final HPLC-

MS stage of analysis. For example, in **Annex Figure A.II.13** it is clearly observable a better detection (higher intensities of peaks) of the digestion products in the sample MO4* as result of an improvement in the purification procedure.

With the aim of deepening the investigation for the remaining amount of GRP2 and ART3 digestion products, A and B fractions were mixed together and prepared for further NMR analysis. In **Annex Figure A.II.17** the monodimensional analysis showing the presence of signals typical of the 4,5-unsaturation introduced by heparin lyases and of anomeric protons is reported. The 2D-NMR spectrum (not shown) was of no use in the understanding of the mixture's structure because of the high presence of salts which covered signals from the oligosaccharides. A purification step is ongoing and will possibly allow the acquisition of a 2D-NMR spectrum to gain more information.

In the near future, derivatization with a fluorophore could be an interesting mean to increase the sensitivity and obtain a quantification of the digestion products. An example of procedure could be reducing end-labeling with the fluorophore BODIPY hydrazide, separation by HPLC, and subsequent fluorescence detection and quantitation [95]. This is a high-sensitivity method that requires nanograms of starting material and is thus the most sensitive method for disaccharide compositional analysis of HS yet reported. Finally, this work pointed out the need of an extremely precise selection of excision areas from cartilage to permit both the definition of the average level of HS within the tissue and/or the understanding of the modulation of HS levels in the different areas of cartilage.

II.6 Experimental section

Fetal growth plate cartilage samples were obtained from courtesy of Dr. Salvatore Romeo and Dr. Angelo Paolo Dei Tos, Pathology Dept. of Treviso Hospital. Healthy and pathologic cartilage samples were provided by the Department of Pathology of Rizzoli Orthopaedic Institute where determination of mutations was also carried out as follows. DNA was extracted from a small part of the tissue by mean of digestion with proteinase K and separation of the genomic DNA onto silica membrane mini spin column (DNeasy Blood & Tissue kit, Qiagen); subsequent pre-screening analysis was performed by denaturing high-performance liquid chromatography (dHPLC, WAVE System Model 3500HT, Transgenomic) followed by Sanger sequencing (ABI PRISM 3100, Applied Biosystems). Samples were snap-frozen and immediately stored in liquid nitrogen after excision. Ethical approval has been obtained for every sample collection and subsequent analysis.

II.6.1 Isolation of GAGs

A published workup procedure was used for the extraction of GAGs from human cartilage [85]. Briefly, GAGs were isolated after digestion with Proteinase K in PIPES buffer and nuclease treatment followed by 3 kDa ultrafiltration for healthy samples or 0.5-1 kDa dialysis for pathologic samples to remove digestion fragments.

II.6.2 Purification of samples by enzymatic digestions

To degrade GAG components excluding HS, freeze-dried GAG mixtures were dissolved in the specific buffer required and after the digestion were loaded onto Amicon ULTRA centrifugal filter units (MWCO 3.0 kDa) to reduce the salt concentration and allow NMR analysis.

Digestion of chondroitin sulfates by chondroitinase ABC (Sigma Aldrich, USA) was carried out in 50 mM phosphate buffer and 50 mM sodium acetate

(1:1 v/v), pH 8 at 37°C for 48 h under continuous dialysis with SpectraPor Float A Lyzer, MWCO 500-1000 Da (Spectrum Medical Industries, Inc., Rancho Dominguez, CA, USA) against 50 mM phosphate buffer and 50 mM sodium acetate (1:1 v/v). Each sample was further treated with hyaluronate lyase (Sigma Aldrich) in 50 mM sodium acetate and 10 mM calcium chloride, pH 6 at 37°C for 48 h and ultrafiltered as described above. keratanase and endo- β -N-acetyl-glucosaminidase digestions were performed in sodium acetate pH 4.6 at 37°C for 48h. Finally, following all degradative enzymatic treatments, samples were fractionated by Amicon ULTRA centrifugal filter units (MWCO 10 kDa) into two fractions: over 10 kDa (A) and between 3-10 kDa (B).

II.6.3 NMR characterization

The samples were dissolved in 1 ml of D₂O, then freeze dried twice. 200 μ l or 600 μ l of D₂O were added to each lyophilized sample and spectra were recorded at 25°C on a Bruker Avance 500 MHz or on a Bruker Avance 600 MHz spectrometer (Karlsruhe, Germany). Both instruments were equipped with 5-mm TCI cryoprobe.

¹H monodimensional NMR spectra were acquired with 128 scans. Water presaturation was applied during each 12 s of relaxation delay.

HSQC spectra were obtained in phase-sensitive, sensitivity pure-absorption mode with decoupling in the acquisition period (Bruker pulse program hsqcetgpsisp.2). Integration of peak volumes in the HSQC spectra was made using standard Bruker TOPSPIN 3.0 software.

II.6.4 HPLC-MS analysis of the digestion products of HS

Enzymatic cleavage of HS

GAG mixtures from cartilage samples underwent a double enzymatic treatment with a mixture of heparin lyases I-II-III (Grampian Enzymes, UK, 2 mU each for 0.1 mg of starting material), in 100 mM sodium acetate buffer,

pH 7, and 10 mM calcium acetate. The reaction was stirred at 37°C (Termo shaker TS-100 Biosan) for 48 h, then stopped by boiling for 10 minutes followed by 0.2 µm filtration (LabService Analytica).

Samples ART2 and GRP1 were divided in two halves and digested either with a cocktail of heparinases or with the single enzymes (2mU for 0.1 mg of starting material).

Isolation of digestion products

Digested samples were loaded onto 3 MWCO Amicon Ultra Centrifugal Devices (Millipore, USA) and recovered after 15 runs of centrifugation at 5000 rpm for 40 minutes (NuveNF200, Turkey). Permeates were freeze-dried, then dissolved in 200 µl of water and loaded onto a G10 desalting column (h 25 cm, Ø 1.2 cm) equilibrated in water and 10% EtOH (Girelli, Italy) previously filtered and degassed. Digestion products were eluted at a flux speed of 0.7 ml/min and fractions of 30s were collected and read at 210-232 nm (Cary50UV, Varian) (see **Annex Figure II.18**). Recovered fractions containing the digestion products were freeze-dried and the desalting step was repeated to allow a better separation between salt and oligosaccharides.

IPRP-HPLC/ESI-TOF-MS analysis

LC-MS analysis was performed on a LC system (Dionex Ultimate 3000, Dionex) equipped with degasing system (model LPG-3400), pump (model LPG-3400A), autosampler (model WPS-3000TSL) and UV-detector (model VWD-3100) and coupled with an ESI-QTOF mass-spectrometer (microQTOF, Bruker Daltonics).

The chromatographic separation was performed using a Kinetex C18 analytical column (100 × 2.1 mm I.D., 2.6 µm particle size, Phenomenex) with Security Guard Cartridges Gemini C18 (4 × 2.0 mm, Phenomenex). A binary solvent system was used for gradient elution.

Solvent A (10 mM DBA, 10 mM CH₃COOH in water or water/methanol 90:10) and solvent B (10 mM DBA and 10 mM CH₃COOH in methanol) were

delivered at 0.1 ml/min. Oligosaccharides were separated using a multi-step gradient that slightly changed, as reported in the table below, to adjust the conditions and this explain the changes in the elution time of oligosaccharides. The solvent composition was held for the last 19 min for equilibrating the chromatographic column before the injection of the next sample.

Sample	Solvent A	Solvent B	Gradient (%B)		Injection (µl)
			t	%B	
ART2 GRP1	H ₂ O/MeOH 90:10	100% MeOH	t=0 t= 30 t=50 t=65 t=76	17 42 50 90 17	10 of 110
ART1, ART3, ART4 GRP2, GRP3 F5, F6 MO and C (all)	100% H ₂ O	100% MeOH	t=0 t= 40 t=85 t=88 t=95	10 35 50 90 10	10 of 110 (ART1) 30 of 100 (all the others)
Unfractionated fetal	H ₂ O/MeOH 90:10	100% MeOH	t=0 t= 60 t=65 t=75	10 40 90 10	30 of 100

The MS spectrometric conditions were as follows: ESI in negative ion mode, drying gas temperature +180°C, drying gas flow-rate 7.0 l/min, nebulizer pressure 0.9 bar; and capillary voltage +3.2 kV. The mass spectra of the oligosaccharides were acquired in a scan mode (*m/z* scan range 200 – 2000). Calibration of the mass spectrometer was obtained by using an ES tuning mix solution acetonitrile solution (Agilent Technologies, Santa Clara, CA) according to a standard procedure. Data were processed by the DataAnalysis software (HyStar Compass, version 3.0, Bruker Daltonics).

CHAPTER III: GLYCOSAMINOGLYCANS IN CYSTIC FIBROSIS

III.1 Introduction

III.1.1 Cystic Fibrosis

Cystic fibrosis (CF) is an autosomal recessive disease occurring in approximately 1 in 3,000 live births in Europe and the USA, and results from mutations in the gene encoding for the CF transmembrane conductance regulator (CFTR) [96] which functions as a channel that regulates the transport of ions and the movement of water across the epithelial barrier. The failure of chloride secretion through CFTR leads to dehydration of endobronchial secretions and prevents mucociliary clearance. Consequently, many CF patients suffer continual bacterial infection, usually caused by *Staphylococcus aureus* or *Pseudomonas aeruginosa*, resulting in chronic inflammation, which is responsible for the characteristic progressive pulmonary disease and the major determinant of life span and quality of life in affected individuals.

Bacterial infection in lungs affected by CF, that are characterized by defective regulation of the inflammatory response [97], results in a vicious circle of events in which the host-mediated response plays a pivotal role in the subsequent chronic airway inflammation. The release of bacterial products influences epithelial cells, modulating the production of pro-inflammatory cytokines such as interleukin-1 (IL-1), tissue necrosis factor-alpha (TNF- α), interleukin-8 (IL-8) and granulocyte/macrophage-colony stimulating factor (GM-CSF), that stimulates the local recruitment of macrophages and neutrophils (**Figure III.1**). Specifically, IL-8 contributes to neutrophil transendothelial migration into CF airways and its expression is prolonged following bacterial, e.g., *P. aeruginosa*, stimulation [98] resulting in excessive neutrophil recruitment, further triggering the release of pro-inflammatory mediators and chemoattractants [99].

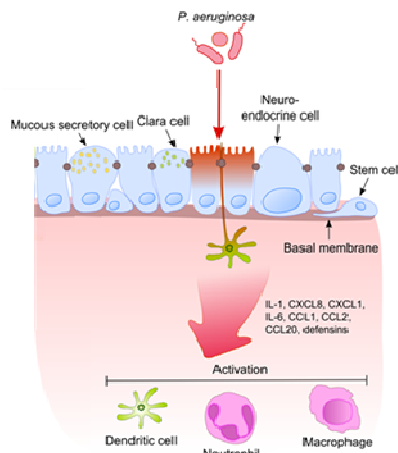


Figure III.1 Bacterial infection. Once pathogenic bacteria (e.g., *P. aeruginosa*) have activated particular pattern recognition receptors on/in epithelial cells, the pro-inflammatory signaling pathways are activated. This results mainly in IL-1, IL-6 and IL-8 production. These cytokines induce chemotaxis to the site of infection in its target cells (e.g., neutrophils, dendritic cells and macrophages).

Neutrophils are primed, activated and engaged in bacterial phagocytosis releasing large amounts of oxidants and proteases, including matrix metalloprotease-9 and neutrophil elastase (NE) [100]. Among the released proteases, NE has the greatest potential to cause undesired tissue injury by escaping from cells and degrading structural proteins such as elastin and fibronectin and interfering with the innate airway immunity by impairing opsonophagocytosis [101]. Marcos *et al.* [102] showed that interleukin-8 (CXCL8), and perhaps other CXC chemokines, can bind the receptor CXCR2 on neutrophils, leading to the formation of networks (NETs) composed of a chromatin backbone with antimicrobial agents such as histones, NE and myeloperoxidase in a cystic fibrosis mouse model and in individuals with cystic fibrosis (**Figure III.2**). The inefficient clearance of NETs results in even more viscous mucus that worsens the airflow in cystic fibrosis and can impair lung function.

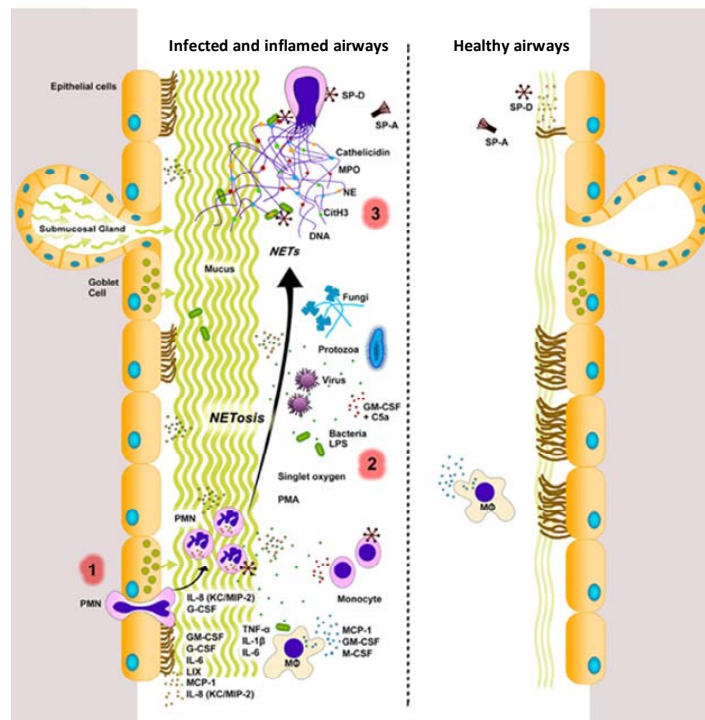


Figure III.2. Illustration of NETs in infected and inflamed airways. Lungs respond to sterile injury or infection by secreting various signaling molecules. During infection and inflammation, various cells express inflammatory cytokines, chemokines, and growth factors to recruit monocytes and neutrophils (e.g., IL-8) into the airway lumen. Neutrophils can be stimulated by a variety of agents to undergo NETosis. A balance between NETosis and NET clearance is essential for effectively clearing infectious agents with minimal damage to the lungs. Dysregulation in these two processes can lead to lung injury and exacerbation of lung diseases. Inflamed airways also have excess mucus. The putative sequence of NETotic events in the lungs are numbered as 1, 2, and 3. Taken from [103]

When the protease burden overwhelms existing anti-protease defenses, injury to the respiratory tissue, i.e., bronchiectasis, occurs, resulting in further weakening of the airway structure. Moreover, apoptotic inflammatory cells accumulate in the airways of young adults with CF, in part through ineffective removal, suggesting that failed phagocytosis may contribute to persistent airway inflammation [104].

Despite identification of the genetic basis of the disease and attempts to realize a gene-based therapy or develop drugs that can correct the defect of the CFTR channel (e.g., Kalydeco or Ivacaftor), anti-inflammatory therapy in CF has assumed an important role over time and more effective anti-inflammatory molecules are necessary. Since inflammation is a key contributor to the pathogenesis of CF lung disease, many studies are focused on finding effective routes by which the respiratory symptoms can be treated, in order to increase the quality of life and the lifespan of patients.

III.1.2 Linkage between CF and GAGs

In the lungs, GAGs are distributed in the interstitium, in the subepithelial tissue and bronchial walls, and in airway secretions (**Figure III.3**). GAGs have important functions in lung ECM: they regulate hydration and water homeostasis; they maintain structure and function, modulate the inflammatory response and influence tissue repair and remodeling.

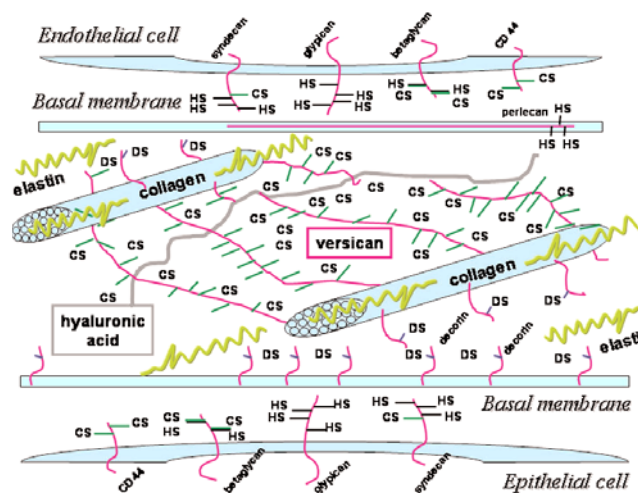


Figure III.3. Extracellular matrix components in lung parenchyma. CS, chondroitin sulfate; DS, dermatan sulfate; HS, heparan sulfate. Taken from [6].

The lung is a rich source of mast cells, which may be the unique cellular source of heparin [105]. Mast cell heparin resides in secretory granules, where most of the GAG chains are linked to a core protein (serglycin), forming macromolecular proteoglycans. Very little heparin is incorporated into cell surface proteoglycans of epithelial and endothelial cells; these are more likely to contain heparan sulfate. Stimulated mast cells secrete heparin along with granule-associated mediators. Other GAGs present in the lungs are HA, CS, HS and DS, while KS is found in airway secretion.

Many studies have demonstrated the importance of HSPGs in pathogen and viral infection and the modulation of inflammatory response by heparan sulfate mimetics [106]. GAG-pathogen interactions affect most, if not all, the key steps of microbial pathogenesis, including host cell attachment and invasion, cell-cell transmission, systemic dissemination and infection of secondary organs, and evasion of host defense mechanisms [107]. Several bacterial pathogens have been shown to induce the release of dermatan sulfate (DS) from the ECM [108] or HS from the cell surface and exploit the ability of solubilized GAGs to counteract cationic antimicrobial factors or neutrophil-mediated host defense mechanisms [109][110]. These data suggest that GAG-pathogen interactions and the ability of pathogens to subvert GAG functions are important virulence mechanisms for a wide variety of microbes [111]. It was also demonstrated that increasing levels of IL-1 beta induce the release of proteoglycans; therefore, modulation of GAGs in infected tissues could be a potential biomarker of inflammation [112] and the idea of interfering with chemokine-GAG binding as an effective strategy for targeting inflammation is supported by several studies [113].

III.1.3 Heparin as an anti-inflammatory drug

Heparin is used widely in the clinic as an antithrombotic agent and is generally well tolerated. It interacts with and inhibits the activity of many regulatory proteins including IL-8 and elastase and it has been shown

capable of modulating growth factor receptor binding and activity [37] **Errore. L'origine riferimento non è stata trovata.**[114] inhibiting the enzyme heparanase [115][116] and reducing selectin-mediated interactions [116][117]. It has been suggested that heparin may have the potential to relieve symptoms in lung conditions, ranging from the excess of NE in CF airways to asthma [118] or even respiratory distress syndrome. Nevertheless, although several studies reported that doses of heparin comparable to those used in antithrombotic protocols did not cause bleeding [119], the effective dose of heparin (or low molecular weight heparin) required to achieve prolonged anti-inflammatory effects could result in anticoagulant complications. Several heparin derivatives have been studied and characterized [120][121][122] and have been shown to exhibit strongly reduced anticoagulation activities, while maintaining the ability to interact with other proteins [123]. Some of their activities, such as angiogenesis inhibition [124], anti-metastatic activity and antagonism of P-selectins [125], have been reported.

Although the precise mechanism of action of heparin in these studies has not been established, it has been proposed that inhibition of the interaction between pro-inflammatory cytokines and membrane-associated GAGs may provide a mechanism for inducing clinically useful immunosuppression [113]. Similarly, it could be postulated that heparin could interfere with the chemokine-GAG interaction.

The chemical modification of heparin, which usually results in a net reduction of the overall charge density and also tends to reduce structural complexity, provides the means by which biochemical processes can be influenced, while attenuating undesired activities. Heparin and its derivatives are often used as experimental proxies because they are more readily available than the naturally occurring GAG heparan sulfate, known to interact with hundreds of proteins, many of them involved in regulation of the extracellular matrix [37].

III.1.4 Objectives of the work

Given the great diversity of GAG structures and the evidence that GAGs may have a protective effect against injury in various respiratory diseases, an understanding of changes in GAG expression that occur in disease may lead to opportunities to develop innovative and selective therapies in the future.

The project is focused on the understanding of the role of glycosaminoglycans in inflammation, particularly in CF. Two aspects are investigated:

- 1) the ability of heparin derivatives to attenuate inflammation by acting on key proteins, specifically neutrophil elastase, interleukin-8 and tumor necrosis factor-alpha
- 2) the possibility of GAGs to act as biomarkers of airway inflammation

The strategy adopted for the development of anti-inflammatory agents is aimed at simultaneously affecting two major points in the inflammation network: IL-8 and NE. Since IL-8 and elastase have been identified as being relevant to chronic inflammatory conditions, particularly lung disease in CF, several heparin derivatives were synthesized and tested for their ability to interfere with multiple effectors of inflammation.

To achieve the first goal of the study the following objectives have been defined:

3. *To create a small library of compounds with reduced sulfation degree*

For this purpose, different derivatives with a lower degree of sulfation than the starting material have been prepared by N-desulfation and N-acetylation and/or by periodate oxidation followed by borohydride reduction, and characterized.

4. *To verify the anti-coagulant and anti-inflammatory activity of the derivatives in vitro*

For this purpose, three anticoagulant tests were performed in different laboratories. Several *in vitro* assays were performed to assess the desired activities, among which were chromogenic assays and circular dichroism.

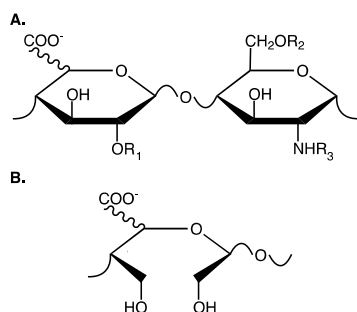
5. *To verify the anti-inflammatory activity of the derivatives in vivo*

In collaboration with Doctor Cigana and her group in San Raffaele Scientific Institute the anti-inflammatory activity of heparin derivatives was investigated *in vivo*. For this purpose, two derivatives were tested in *P. aeruginosa* infected mice and markers of the inflammation were measured after sacrifice.

To achieve the second goal of the study, a chronic model of *P. aeruginosa* infection was used and GAGs were isolated from lung homogenates and characterized by cellulose acetate electrophoresis and enzymatic digestion followed by HPLC-MS analysis.

III.2 Preparation of heparin derivatives as possible anti-inflammatory agents

Two series of heparin derivatives were generated based on a porcine mucosal heparin (PMH, compound **1**) scaffold; series **A** (**1a-1c**) and **B** (**2** and **2a-2d**). Both sets of compounds contained varying amounts of N-acetylation. In series **B**, the non-sulfated uronate residues containing 2,3 vic-diols underwent periodate oxidation, forming a glycol-split uronic acid residue [124]. Furthermore, prior to N-acetylation of compound **2b** the sample was partially 2-O-desulfated, thereby providing a derivative with a higher percentage of glycol-split uronic acids. **Scheme III.1** contains the major repeating disaccharide unit of heparin and the structure of the glycol-split uronic acid.



Scheme III.1. The repeating disaccharide unit of heparin (R_1 and $R_2 = \text{H}/\text{SO}_3^-$, $R_3 = \text{H}/\text{SO}_3^-/\text{COCH}_3$), in the compounds comprising series **A** and **B**. The main disaccharide of compound **1** is characterized by R_1 , R_2 and $R_3 = \text{SO}_3^-$. The uronic acid in PMH is predominantly in the form L-iduronic acid (L-IdoA and L-IdoA-2-O-sulfate; ~ 80%) with D-glucuronic acid (D-GlcA; ~ 20%) making up the remainder. **B.** The glycol-split uronic acid residue present in the series **B** compounds.

III.2.1 Structural characterization of compounds

The compounds in series **A** and **B** are listed in **Table III.1**. It should be noted that, as the degree of N-acetylation increases, the overall level of sulfation

decreases, as expected. The degree of N-acetylation and periodate oxidation in the heparin compounds was quantified by ^{13}C NMR (see **Annex Figure A.III.1**), while SEC-TDA was used to determine the weight average molecular weight of the compounds (see **Annex, Figure A.III.2** for an example) [126].

Table III.1. Structural characteristics of the compounds originating from heparin (series A; **1-1c**) and glycol-split heparin (series B; **2-2d**) derivatives. The table contains the materials weight average molecular weight (Mw), percentage of N-acetyl substitution in glucosamine residues and percentage of glycol-split uronate residues. Compound **1** is unmodified PMH, used as reference for series A, while compound **2** is glycol-split heparin, used as reference for series B.

Series	Compound	M _w (kDa)	% N-acetyl	% Glycol-split
	1 (PMH)	20.0	15	0
A	1a	21.0	45	0
	1b	22.0	64	0
	1c	17.0	100	0
	2	16.5	15	20
B	2a	17.0	27	27
	2b	13.0	49	35
	2c	15.0	64	25
	2d	16.0	100	25

Size can be an influential parameter on the binding of polysaccharides to proteins, especially the minimum length that is required to establish an interaction. The molecular weight of the test compounds ranged from 13 to 22 kDa, assuring an interaction with both IL-8 and human leukocyte elastase (HLE).

III.2.2 Inhibition of Elastase activity

Two inhibition assays were used to test the inhibition activity of heparin derivatives; the first is based on the release of *p*-nitroaniline from a small chromogenic substrate (500Da) following the cleavage by human leukocyte

elastase, while the other measured the inhibition of digestion of soluble α -elastin (10-60 kDa).

All heparin derivatives proved able to inhibit digestion of the synthetic peptide, similar to standard heparin (compound **1**), at concentrations above 20 nM, while little differences were observed at lower concentrations, probably due to different modes of interaction (**Figure III.4**). The inhibitory effect of **1a-1c** increased with the degree of N-acetylation using the peptide substrate, but no significant differences were found when α -elastin was used. The glycol-split modification had no effect on the inhibitory capacity of compounds in either of the assays.

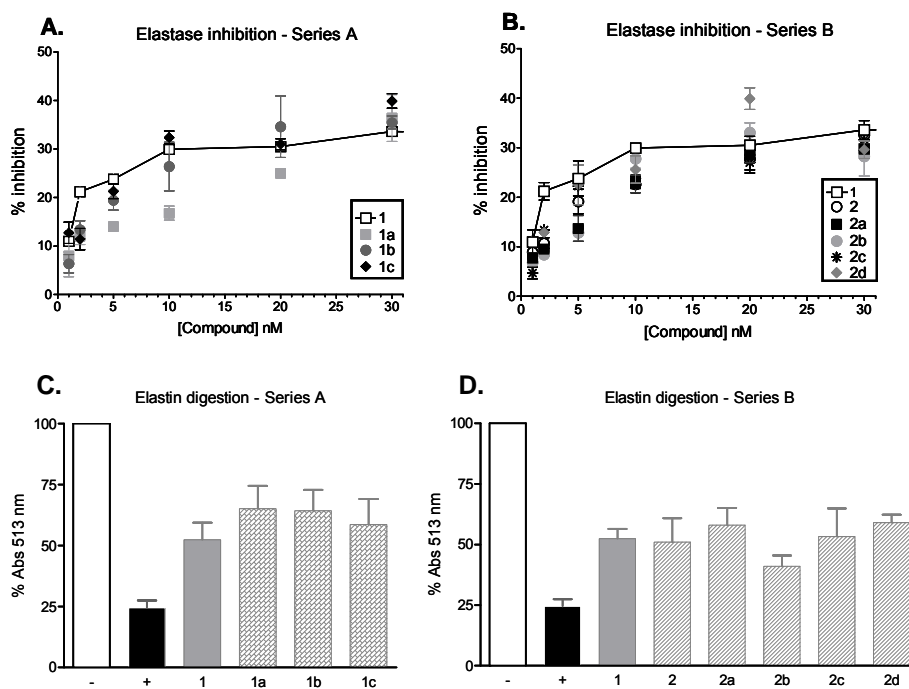


Figure III.4. Inhibition of human leukocyte elastase by heparin derivatives. In **A** and **B**: inhibition of elastase measured by decrease in absorbance at 405 nm and reported as % of inhibition. In **C** and **D**: the increase in absorbance at 513 nm reports the inhibition of digestion of the natural substrate (α -elastin); the negative control is the level of digestion in the presence of inactive enzyme, while the positive control is the digestion in the absence of inhibitors.

Results shown are averages of 3 independent experiments, each with 2 replicates, \pm standard errors. Error bars on the negative controls are negligible.

Derivatives were tested at higher concentrations and an increase of HLE inhibition up to 40% was observed (up to 200 nM, see **Annex Figure A.III.3** for an example). However, neither a 3–4 fold increase in the concentration of heparin nor any of the derivatives proved able to inhibit the enzyme completely.

III.2.3 Interaction with IL8

The ability of the heparin derivatives to interact with IL-8, a key modulator of inflammation, was also tested by two independent methods. The first measured their ability to displace IL-8 in solution from surface-bound heparin using a competitive ELISA (**Figure III.5** and **Annex Figure A.III.4**). All of the heparin derivatives were able to compete with heparin for IL-8 binding and were, therefore, able to displace it. Several derivatives turned out to be more active than the reference heparin (**1**), which was able to displace less than 50%, before reaching a plateau. In series **A**, **1a** (45% NAc) promoted a more effective displacement; up to almost 90% and in a different manner to both **1** and **1b** (64% NAc) or **1c** (100% NAc), suggesting distinct modes of interaction. The differences between **1b** and **1c**, **2** and **2b** were not statistically significant. The glycol-split modification of heparin (**2**) did not improve its ability to compete with the standard heparin bound to the plate, although a concentration-dependent effect was detected, distinct from that observed for unmodified heparin. Compound **2b** (49% NAc, 35% gs) was less efficient than the N-acetylated counterpart in detaching IL-8, perhaps because of the smaller molecular weight, in contrast to compounds **2c** (64% NAc gs) and **2d** (100% NAc gs).

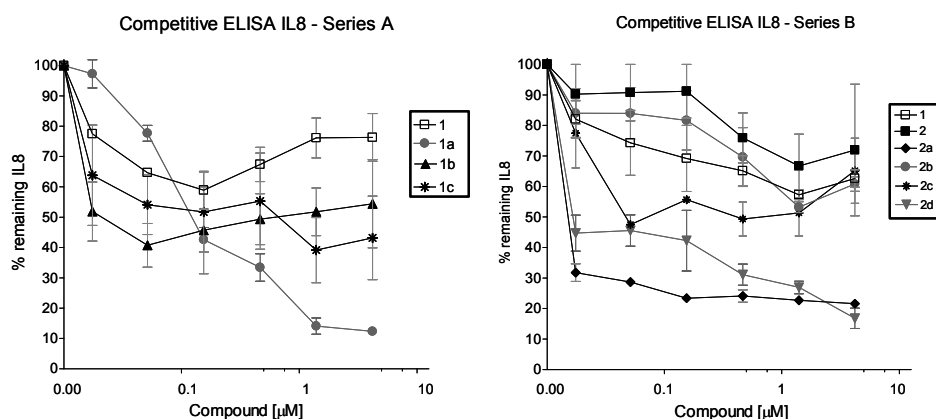


Figure III.5. Interaction with IL8. Competitive ELISA showing displacement of bound IL-8 from surface immobilized heparin by compounds of series A, on the left and compounds of series B, on the right. Reference heparin 1 is shown on both graphs.

The second method monitored direct binding in solution to IL-8 through changes in IL-8 protein secondary structure, detected *via* chiral chromophores present in the protein backbone. Such chromophores are sensitive to conformational changes when probed using synchrotron radiation circular dichroism (SRCD) spectroscopy (**Figure III.6**). SRCD in the range 185-260 nm is sensitive to secondary structure changes in proteins and was used to establish, unequivocally, the interaction between IL-8 and heparin derivatives in solution. Profound structural changes in IL-8 were observed in the presence of both standard heparin and selected derivatives. The CD spectrum of IL-8 recorded resembles that of a previously reported spectrum of IL-8 (amino acids 1-66) [127]. The two minima located at ~204 and ~224 nm are characteristic of the chemokine as a monomer; the addition of the heparin derivatives to IL-8, in molar ratio of ~1:1, caused structural rearrangement of the protein, with the resulting spectra resembling that of a protein with a random-coil structure. Further information on the changes in secondary structure of IL8 bound to derivatives could be calculated by Dichroweb [128] [129] by comparison with the CD spectra of a defined set of proteins and using a deconvolution program. Owing to the significant difference

among the spectra, it was not possible to use a unique dataset of proteins to compare the spectra with and therefore, no additional information was deduced.

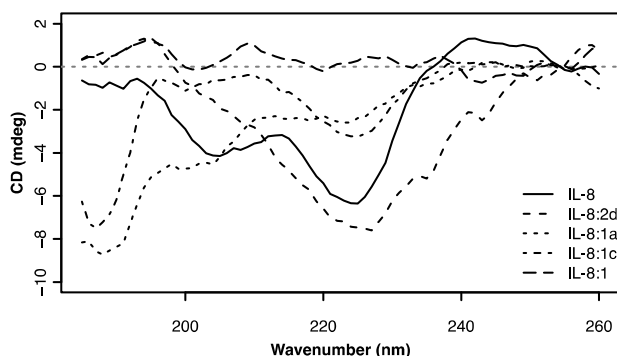


Figure III.6. Interaction of heparin and derivatives in solution with IL-8. SRCD spectra (185–260 nm) of IL-8 in the presence of selected test compounds (**1a**, **1c**, **2d**), unmodified porcine mucosal heparin (**1**) a 1:1 molar ratio. The spectra of heparin and derivatives alone were subtracted.

III.2.4 Interaction with TNF- α

The interaction of selected heparin derivatives with TNF- α , which is involved in the inflammatory response was also explored in solution. The SRCD spectra of TNF- α , alone, and in the presence of either unmodified heparin (**1**), or heparin derivatives **1a**, **1c** and **2d**, which all exhibited favorable IL-8 binding and elastase inhibition are shown in **Figure III.7**. The TNF- α active form is a 51 kDa trimer held together by non-covalent interactions and its secondary structure comprises predominantly β -sheet and turns as evinced by the positive peak at 205 nm and a negative peak between 216 and 225 nm, although little α -helix is present. These data are consistent with previous CD and IR studies indicating that TNF- α contains about 60% β -sheet or turns and a significant amount of irregular structures [130][131]. Binding of both standard heparin and derivatives, although present only in a 1:10 molar ratio, caused significant and distinct changes in

the CD spectra of TNF- α . Calculation of the percentage of secondary structure changes with Dataset 7 was possible only for (1), which caused a 40% increase in β -sheet, while changes induced by its derivatives, which influenced the secondary structure of TNF in different ways, were not described adequately by the same Dataset of proteins.

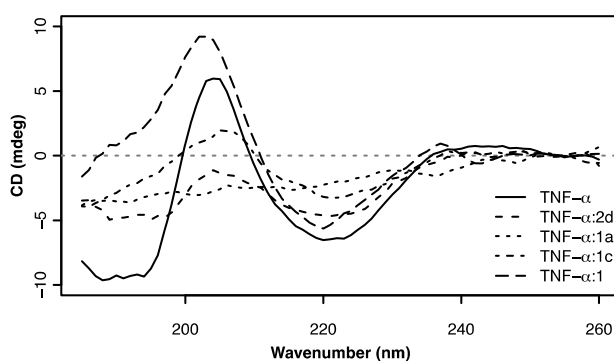


Figure III.7. SRCD spectra (185–260 nm) of TNF- α . The presence of heparin derivatives **1a**, **1c**, **2d** and unmodified porcine mucosal heparin (**1**) induces changes in the secondary structure of the protein, demonstrating a direct interaction in solution. The spectra of heparin and derivatives alone were subtracted.

III.2.5 Anticoagulant activity

The activities of the series A and B compounds are summarized in **Table III.2**. The anticoagulant activities (anti-factor Xa, aPTT, PT), which are the major potential side-effects of heparin derivatives, are shown together with values for the inhibition of HLE and IL-8 displacement.

Three assays are commonly available to determine the anticoagulant activity of heparin and have been used in this study. The antiXa assay measures the antithrombin (AT)-catalyzed inhibition of factor Xa. The aPTT is a performance indicator of the efficacy of both the "intrinsic" (now referred to as the contact activation pathway) and the common coagulation pathways.

Table III.2. Summary of the activities of series A and B compounds. § Reported values are normalized relative to control heparin (1), which had APTT and PT activities (EC_{50}) of 2.1 and 23.9 $\mu\text{g/mL}$. Higher values denote a weaker anticoagulant activity than heparin. # The percentage reported is relative to a specific concentration of the compounds as indicated in the headings of each column, for a range of concentrations see **Figure III.4**. ° Comparison with positive control (absence of inhibitor): one way ANOVA - Dunnett's Multiple Comparison Test (* $p < 0.05$, ** $p < 0.01$).

Series	Compound	% Factor Xa inhibition	APTT§	PT§	% HLE inhibition (peptide) #	% HLE inhibition (α -elastin) °
					10 nM	0.54 μM
A	1 (PMH)	79.6	1.0	2.0	30.0	35
	1a	24.1	4.0	2.5	19.0	48**
	1b	22.4	2.0	3.0	26.0	46**
	1c	6.0	27.3	14.7	32.4	42*
B	2	17.0	8.7	9.1	22.6	39
	2a	10.5	7.3	91.2	22.7	41*
	2b	12.8	15.2	90.8	27.7	28
	2c	11.0	178.8	237.0	24.0	41*
	2d	13.5	264.0	> 237	25.6	39*

It is used in conjunction with the prothrombin time (PT) which measures the extrinsic pathway (Tissue Factor Pathway) (**Figure III.8**).

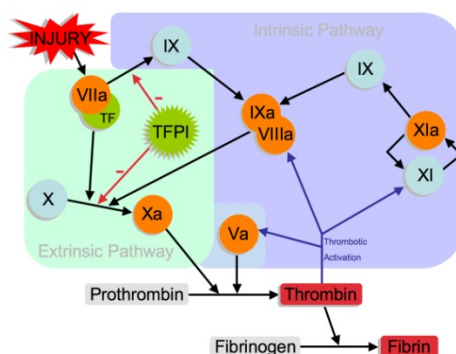


Figure III.8. Scheme of a simplified coagulation cascade. The coagulation cascade is basically a series of steps whereby coagulation factors become activated in order to generate thrombin from its precursor, prothrombin, and fibrin from its precursor, fibrinogen, and make clots to stop bleeding. Red arrows indicate inhibition. TFPI= Tissue Factor Pathway Inhibitor, TF= Tissue Factor, Coagulation factors are shown in circles (blue= inactive, orange= activated).

Results confirmed the decrease in anticoagulant activity of the derivatives, which correlates with the decrease of sulfation degree, while the glycol-split modification, whilst present in only 25–35% of disaccharides, abolished the anticoagulant activities principally by affecting the glucuronic residue present in the pentasaccharide sequence responsible for the interaction with ATIII.

III.2.6 Neutrophil chemotaxis

Compounds were also tested for their ability to inhibit the recruitment of neutrophils in a Boyden chamber migration assay performed on the neutrophils freshly isolated from the blood of healthy volunteers. This test was performed independently in two different laboratories with slightly different protocols and in both cases high variability was found among volunteers (**Figure III.9**, only data obtained in the Liverpool laboratory are shown).

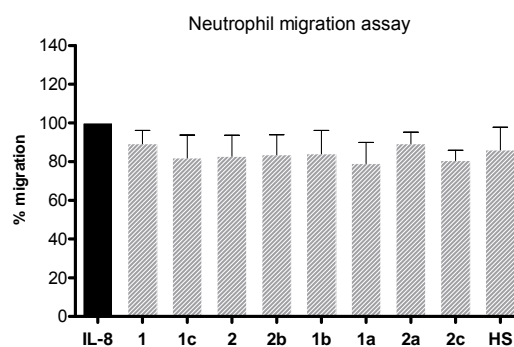


Figure III.9. The graph shows the average effect of 100 µg/ml derivatives on human neutrophil chemotaxis from four healthy volunteers. Each compound was measured twice and compared to the respective control for each patient. There is no significant difference between samples and control (one way ANOVA - Dunnett's Multiple Comparison Test $p > 0.05$).

These results were inconclusive and repetitions under standardized conditions, together with close matching of the volunteers would be necessary to obtain consistent results.

III.2.7 Ability of PS to reduce inflammation and tissue damage in vivo

Heparin derivatives **2** and **1a** were tested in the murine model of *P. aeruginosa* acute and chronic infection (**Figure III.10**). Regarding acute infection C57Bl/6Ncr1BR mice were treated twice subcutaneously with a dose of 30 mg/Kg, two hours before and two hours after the infection and sacrificed 6 hours after bacterial challenge. The analysis of samples showed that mice treated with **1a** reduced significantly the number of total leukocytes in comparison to Ctrl mice treated with saline (**Figure III.10.A**) and in particular neutrophils (**Figure III.10.B**) in bronchoalveolar lavage fluid (BALF). In addition, this compound also decreased the number of epithelial cells, suggesting a reduction in the damage to the epithelial barrier (**Figure III.10.C**). Then **1a** and **2** were administered to in C57Bl/6Ncr1BR mice chronically infected to test the potential long term anti-remodeling activity of these polysaccharides. Mice infected were treated subcutaneously daily with 30mg/Kg of the compounds and sacrificed 14 days after infection. Treatment with **1a** reduced significantly the number of total leukocytes in the BALF in comparison to Ctrl mice treated with saline (**Figure III.10.D**). In addition, **1a** treatment reduced significantly TGF- β content in the BALF in comparison to Ctrl mice (**Figure III.10.E**).

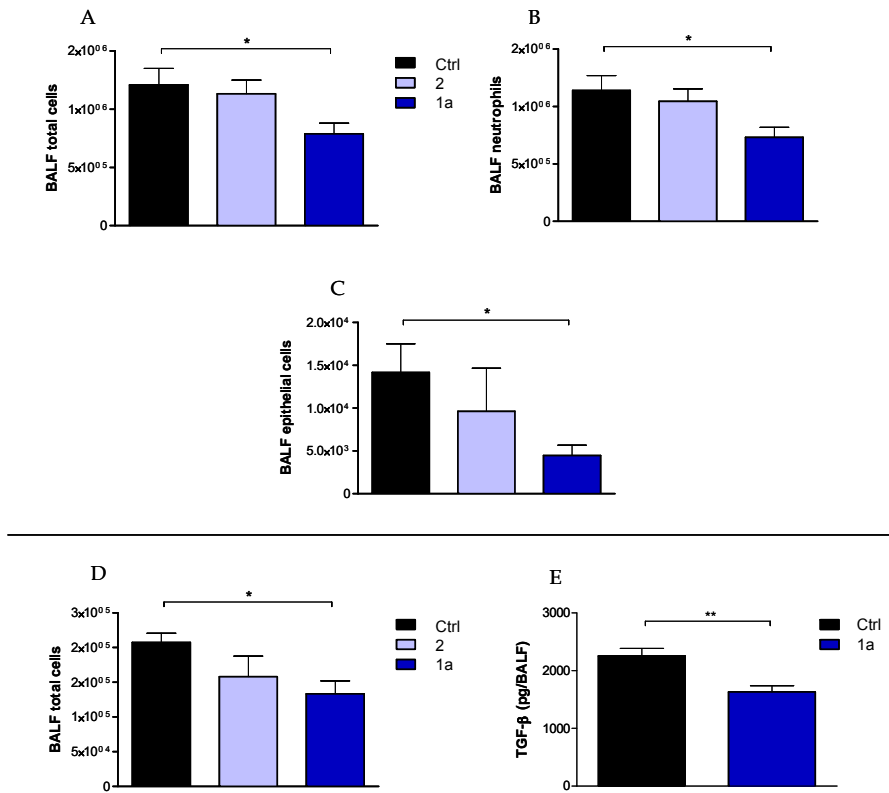


Figure III.10. Inflammation and tissue damage modulation by PS after *P. aeruginosa* acute and chronic lung infection. A) Total cell recruitment, B) neutrophils recruitment, and C) epithelial cells were analyzed in BALF of C57Bl/6 mice acutely infected with the early *P. aeruginosa* strain AA2 and treated subcutaneously 2 hours before and 2 hours post infection with **1a** and **2**. D) Total cells recruitment and E) TGF- β were quantified in the BALF of mice chronically infected with the late *P. aeruginosa* strain AA43 and treated daily subcutaneously with **1a** and **2**. Statistical significance by Mann Whitney test is indicated: * $p < 0.05$, ** $p < 0.01$.

Compound **1a** induced a statistically significant decrease of total cells recruited in bronchia, in particular of neutrophils and epithelial cells during acute infection. It also reduced total cell recruitment and TGF- β in the BALF during chronic lung infection, indicating that it modulates both inflammation and tissue damage.

III.3 Evaluation of GAGs level in a murine model of *P. aeruginosa* infection

To better characterize and possibly quantify GAG species, a group of mice C57Bl/6Ncr1BR was chronically infected for 28 days with late strain AA43 (mucoid) and with sterile agar beads. Murine lungs were perfused before being recovered; this procedure allows exclusion of the 'contamination' of lung homogenates by circulating GAG present in the blood; moreover, homogenates were separated into pellets and supernatants to distinguish released GAG from those present as structural components of the extracellular matrix. The presence of GAG after digestion of both the protein and nucleic components was verified through $^1\text{H-NMR}$ (**Figure III.11**); no significant differences were found between spectra of control and infected mice.

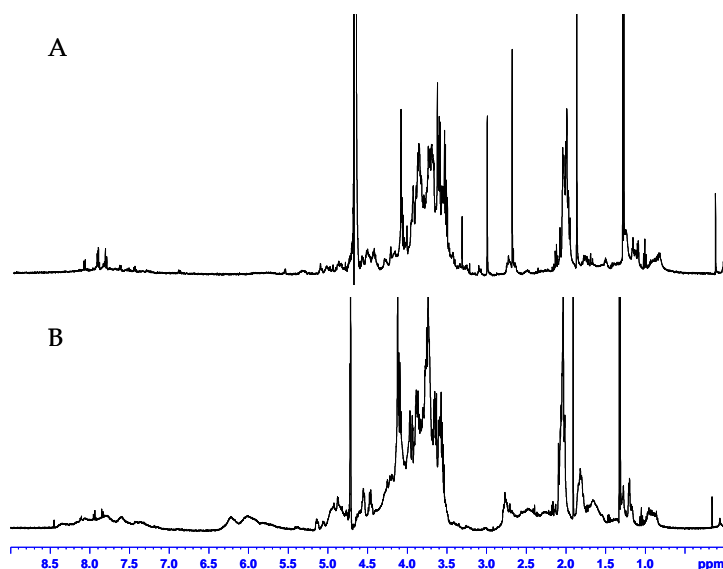


Figure III.11. $^1\text{H-NMR}$ of GAGs from control and infected mice. A) supernatant and B) pellet of a control mouse after proteinase K and DNase I digestion and ultrafiltration.

Spectra resemble a mixture of polysaccharides; particularly, acetyl groups at ~ 2 ppm and backbone signals between 3.2 and 5.4 ppm are distinguishable.

Signals in aliphatic (0.5-2 ppm) and aromatic (7-8.5 ppm) regions are due to residual proteins, lipids and nucleic acid. Owing to the scarcity of isolated GAGs (0,1-0,7 mg corresponding to ~0,05-0,3% of the starting lyophilized material), in deep NMR characterization was not possible, thus both supernatants and pellets were digested with specific enzymes to identify specific GAG and desalted digestion products were analyzed by HPLC-mTOFQ analysis.

The HPLC-MS profiles showed the presence of digestion products from heparin/HS (**Figure III.12**), but not from CS or DS. The presence of ChABC digestion products was expected in relation to the detection at both 210nm and 232nm of a significant amount of a component from the desalting chromatography (see **Annex Figure A.III.5**) which instead turned out to be other than CS. Even if HPLC-MS analysis is not quantitative, comparison among samples is possible under identical conditions and by comparing the integrals of HPLC peaks of disaccharides to the sum of the relative integrals. In this way it is possible to observe an increase in heparin/heparan sulfate digestion products in infected mice compared to controls.

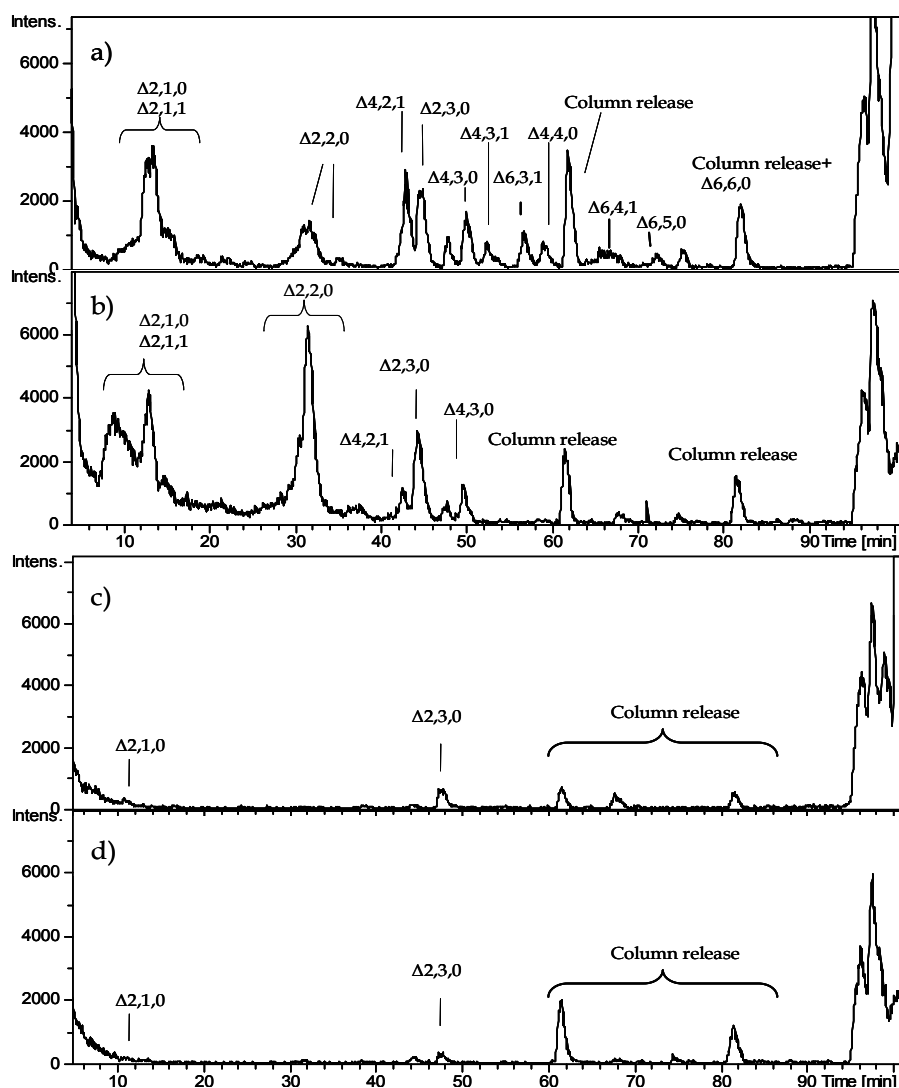


Figure III.12. Example of HPLC profiles of heparinase digestion products. A) pellet from a control mouse; B) pellet from an AA43 mouse, c) supernatant from a control mouse, d) supernatant from an AA43 mouse. Oligosaccharides were identified by their mass/charge ratio and labeled as follow. The unsaturated bond of the terminal uronic acid is indicated by Δ , and the number of monomers, the number of sulfates and the number of acetyls are reported.

The highest value of the sum is set as 100% and the relative percentage of disaccharides is reported in **Figure III.13** as a mean of three samples per type (see **Annex Table A.III.1**).

No significant differences were found between the supernatants in the control and infected mice, while an increase in digestion products in the pellets of AA43 mice compared to the controls was observed, with the prevalence of the monosulfated disaccharide $\Delta 2,1,0$ over the other three species detected.

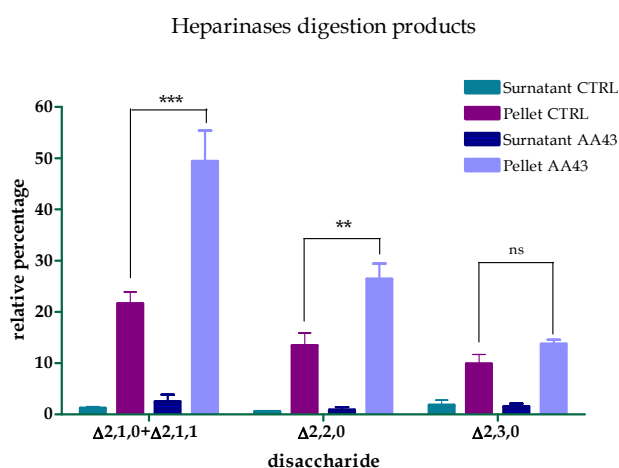


Figure III.13. Disaccharide products of the digestion of HEP/HS from murine lungs. The graph shows the percentage of each disaccharide species relative to the disaccharide moiety in each sample. 100% is considered the sum of integrals of AA43 pellet. Two-way ANOVA with Bonferroni's post-test was used to statistically analyze results. Data are the mean of three samples per type which have been processed independently.

Results indicate the presence of a structure with a lower degree of sulfation than commercial heparin (the heparin disaccharides contain an average of ~ 2.7 sulfate groups, whereas those of HS only ~ 1 sulfate group [45]). In particular, the estimated sulfation degree of HS/HEP from both control and infected mice is ~ 1.8 and these values are closer to those of a canonic HS. The same calculations were done for the tetrasaccharide moiety (see **Annex Figure A.III.6**) that is the second most abundant family after disaccharides. Owing to the different response of oligosaccharides compared to disaccharides, direct comparison between different families cannot be made, although an estimation of the amount of tetrasaccharides can be obtained by

confronting the integrals of the two families. The amount of tetrasaccharides is only the 6% in infected mice and 10% in control mice compared to disaccharides and even if this number was underestimated, it is not sufficient to cover the gap in disaccharides between controls and infected mice which is around the 50%.

Prior studies have reported the release of heparin from human lung mast cells in response to allergen exposure, and increased levels of a heparin-like substance have been reported in the plasma of asthmatic [132]. For this reason, in our experiments, lungs were perfused to avoid the detection of released heparin; as a consequence, observed disaccharides originate from HS bound to PGs on the surface of cells or HEP stored in mast cells' granules.

It is probable that the amount of CS/DS was not sufficient for detection; therefore, to verify the presence of these two species, and to detect hyaluronic acid (HA), which is known to be present in lungs but is extremely difficult to digest either with bacterial or mammalian hyaluronidase, cellulose acetate electrophoresis was performed on GAGs from a healthy isogenic mouse. Under these conditions, migration depends on the sulfation degree and follows this order from the loading point toward the positive electrode: HA, CS, HS/HEP.

From the NMR spectra the presence of other components was apparent, that could have had a high impact on the final weight and led to overestimation of GAGs. For this reason, samples were 4 times more concentrated than the standard mixture but, the amount of GAGs was insufficient for detection (see **Annex Figure A.III.7**).

Future perspectives are the use of another electrophoretic technique that has been successfully applied to GAGs, i.e. PAGE, to increment sensitivity or another colorimetric method to be used directly in solution.

III.4 Discussion and future perspectives

The prepared heparin derivatives from both series were able to bind and displace IL-8 from the surface of the ELISA plate and interaction was confirmed in solution independently using SRCD. It is apparent from the SRCD spectra of IL-8 with the modified polysaccharides, that each derivative induces distinct structural changes in IL-8, implying either distinct binding modes, the induction of different structural changes by distinct structures binding the same binding site, or a mixture of both. The ELISA results showed that **1a** was able to displace up to 90% of IL-8 from the plate at 3.3 μM , while the glycol-split modification, that increases the flexibility of the chains [133], diminished the affinity of **1a** (45% NAc) compared to its glycol-split counterpart **2b** (49% NAc, 35% gs). In contrast, the glycol-split modification of **1c** (100% NAc) increased the affinity for IL-8. From another perspective, with the exception of **2b** in which partial 2-O desulfation did not promote further activity, the increase of N-acetylation in glycol-split compounds promoted affinity for IL-8, suggesting that factors besides pure electrostatics were responsible for the interaction [122].

The heparin derivatives prepared here interacted with IL-8 and TNF- α and partially inhibited cleavage of both a synthetic peptide and a natural substrate by human sputum elastase *in vitro*.

Other groups report the complete inhibition of the enzymatic activity by heparin and its derivatives. The explanation could be due to the difference between the experimental procedures. In fact, in the work by Frier *et al.* [134], inhibition was assessed by pre-incubation of HLE with various molar ratios of heparin or derivatives, while here the inhibitor was already present in the buffer, thus mimicking the probable *in vivo* situation in which compounds would act.

The partial, rather than the complete inhibition of key elements involved in the excessive inflammation response could return the immune response

towards normal levels, thereby reducing damage to lung tissue, while maintaining some capacity to combat infection. The compounds identified offer a starting point for future drug development, opening-up the possibility of the synthesis of polysaccharides or analogues with lower molecular weight, capable of acting on multiple cytokines with the ability to decrease inflammation through several targets simultaneously, while minimizing unwanted side-effects. In addition to *in vitro* tests, compounds **1a** and **2** that were tested in a murine model of *P.aeruginosa* infection, proved able to modulate inflammation during both acute and chronic lung infection. Among the two, the most interesting one proved to be **1a** which induced decrease of recruited neutrophils and epithelial cells in bronchia during acute infection and of the cytokine TGF- β in the BALF during chronic lung infection, indicating that it modulates both inflammation and tissue damage. It is unknown the mechanism of action of heparin derivatives, although the interaction with inflammatory molecules is thought to provide a mechanism for both their presentation to respective receptors and protection from proteolytic degradation and the establishment of chemokine gradients in order to provide directional signals for migrating cells [135].

As reported in **Section III.I.2**, modulation of GAGs in infected tissues could be a potential biomarker of inflammation [112]. Preliminary results from the HSR group indicated that levels of GAGs (detected with sGAG assay (Kamiya Biomedical Company)) were higher in CF patients chronically and intermittently infected by *P. aeruginosa* in comparison to those free from this bacterium (data not shown). The hypothesis that *P. aeruginosa* chronic infection could modulate the levels and the proportions of the GAGs present in the matrix is supported by our data obtained by enzymatic degradation of GAGs and characterization of their digestion products. Indeed, an increase in heparin lyases digestion products was observed in *P.aeruginosa* AA43 infected mice compared to wild type mice, thus demonstrating a higher presence of a HS-like component following bacterial infection.

In addition to the series shown, it is possible to introduce modifications in other positions along heparin chains and to control the reactions to generate compounds with lower MW or to isolate specific fractions of desired dimensions to reduce the polydispersity. Some low molecular weight (LMW) heparin derivatives are now under preparation and will be tested for their interaction with elastase and IL-8.

Further *in vivo* experiments are ongoing to verify the ability of other derivatives to modulate inflammation and to confirm results.

In addition, to better characterize the implication of GAGs in CF disease, Cfr^{tm1UncTgN} (FABPCFTR) and their isogenic wild type mice were infected with *P. aeruginosa* AA43 strain for 28 days. The supernatants and pellet of mice lungs will be analyzed to identify GAG species and verify if modulation of their level occurs.

III.5 Experimental section

III.5.1 Preparation and characterization of heparin derivatives

The N-acetylated heparin and glycol-split derivatives were prepared as described previously [125][126] starting from unmodified pig mucosal heparin (PMH or compound **1**, Bioiberica S.A., Spain) and characterized by ¹³C NMR (see **Annex figure A.III.1** for ¹³C spectra of **1** and derivatives **1a**, **2**). The weight average molecular weights (Mw) were determined in sodium nitrate at a concentration of 5 mg/mL and at 313 K employing Viscotek HP-SEC-TDA (**Table III.1** and **Annex Figure A.III.2**) equipped with a SEC column coupled with triple detector array (TDA), including three online detectors, right-angle laser light scattering (RALLS), refractometer (measuring refractive index (RI)) and viscosimeter [136].

III.5.2 Anticoagulant assay

The anticoagulant activity of the derivatives was assayed using the COATEST® Heparin (Chromogenix) following the manufacturer's instructions. Briefly, heparin reacts with Antithrombin and an excess of Factor Xa was added leading to the formation of a ternary complex. Free Factor Xa cleaves a chromogenic substrate and the absorbance is read at 405 nm. Several concentrations of standard heparin were tested and a standard curve was obtained from 0 to 0.35 µg/mL. Then, the heparin derivatives (0.25 µg/mL) were tested and compared to the same concentration of standard heparin. The test was performed twice in duplicate in a 96-well plate and the colour read photometrically (VersaMaxmicroplate reader, Molecular Devices, USA).

The PT assay was performed as per the manufacturer's instructions with some minor modifications. Pooled (normal) human plasma was obtained from Technoclone Ltd (UK). Briefly, the test sample was incubated with plasma prior to the addition of Thromborel S (Siemens, at 2X concentration).

The time taken for clot formation was monitored using a thrombotic coagulometer (Stage Diagnostics) and recorded if the clot formation occurred before 120 s.

APTT assays were performed essentially according to the manufacturer's instructions. Briefly, human plasma test sample and Pathromtin SL (Siemens) were incubated for 2 min at 37 °C, 50 mM CaCl₂ was then added to initiate coagulation. The time taken for clot formation was observed as per PT assay.

III.5.3 Competitive ELISA to measure IL-8 displacement from heparin

The test performed was a modified version of the classic competitive ELISA. Streptavidin (30 µg/mL, Sigma Aldrich, USA) was used to coat a Maxibinding 96-well plate (SPL Lifesciences) overnight (4 °C). The plate was then incubated with heparin-biotin (0.1 mg/mL, Sigma Aldrich, USA) at room temperature, followed by blocking (2% BSA in DPBS overnight at 4 °C). The next step was the binding of 1.5 µg/mL IL-8 (Millipore, USA) to the plate, in the absence and presence of a heparin derivative ranging from 0 to 10 µM and subsequent incubation with a rabbit anti-human IL-8 primary (Millipore, Bedford, MA) (1:500, 50:l, 1 h) and a goat anti-rabbit-HRP-conjugated secondary (Millipore, Bedford, MA) (1:1000, 50:l, 1 h) antibody. All incubations were followed by triplicate washes in DPBS with the addition of 0.05 % Tween-20. Finally, 0.4 mg/mL *o*-phenylenediamine (Sigma Aldrich, USA) in 50 mM citrate/dibasic sodium phosphate and 0.0004 % hydrogen peroxide (Sigma Aldrich, USA) was added. The enzymatic reaction was terminated by addition of 1 M H₂SO₄. Absorbance measurements were made at 492 nm (VersaMaxmicroplate reader, Molecular Devices, USA). A calibration curve of IL-8 from 0 to 1.5 µg/mL was set up for each experiment (see **Annex Figure A.III.4** for an example).

III.5.4 Elastase inhibition assays

The inhibition test of Human Leukocyte Elastase (EPC, Owensville, USA) was based on the release of ρ -nitroaniline from the chromogenic substrate MeO-Suc-Ala-Ala-Val- p NO₂-anilide (EPC, Owensville, USA). The reaction was conducted at 37 °C in 96-well plates and monitored by reading at 405 nm continuously for 25 minutes (VersaMax microplate reader, Molecular Devices, USA). The substrate (240 μ M final; 2.1 mM stock in phosphate buffer 50 mM, pH 7.4, 15 mM DMSO, 0.13 M NaCl) was incubated for 10 min in the presence or absence of increasing concentrations of derivatives before adding the enzyme (60 nM; 800 nM stock in sodium acetate 70 mM, pH 4.5). As control, the enzyme was inactivated with sulfuric acid (1 M, to a final concentration of 0.5 M) prior to the addition to the reaction mix.

The ability of the derivatives to inhibit α -elastin digestion by Human Sputum Elastase (EPC, Owensville, USA) was tested using a FastinTM Elastin kit (Bicolor, Carrickfergus, N. Ireland), employing an adaptation of the method recommended by the manufacturer. The modified procedure involved the digestion of a solution of α -elastin (20 μ L, 1 mg/mL) in 50 mM phosphate buffer pH 7.4 by elastase (100 μ L final volume, 0.54 μ M, 37 °C, 1 h) in the presence or absence of 0.54 μ M derivatives (1:1 molar ratio to elastase), inactivation with oxalic acid (1 M, to a final concentration of 0.25 M) and staining with the FastinTM kit, according to the manufacturer's instruction. Briefly, α -elastin was precipitated using 50 μ L of Precipitating Reagent and the tubes were then centrifuged (10,000 \times g, 10 min). After the removal of the liquid, 500 μ L of dye were added and the tubes were mixed (90 min, room temperature). After centrifugation and careful removal of the liquid, 250 μ L of the Dye Dissociation Reagent were added. After mixing, the contents of the tubes were transferred to a 96-well plate and read at 513 nm (VersaMax microplate reader, Molecular devices, USA). A calibration curve of α -elastin from 0 to 50 μ g was obtained to verify the efficacy of the

assay. As control, the enzyme was inactivated with oxalic acid (1 M, to a final concentration of 0.25 M) prior to the addition of the substrate.

III.5.5 Nuclear Magnetic Resonance

The ^{13}C NMR spectra of the heparin chemical derivatives (100 mg/ml) were recorded in D_2O at 313 K on Bruker AC300 and AMX400 spectrometers. The ^1H NMR spectra of lung extracts were recorded in D_2O at 313 K on the Bruker AV500 spectrometer. The data were processed using Topspin 3.0 software.

III.5.6 Circular Dichroism

The synchrotron radiation circular dichroism (SRCD) spectra were recorded (180 to 260 nm) on a purpose-built CD beam line (B23 at Diamond Light Source, Didcot, Oxfordshire, UK) using a CaF_2 sample cell with 0.02 cm path length, employing 1 nm resolution. The slit widths for all spectra were 0.5 mm, 1 s integration time was used and the storage ring current was 250 mA for the duration of the experiments. SRCD spectra of the derivatives alone were also recorded and subtracted. Spectra of IL-8 were recorded at a concentration of 0.5 mg/mL in 17.5 mM phosphate buffer, the concentration of the derivatives were at equal weight ratios for all samples. TNF- α spectra were recorded at 10 mg/mL, with 0.1 mg/mL derivatives, in 17.5 mM phosphate buffer. Deconvolution of CD spectra was made with Dichroweb [128] [129] using the program CONTIN and several of the protein spectra reference Datasets provided, amongst which Dataset 7 proved to better estimate the secondary structure's content of TNF- α .

III.5.7 Neutrophil isolation

Whole blood was collected in Sodium Citrate vacutainers from healthy volunteers, via protocols approved by the University of Liverpool Committee on Research Ethics. Neutrophils were isolated using

Polymorphprep (Axis Shield), and contaminating erythrocytes were removed by hypotonic lysis. Neutrophil purity and viability was routinely found to be >97% and 98% respectively (as assessed by Wright' staining and trypan blue exclusion, respectively). Freshly isolated neutrophils were re-suspended at 5×10^6 /mL in RPMI media (Gibco).

III.5.8 Neutrophil chemotaxis assay

The chemotaxis assay was carried out in 24-well tissue culture plates coated with 12mg/mL poly-hema (Sigma) to prevent cell adhesion, using hanging inserts (Millipore) with a 3 μ m porous membrane separating media from the top and bottom chambers. Heparin derivatives (100 μ g/mL) and/or IL-8 (100ng/mL, Sigma) were added to 800 μ l RPMI media in the bottom chamber. Neutrophils (10^6) were added to the top chamber and the plate incubated for 90 min at 37°C with 5% CO₂. The number of migrated neutrophils (into the bottom chamber) after 90 min was measured using a Coulter Counter Multisizer 3 (Beckman Coulter).

III.5.9 Acute and chronic infection

Acute infection (6 hours) in C57Bl/6Ncr1BR male mice (obtained from Charles River Laboratories, Italy) was established with early *P. aeruginosa* clonal strain AA42. Mice were intratracheally challenged with 1×10^6 CFU of AA2 strain given as planktonic bacterial cells and were treated twice subcutaneously with the two molecules at a dose of 30mg/Kg two hours before and two hours after the inoculation and sacrificed 6 hours post infection. 14-days chronic infection in C57Bl/6Ncr1BR male mice (Charles River Laboratories, Italy) was established with late *P. aeruginosa* clonal strains AA43 and AA44. $1-2 \times 10^6$ bacteria were embedded in agar beads to mimic the microanaerobic condition of *P. aeruginosa* growth in CF airways and were intratracheally injected in mice. Animal studies were conducted according to protocols approved by the San Raffaele Scientific Institute (Milan, Italy) Institutional Animal Care and Use Committee (IACUC) and

adhered strictly to the Italian Ministry of Health guidelines for the use and care of experimental animals. Mice were sacrificed and lung homogenates and BALF recovered. Differential cell count was performed on cytopins. TGF- β in supernatants of BALF and lung homogenates was analyzed by Bioplex. MMPs activity was determined in the BALFs and lung homogenates using a 5-FAM/QXL 520 FRET peptide as a substrate.

III.5.10 Isolation of GAGs

Freeze-dried lung homogenates from control and infected mice were from Dr. Cigana at San Raffaele Scientific Institute (Milan, Italy). Samples were kept in cold acetone (Sigma Aldrich, USA) overnight at 4°C, then defatted by washing with a solution of 2:1 chloroform/methanol (Sigma Aldrich, USA) and filtration on a 3 μ m filter to discard solvents. After washing with ethyl ether (Sigma Aldrich, USA), samples were freeze-dried then dissolved in dPBS with 2mM CaCl₂ and subjected to proteolytic cleavage with Proteinase K (Sigma Aldrich, USA) at 55°C for 48h. After inactivation by boiling for 10 minutes, the temperature was set to 37°C, MgCl₂ was added at a final concentration of 2 mM and DNase I (Sigma Aldrich, USA) digestion was carried out for 48h. Reaction was stopped by boiling for 10 minutes followed by filtration on 0.2 μ m filters (Millipore, USA). Samples were purified by 3 kDa ultrafiltration (Amicon ULTRA, Millipore, USA) to remove digestion fragments, then analyzed by ¹H-NMR.

III.5.11 Enzymatic digestions

Digestion of chondroitin sulfates by chondroitinase ABC (Sigma, USA, 4 mU for 0.1 mg of starting material) was carried out in 50 mM phosphate buffer and 50 mM sodium acetate (1:1 v/v), pH 8 at 37°C for 48 h. The reaction was stopped by boiling for 10 minutes followed by 0.45 μ m filtration (LabService Analytica).

Digestion of heparin and heparan sulfate with a cocktail of heparin lyases I-II-III (Grampian Enzymes, UK, 2 mU each for 0.1 mg of starting material),

was carried out in 100 mM sodium acetate buffer and 10 mM calcium acetate, pH 7. The reaction was stirred at 37°C in a thermostated bath for 48 h, then stopped by boiling for 10 minutes followed by 0.2 µm filtration (LabService Analytica).

Products were recovered by Amicon ULTRA centrifugal filter units (MWCO 3 kDa) and desalted using a G-10 column (h 25cm, Ø 1.5 cm) eluting with 10% EtOH. Collected fractions of 400µl were read at 210 nm (Cary50 UV). After freeze-drying, products were dissolved in 100 µl for HPLC-MS analysis (30µl injection).

LC-MS analysis was performed on a LC system (Dionex Ultimate 3000, Dionex) equipped with degassing system (model LPG-3400), pump (model LPG-3400A), autosampler (model WPS-3000TSL) and UV-detector (model VWD-3100) and coupled with an ESI-QTOF mass-spectrometer (microQTOF, Bruker Daltonics).

The chromatographic separation was performed using a Kinetex C18 analytical column (100 × 2.1 mm I.D., 2.6 µm particle size, Phenomenex) with Security Guard Cartridges Gemini C18 (4 × 2.0 mm, Phenomenex). A binary solvent system was used for gradient elution.

Solvent A (10 mM DBA, 10 mM CH₃COOH in water) and solvent B (10 mM DBA and 10 mM CH₃COOH in methanol) were delivered at 0.1 ml/min. Oligosaccharides were separated using a multi-step gradient as reported in the table below.

Gradient (%B)	
t=0	10
t= 40	35
t=85	50
t=88	90
t=95	10

The solvent composition was held for the last 19 min for equilibrating the chromatographic column before the injection of the next sample. The MS

spectrometric conditions were as follows: ESI in negative ion mode, drying gas temperature +180°C, drying gas flow-rate 7.0 l/min, nebulizer pressure 0.9 bar; and capillary voltage +3.2 kV. The mass spectra of the oligosaccharides were acquired in a scan mode (m/z scan range 200 – 2000). Calibration of the mass spectrometer was obtained by using an ES tuning mix solution acetonitrile solution (Agilent Technologies, Santa Clara, CA) according to a standard procedure. Data were processed by the DataAnalysis software (HyStar Compass, version 3.0, Bruker Daltonics).

III.5.12 Cellulose acetate electrophoresis

The electrophoresis was run in HCl/KCl buffer at 4°C. Cellulose acetate strips (Sartorius, Germany) of 2 cm-width were wetted in the buffer, then 1 ul of 2 mg/ml sample were loaded and a constant current of 2mA/strip was applied for 5 hours. Detection was performed by staining for 15 minutes with Alcian Blue (in sodium acetate pH 5.6 and 1% EtOH) and discoloring with 5% acetic acid. GAGs standards (HA, C4S, HS, HEP and a mixture of the four) were used as control of the migration points.

RIASSUNTO IN ITALIANO

I GLICOSAMINOGLICANI IN DUE MALATTIE GENETICHE AUTOSOMICHE: OSTEOCONDROMI MULTIPLI E FIBROSI CISTICA

E' noto da tempo l'importante ruolo biologico svolto dai glicosamminoglicani (GAGs), polisaccaridi in grado di interagire con una serie di fattori di crescita, citochine e componenti della matrice extracellulare modulandone l'attività, e in grado di partecipare alle principali fasi del processo di infezione batterica. Il progetto di dottorato si è incentrato sul ruolo dei GAGs in due patologie genetiche, una autosomica dominante e una autosomica recessiva, rispettivamente Osteocondromi Multipli (OM) e Fibrosi Cistica (FC). Gli OM sono escrescenze ossee ricoperte da cartilagine che si formano in più punti dello scheletro a causa dell'errata regolazione del processo di ossificazione durante lo sviluppo causato da mutazioni nei geni EXT che codificano per glicosiltransferasi coinvolte nella biosintesi del GAG eparansolfato (HS), responsabile del corretto signaling durante l'osteogenesi. In letteratura sono riportate numerose indagini su cartilagine affetta da OM, ma nessuno studio strutturale sull'HS proveniente da tale cartilagine ed è dunque assente una correlazione genotipo-fenotipica. Il progetto di ricerca si è focalizzato sulla caratterizzazione strutturale dell'HS isolato sia da cartilagine umana sana proveniente da pazienti di diversa età, dallo stadio fetale a quello adulto, che da cartilagine patologica. La correlazione delle mutazioni nei geni EXT con la struttura dell'HS aiuterà ad individuare possibili biomarkers della malattia e della progressione maligna e fornirà indicazioni su una possibile terapia. 13 excisioni cartilaginee da individui sani, di cui 6 fetali, e 11 campioni patologici sono stati analizzati per il contenuto in HS. L'identificazione delle specie presenti ed i controlli delle fasi del lavoro sono avvenuti mediante spettroscopia NMR. L'isolamento dell'HS si è rivelato difficoltoso a causa della presenza di

keratan solfato (KS) resistente alla degradazione enzimatica con keratanasi I e II ed è dunque risultato impossibile caratterizzare l'HS tramite NMR. Un unico campione MO è risultato essere privo di KS ed è stato possibile registrare uno spettro monodimensionale dell'HS in esso presente. La caratterizzazione strutturale dell'HS è avvenuta quindi tramite depolimerizzazione con enzimi specifici ed analisi HPLC-MS dei prodotti di digestione ed ha permesso di rilevare differenze composizionali nei diversi campioni analizzati.

Molti studi riportano che non si possa descrivere l'eparan solfato come una struttura ben definita, ma che esistano più eparan solfati con diversi gradi di solfatazione a seconda del tessuto di estrazione. In accordo, i risultati di questo studio hanno rivelato estrema variabilità composizionale nell'HS da cartilagine umana sana, imputabile a due fattori principali: 1) i soggetti sono considerati sani, in merito alla patologia in esame, se non affetti da disturbi noti per inficiare la composizione e/o struttura della cartilagine; 2) l'area di escisione è di fondamentale importanza, poiché la cartilagine è organizzata in zone differenti in cui il gradiente dei fattori di crescita è regolato dal gradiente di HS. I campioni fetali hanno mostrato maggiore uniformità composizionale dell'HS e sono l'esempio per eccellenza di cartilagine da piatto di crescita, per il confronto con HS da esostosi e/o condrosarcomi. I risultati hanno mostrato la presenza di HS in entrambe le condizioni patologiche, con un aumento del grado di solfatazione nei tre campioni da condrosarcoma con mutazioni nei geni EXT rispetto all'unico campione senza mutazioni. Questo trend dovrà essere confermato con un maggior numero di campioni. La biosintesi dell'HS in presenza di mutazioni nei geni EXT avviene ad opera di altri geni EXTL che probabilmente portano alla sintesi di catene "non convenzionali" che non sono in grado di regolare il processo di ossificazione. In merito alla quantificazione dei prodotti di digestione, un metodo applicabile nell'immediato futuro potrebbe essere la derivatizzazione dell'estremità riducente degli oligosaccaridi con un

fluoroforo come BODIPY, che permetterebbe di accertare variazioni nei livelli di HS. Tuttavia, è emersa da questo studio la necessità di una maggiore precisione nell'effettuazione delle excisioni, la cui profondità e ampiezza sembra incidere notevolmente sui risultati finali.

La fibrosi cistica è caratterizzata da mutazioni nel canale di trasporto del cloro CFTR, che causano scorretta traslocazione degli ioni cloro con conseguente accumulo di muco viscoso all'esterno delle cellule epiteliali polmonari, infiammazione persistente e infezione batterica cronica, portando infine a numerosi scompensi a livello sistemico. In letteratura alcuni studi dimostrano una modulazione della biosintesi di alcuni glicosaminoglicani durante i processi infiammatori ed è inoltre riportato l'effetto antiinfiammatorio di alcuni derivati del glicosaminoglicano eparina (HEP), sottolineandone la possibilità di utilizzo senza provocare fenomeni di sanguinamento, tipici invece di trattamenti con farmaci anticoagulanti. Il lavoro si è incentrato su due aspetti inerenti i GAGs: da un lato, due serie di polisaccaridi, provenienti da modificazione chimica dell'eparina sono stati generati, alla ricerca di composti con attività anti-infiammatoria multipla, dapprima *in vitro* ed in seguito *in vivo* in un modello di infezione cronica indotta. La modificazione chimica dell'eparina ha comportato riduzione dell'attività anticoagulante e acquisizione di proprietà anti-infiammatorie, quali la capacità di inibire l'azione dell'elastasi neutrofila e di interagire con interleuchina-8 e TNF-alfa, *in vitro*. Inoltre, alcuni composti sono stati testati in un modello di infezione murina indotta da *P.aeruginosa*, uno dei principali patogeni rinvenuti nei polmoni di pazienti affetti dalla malattia. I composti sono stati somministrati a livello sottocutaneo ed è stata riscontrata diminuzione del numero di cellule totali e di TGF-beta nei lavaggi broncoalveolari *in vivo* sia in presenza di infezione acuta che di infezione cronica (14 giorni), dimostrando così capacità di modulazione della risposta infiammatoria da parte dei composti. In seguito a questo incoraggiante

risultato, è ora in corso la valutazione dell'effetto antiinfiammatorio in presenza di infezione cronica da 28 giorni per verificare l'effetto a lungo termine, in presenza o assenza di un comune antibiotico per verificare la possibilità di potenziare trattamenti già esistenti. Inoltre, si è valutata la modulazione dei GAGs in omogenati polmonari murini in presenza di infezione indotta da *P.aeruginosa*, tramite isolamento e caratterizzazione dei GAGs presenti. I polmoni sono stati perfusi per eliminare il sangue presente e dunque la componente eparinica in circolo e sono stati poi sottoposti a digestioni enzimatiche selettive per identificare le diverse specie di GAGs presenti. I risultati hanno mostrato un aumento significativo dei livelli di eparansolfato in presenza di infezione batterica, confermando dati precedenti ottenuti mediante un dosaggio colorimetrico. Campioni provenienti da topi FC, recanti la mutazione in CFTR, sono in corso di studio.

ACKNOWLEDGEMENTS

I would like to sincerely thank many people accompanying me along the long way. I would like to, first and foremost, thank my family who has always encouraged me and supported my decisions, who has shared both happy and stressing moments with love and comprehension.

I would like to thank my supervisor, Dr. Antonella Bisio, for many reasons. I really appreciate her openness of mind and the interesting conversations both related to work and to personal issues. She always reminded me to look at the bright side of the difficult situations and encouraged me.

I would also like to thank Dr. Annamaria Naggi, for scientific advisement and for interesting discussion, especially on the topic of cystic fibrosis, and Dr. Giangiacomo Torri for giving me the opportunity to carry out my PhD research at the "Ronzoni" Institute.

Many grateful thanks also to the Italian Cystic Fibrosis Foundation for financing part of the work, and to the many foreign collaborators which supported me abroad, making the experience enjoyable and valuable, among which Dr. Ed Yates, Dr. Tim Rudd and Dr. Janis Shute. My PhD research would have been much more difficult without the contributions of several people. Many thanks to Cesare Cosentino and Lucio Mauri, for performing NMR measurements, Anna Alekseeva and Elena Urso, for performing HPLC-MS analysis and for technical and moral support. Many thanks to Dr. Alessandro Parra for his critical reading of my PhD dissertation and for his availability. Many sincere thanks to my lab-neighbors for providing a great work environment. In particular, I would like to sincerely thank all of them for their friendship and support.

REFERENCES

- [1] Afratis N., Gialeli C., Nikitovic D., Tsegenidis T., Karousou E., Pava M. S., Tzanakakis G. N. and Karamanos N. K., *FEBS Journal*, **2012**, 279:1177–1197.
- [2] Carey DJ., *Biochem J*, **1997**, 327:1–16.
- [3] Filmus J., Selleck S.B., *J Clin Invest*, **2001**, 108:497–501.
- [4] Bishop J.R., Schuksz M., Esko J.D., *Nature*, **2007**, 446(7139):1030–1037.
- [5] Rahmoune H., Lamblin G., Lafitte J.J., Galabert C., Filliat M., Roussel P., *Am J Respir Cell Mol Biol*, **1991**, 5(4):315–20
- [6] Souza-Fernandes A.B., Pelosi P. and Rocco P.R.M., *Critical Care*, **2006**, 10:237 (review)
- [7] Esko J.D., Kimata K., Lindahl U., In: Varki A., Cummings R., Esko J., Freeze H.H., Stanley P., Bertozzi C.R., Hart G.W., Etzler M.E., eds. *Essential of Glycobiology. 2nd ed.*, Cold Spring Harbor (NY): Cold Spring Harbor Laboratory Press, **2009**.
- [8] Tone Y., Pedersen L. C., Yamamoto Y., Izumikawa T., Kitagawa H., Nishihara Y., Tamura J., Negishi M. and Sugahara K., *J Biol Chem*, **2008**, 283:16801–16807.
- [9] Ahn J., Lüdecke H.J., Lindow S., Horton W.A., Lee B., Wagner M.J., Horsthemke B., Wells D.E., *Nat Genet*, **1995**, 11:137–143.
- [10] Stickens D., Clines G., Burbee D., Ramos P., Thomas S., Hogue D., Hecht J.T., Lovett M., Evans G.A., *Nat Genet*, **1996**, 14:25–32.
- [11] Wuyts W., Van Hul W., Wauters J., Nemtsova M., Reyniers E., Van Hul E.V., De Boule K., de Vries B.B., Hendrickx J., Herrygers I., et al., *Hum Mol Genet*, **1996**, 5:1547–1557.
- [12] Lind T., Tufaro F., McCormick C., Lindahl U., Lidholt K., *J Biol Chem*, **1998**, 273:26265–26268.
- [13] McCormick C., Duncan G., Goutsos K.T., Tufaro F., *Proc Natl Acad Sci USA*, **2000**, 97:668–673.
- [14] Cheung P.K., McCormick C., Crawford B.E., Esko J.D., Tufaro F., Duncan G., *Am J Hum Genet.*, **2001**, 69:55–66.
- [15] Duncan G., McCormick C., Tufaro F., *J Clin Invest*, **2001**, 108:511–516. Ori A., Wilkinson M.C., Fernig D.G., *Front Biosci*, **2008**; 13:4309–38 (Review).
- [16] Bame K.J., Reddy R.V., Esko J.D., *J Biol Chem*, **1991**, 266(19):12461–12468
- [17] Raman K., Nguyen T.K., Kuberan B., *FEBS Lett*, **2011**, 585(21):3420–3.
- [18] Sheng J., Liu R., Xu Y., Liu J., *J Biol Chem*, **2011**; 286(22):19768–76.
- [19] Chavaroche A.A.E., van den Broek L.A.M., Eggink G., *Carbohydr Polym*, **2013**, 93: 38–47.
- [20] Wei Z., Swiedler Stuart J., Ishihara M., Orellana A., *Proc Natl Acad Sci USA*, **1993**, 90:3885–3888.
- [21] Rabenstein D.L., *Nat Prod Rep*, **2002**, 19: 312–331 (review)
- [22] Esko J.D., Selleck S.B., *Annu Rev Biochem*, **2002**, 71:435–71.

- [23] Ai X., Do A.T., Kusche-Gullberg M., Lindahl U., Lu K., Emerson C.P. Jr., *J Biol Chem*, **2006**, 281:4969–4976
- [24] Lamanna W.C., Kalus I., Padva M., Baldwin J., Merry C.L., Dierks T., *J Biotechnol*, **2007**, 129: 290–307
- [25] Rudd T.R., Yates E.A., *Mol BioSyst*, 2012, 8, 1499–1506
- [26] Coombe D.R., Kett W.C., *Cell Mol Life Sci*, **2005**, 62(4):410-24.
- [27] De Agostini A.; Watkins S. C.; Slayter H. S.; Youssoufian H., Rosenberg R. D., *J Cell Biol*, **1990**, 111, 1293–1304.
- [28] Forsberg E., Pejler G., Ringvall M., Lunderius C., Tomasini-Johansson B., Kusche-Gullberg M., Eriksson I., Ledin J., Hellman L., and Kjellen L., *Nature*, **1999**, 400:773–776.
- [29] Dagälv A., Holmborn K., Kjellén L., Abrink M., *J Biol Chem*, **2011**, 30;286(52):44433-40.
- [30] Capila I., Linhardt R., *Angew. Chem.*, **2002**, 41:390-412
- [31] Kjellen L., Carlsson P., In: Lever R., Mulloy B, Page C.P., eds, *Heparin - a century of progress*, Handbook of experimental pharmacology 207, Springer-Verlag Berlin Heidelberg, **2012**.
- [32] Liu Z., Lavine K.J., Hung I.H., Ornitz D.M., *Dev Biol*, **2007**, 302:80–91.
- [33] Iozzo R.V., *Annu Rev Biochem*, **1998**, 67:609-52.
- [34] De Cat B., David G., *Semin Cell Dev Biol*, **2001**, 12(2):117-25.
- [35] Dreyfuss J.L., Regatieri C.V., Jarrouge T.R., Cavalheiro R.P., Sampaio L.O., Nader H.B., *Ann Braz Acad Sci*, **2009**, 81(3):409–429.
- [36] Heinegård D., *Int J Exp Path*, **2009**, 90:575–586.
- [37] Ori A., Wilkinson M.C., Fernig D.G., *J Biol Chem*, **2011**, 286, 19892–19904.
- [38] Ornitz D.M., *Bioessays*, **2000**, 22:108–112.
- [39] Goldfarb M., *Cytokine Growth Factor Rev*, **1996**, 7:311–325.
- [40] Yayon A., Klagsbrun M., Esko J.D., Leder P., and Ornitz D.M., *Cell*, **1991**, 64:841–84.
- [41] Rapraeger A.C., Krufka A., and Olwin B.B., *Science*, **1991**, 252:1705–1708.
- [42] Allen B.L., Rapraeger A.C, *J Cell Biol*, **2003**, 163(3): 637–648.
- [43] Wesche J., Haglund K., Haugsten E.M., *Biochem J*, **2011**, 437 (2), 199-213.
- [44] Fitzgerald K.A., O’neill L.A., Geraring A.J, Callard R.E. *The Cytokine Factsbook and Webfacts, 2nd edition*, Burlington: Elsevier Siene, **2001**.
- [45] Fernandez E. J., Lolis E., *Annu Rev Pharmacol Toxicol*, **2002**, 42, 469–499.
- [46] Ishitsuka R., Kojima K., Utsumi H., Ogawa H., Matsumoto I., *J Biol Chem*, **1998**, 273 (1998) 9935–9941.
- [47] Capila I., Hernáiz M. J., Mo Y. D., Mealy T. R., Campos B., Dedman J. R., Linhardt R. J., Seaton B. A., *Structure*, **2001**, 9:57–64.
- [48] Cooper A.D., *J Lipid Res*, **1997**, 38:2173-2192.
- [49] Mahley R. W., Ji Z.S., *J Lipid Res*, **1999**, 40(1):1-16.
- [50] Ji Z. S., Pitas R. E., Mahley R. W., *J Biol Chem*, **1998**, 273: 13452–13460.

- [51] Celie J. W. A. M., Keuning E. D., Beelen R. H. J., Dräger A. M., Zweegman S., Kessler F. L., Soininen R., van den Born J., *J Biol Chem*, **2005**, 280(29): 26965-26973.
- [52] Nelson R.M., Cecconi O., Roberts W.G, Aruffo A., Linhardt R.J., Bevilacqua M.P., *Blood*, **1993**, 82:3253-3258.
- [53] Armistead J.S., Wilson I.B., van Kuppevelt T.H., Dinglasan R.R., *Biochem J*, **2011**, 438(3):475-83.
- [54] Galliher P. M., Cooney C. L., Langer R. and Linhardt R. J., *Appl Environ Microbiol*, **1981**, 41(2): 360-365.].
- [55] Godavarti R., Sasisekharan R., *Biochem Biophys Res Commun*, **1996**, 229, 770-777.
- [56] McKenzie E. A., *Br J Pharmacol*, **2007**, 151(1): 1-14.
- [57] Valstar M.J., Ruijter G.J., van Diggelen O.P., Poorthuis B.J., Wijburg F.A., *J Inherit Metab*, **2008**, 31:240-252.
- [58] DeBaun M.R., Ess J., Saunders S., *Mol Genet Metab*, **2001**, 72:279-286.
- [59] Cook A., Raskind W., Blanton S.H., Pauli R.M., Gregg R.G., Francomano C.A., Puffenberger E., Conrad E.U., Schmale G., Schellenberg G., et al., *Am J Hum Genet*, **1993**, 53(1):71-79.
- [60] Wuyts W., Van Hul W., De Boule K., Hendrickx J., Bakker E., Vanhoenacker F., Mollica F., Lüdecke H.J., Sayli B.S., Pazzaglia U.E., et al., *Am J Hum Genet*, **1998**, 62(2):346-354.
- [61] Wuyts W., Van Hul W., *Hum Mutat*, **2000**, 15(3):220-227.
- [62] Solomon L., *J Bone Joint Surg [Br]*, **1963**, 45:292-304.
- [63] Wu Y., Heutink P., de Vries B., Sandkuijl L.A., van den Ouweland A.M.W., Niermeijer M.F., Galjaard H, et al., *Hum Mol Genet*, **1994**, 3:167-171.
- [64] Le Merrer M., Legeai-Mallet L., Jeannin P.M., Horsthemke B., Schinzel A., Plauchu H., Toutain A., Achard F., Munnich A., Maroteaux P., *Hum Mol Genet*, **1994**, 3(5):717-22.
- [65] Porter D.E., Lonie L., Fraser M., Dobson-Stone C., Porter J.R., Monaco A.P., Simpson A.H., *J Bone Joint Surg Br*, **2004**, 86(7):1041-6.
- [66] Zak B.M., Crawford B. E., Esko J. D., *Biochim Biophys Acta*, **2002**, 1573: 346- 355 (review)
- [67] Li Z., Yasuda Y., Li W., Bogyo M., Katz N., Gordon R.E., Fields G.B., Bromme D., *J Biol Chem*, **2004**, 279:5470-5479.
- [68] Hall C. R., Cole W. G., Haynes R., Hecht, J. T., *Am J Med Genet*, **2002**, 112: 1-5.
- [69] Bovée J.V., Cleton-Jansen A.M., Wuyts W., Caethoven G., Taminiou A.H., Bakker E., Van Hul W., Cornelisse C.J., Hogendoorn P.C., *Am J Hum Genet*, **1999**, 65(3):689-98.
- [70] Ropero S., Setien F., Espada J., Fraga M.F., Herranz M., Asp J., Benassi M.S., Franchi A., Patiño A., Ward L.S., Bovee J., Cigudosa J.C., Wim W., Esteller M., *Hum Mol Genet*, **2004**, 13(22):2753-65.
- [71] Hecht J.T., Hayes E., Haynes R., Cole W.G., Long I.J., Farach-Carson M.C., Carson D.D., *Differentiation*, **2005**, 73:212-221.

- [72] Stickens D., Brown D., Evans G.A., *Dev Dyn*, **2000**, 218:452–64.
- [73] Bernard M.A., Hogue D.A., Cole W.G., Sanford T., Snuggs M.B., Montufar-Solis D., Duke P.J., Carson D.D., Scott A., Van Winkle W.B., Hecht J.T., *J Bone Miner Res*, **2000**, 15(3):442-50.
- [74] Wuyts W., Ramlakhan S., Van Hul W., et al., *Am J Hum Genet*, **1995**, 57: 382-387.
- [75] Hameetman L., David G., Yavas A., et al., *J Pathol*, **2007**, 211: 399–409
- [76] Shieh M. T., Spear P. G., *J Virol*, **1994**, 68: 1224-1228.
- [77] Shieh M.T., WuDunn D., Montgomery R.I., Esko J.D., Spear P.G., *J Cell Biol*, **1992**, 116: 1273– 1281.
- [78] Tufaro F., Snider M.D., McKnight S.L., *J Cell Biol*, **1987**, 105: 647–657.
- [79] McCormick C., Leduc Y., Martindale D., Mattison K., Esford L.E., Dyer A.P., Tufaro F., *Nat Genet*, **1998**, 19:158– 161.
- [80] Lidholt K., Weinke J.L., Kiser C.S., Lagemwa F.N., Bame K.J., Cheifetz S., Massagué J., Lindahl U., Esko J.D., *Proc Natl Acad Sci USA*, **1992**, 89:2267– 2271.
- [81] Lind T., Lindahl U., Lidholt K., *J Biol Chem*, **1993**, 268:20705– 20708.
- [82] Brandt K.D., Doherty M., Lohmander L.S., *Osteoarthritis*, **1998**, 108-122.
- [83] Sauerland K., Plaasb A.H.K, Raissc R.X., Steinmeyer J., *Biochim Biophys Acta*, **2003**, 1638 (3):241–248.
- [84] Ballock R.T., O'Keefe R.J., *Birth Defects Res C Embryo Today*, **2003**, 69(2):123-43.
- [85] Parra A., Veraldi N., Locatelli M., Fini M., Martini L., Torri G., Sangiorgi L., and Bisio A., *Glycobiology*, **2012**, 22(2): 248–257.
- [86] Tai G.-H., Huckerby T.N., Nieduszynski I.A., *Biochem J*, **1993**, 291:889-894.
- [87] Brown G.M., Huckerby T.N., Morris H.G., Nieduszynski I.A., *Biochem J*, **1992**, 286:235-241.
- [88] Reantragoon S, Arrigo L M, Dweck H S, Rosenfeld L., *Arch Biochem Biophys*, **1996**, 327:234–238.
- [89] Yamada S., Sakamoto K., Tsuda H., Yoshida K., Sugahara K., Khoo K., Morris H.R., Dell A., *Glycobiology*, **1994**, 4, 69-78.
- [90] Mao Y., Huang Y., Zong C., Lin C., Boons G.-J., and Zaia J., *Anal Chem*, **2015**, 6;87(1):592-600.
- [91] Toida T., Toshida H., Totoda H., Koshiishi I., Imanari T., Hileman R. E., Fromm J. R., Linhardt R. J., *Biochem J*, **1997**, 322, 499-506
- [92] Nordgard-Sumnicht, K. and Varki, A., *J Biol Chem*, **1995**, 270, 12012-12024.
- [93] Jandik K.A., Kruep D., Cartier M., Linhardt R.J., *J Pharm Sci*, **1996**, 80, 45-51.
- [94] Warda M., Toida T., Zhang F., Sun P., Munoz E., Linhardt R.J., *Glycoconj J*, **2006**, 23(0): 555–563.
- [95] Skidmore M.A., Guimond S.E., Dumax-Vorzet A.F., Yates E.A., Turnbull J.E., *Nat Protoc*, **2010**, 5, 1983–1992.
- [96] Rowe S. M., Miller S., Sorscher E. J., *N Engl J Med*, **2005**, 352, 1992-2001.

- [97] Muhlebach M. S., Noah T. L., *Am J Resp Crit Care*, **2002**, 165, 911-915.
- [98] Joseph T., Look D., Ferkol T., *Am J Physiol- Lung C*, **2005**, 288, L471-479.
- [99] Cosgrove S., Chotirmall S. H., Greene C. M and McElvaney N. G., *J Biol Chem*, **2011**, 286, 7692-7704.
- [100] Downey D.G., Bell S.C. and Elborn J.S., *Thorax*, **2009**, 64, 81-88.
- [101] Tosi M.F., Zakem H. and Berger M., *J Clin Invest*, **1990**, 86, 300-308.
- [102] Marcos V., Zhou Z., Yildirim A.O., Bohla A., Hector A., Vitkov L., Wiedenbauer E.M., Krautgartner W.D., Stoiber W., Belohradsky B.H., Rieber N., Kormann M., Koller B., Roscher A., Roos D., Griese M., Eickelberg O., Döring G., Mall M.A., Hartl D., *Nat Med*, **2010**, 16, 1018-1023.
- [103] Cheng O.Z., Palaniyar N., *Front Immunol*, **2013**, 4:1 (review).
- [104] Vandivier R.W., Fadok V.A., Hoffmann P.R., Bratton D.L., Penvari C., Brown K.K., Brain J.D., Accurso F.J., Henson P.M., *J Clin Invest*, **2002**, 109, 661-670.
- [105] Poole A.R., *Biochem J*, **1986**, 236:1-14.
- [106] Darville T., Yedgar S., Krinsky M., Andrews C.W. Jr, Jungas T., Ojcius D.M., *Microbes Infect*, **2004**, 6(4):369-76.
- [107] Aquino R.S., Lee E.S., Park P.W., *Prog Mol Biol Transl Sci*, **2010**, 93:373-94.
- [108] Schmidtchen A., Frick I., Björck L., *Mol Microbiol*, **2001**, 39:708-713.
- [109] Chen Y., Bennett A., Hayashida A., Hollingshead S., Park P.W., *J Biol Chem*, **2005**, 282:159-167.
- [110] Hayashida A., Amano S., Park P.W., *J Biol Chem*, **2011**, 285:3288-3297
- [111] Duensing T.D., Wing J.S., van Putten J.P.M., *Infect Immun*, **1999**, 67:4463-4468.
- [112] Zanni M., Tamburro A., Santone I., Rotilio D., *Semin Thromb Hemost*, **1994**, 20(2):159-67.
- [113] Johnson Z., Kosco-Vilbois M.H., Herren S., Cirillo R., Muzio V., Zaratin P., Carbonatto M., Mack M., Smailbegovic A., Rose M., Lever R., Page C., Wells T.N., Proudfoot A.E., *J Immunol*, **2004**, 173 (9):5776-85.
- [114] Jayson G.C., Gallagher J.T., *Brit J Cancer*, **1997**, 75(1), 9-16.
- [115] Brown R.A., Lever R., Jones N.A., Page C.P., *Brit J Pharmacol*, **2003**, 139(4), 845-853.
- [116] Vlodaevsky I., Mohsen M., Lider O., Svahn C.M., Ekre H.P., Vigoda M. et al. , *Invas Metastas*, **1994**, 14(1-6), 290-302
- [117] Borsig L., Wong R., Feramisco J., Nadeau D.R., Varki N M., Varki, A., *PNAS*, **2001**, 98(6), 3352-3357
- [118] Varki N.M., Varki, A., *Semin Thromb Hemost*, **2002**, 28(1), 53-66.
- [119] Diamant, Z., Timmers, M. C., van der Veen, H., Page, C. P., van der Meer, F. J., & Sterk, P.J., *Am J Resp Crit Care*, **1996**, 153(6 Pt 1), 1790-1795.
- [120] Yip L.Y., Lim Y.F., Chan H.N., *Burns*, **2011**, 37(7), 1154-1160

- [121] Mulloy B., Forster M. J., Jones C., Davies D. B., *Biochem J*, **1993**, 293(Pt 3), 849–858.
- [122] Rudd T.R., Skidmore M.A., Guimond S.E., Cosentino C., Torri G., Fernig D. G. et al., *Glycobiology*, **2009**, 19(1), 52–67.
- [123] Yates E.A., Santini F., Guerrini M., Naggi A., Torri G., Casu B. *Carbohydr Res*, **1996**, 294,15–27
- [124] Guimond S.E., Turnbull J.E., Yates E.A., *Macromol Biosci*, **2006**, 6(8), 681–686.
- [125] Casu B., Guerrini M., Guglieri S., Naggi A., Perez M., Torri G., et al., *J Med Chem*, **2004**, 47(4), 838–848.
- [126] Naggi A., Casu B., Perez M., Torri G., Cassinelli G., Penco S. et al., *J Biol Chem*, **2005**, 280(13), 12103–12113.
- [127] Fernando H., Nagle G.T., Rajarathnam K., *FEBS J*, **2007**, 74(1), 241–251.
- [128] Whitmore L., Wallace B.A., *Biopolymers*, **2008**, 89: 392-400
- [129] Whitmore L., Wallace B.A., *Nucleic Acids Res*, **2004**, 32:W668-673
- [130] Eck M.J., Sprang S.R., *J Biol Chem*, **1989**, 264(29), 17595–17605.
- [131] Jones E.Y., Stuart D.I., Walker N.P., *Nature*, **1989**, 338(6212), 225–228
- [132] Green W.F., Konnaris K., Woolcock A.J., *Am J Respir Cell Mol Biol*, **1993**, 8:518-521.
- [133] Casu B., Guerrini M., Naggi A., Perez M., Torri G., Ribatti D. et al., *Biochemistry*, **2002**, 41(33),10519–10528.
- [134] Fryer A., Huang Y.C., Rao G., Jacoby D., Mancilla E., Whorton R., et al., *JPET*, **1997**, 282(1), 208–219.
- [135] Kuschert G.S., Coulin F., Power C.A, Proudfoot A.E, Hubbard R.E., Hoogewerf A.J., Wells T.N., *Biochemistry*, **1999**, 38: 12959–12968
- [136] Bertini S., Bisio A., Torri G., Bensi D., Terbojevich M., *Biomacromolecules*, **2005**, 6(1), 168–173.

ANNEX
CHAPTER II

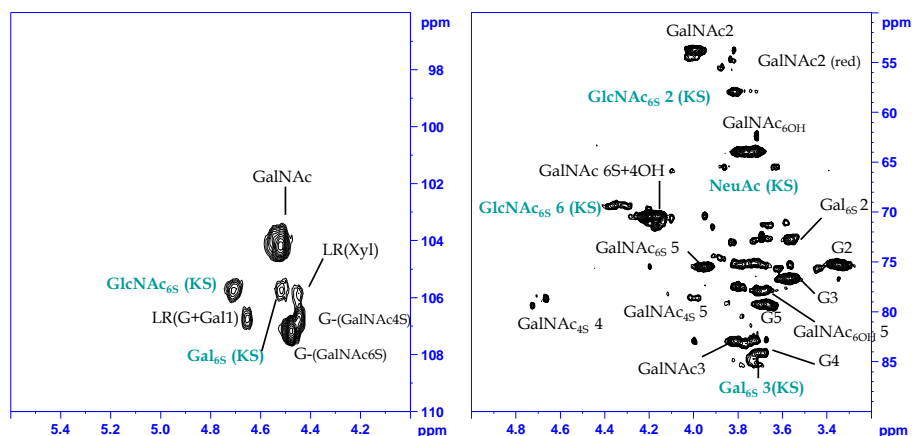


Figure A.II.1. HSQC-NMR spectrum of GAGs from Aggrecan. Signals of the anomeric region are shown on the left while signals from the backbone are shown on the right. Signals specific to KS are indicated in green, while signals specific to CS are indicated in black. Signals of residues from the linkage region (LR) were also detected. NeuAc is neuraminic acid and Xyl is xylose.

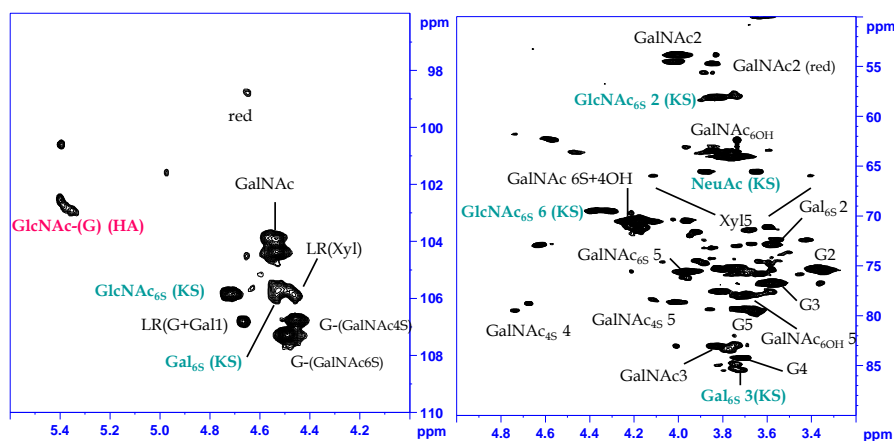


Figure A.II.2. HSQC-NMR spectrum of GAGs from ART5. Signals of the anomeric region are shown on the left while signals from the backbone are shown on the right. Signals specific to KS are indicated in green, while signals attributable to HA are indicated in red. Signals of residues from the linkage region (LR) were also detected. The signal attributable to the C2 of GlcA of HA overlaps with CS. NeuAc is neuraminic acid and Xyl is xylose. Red indicates protons from the reducing end.

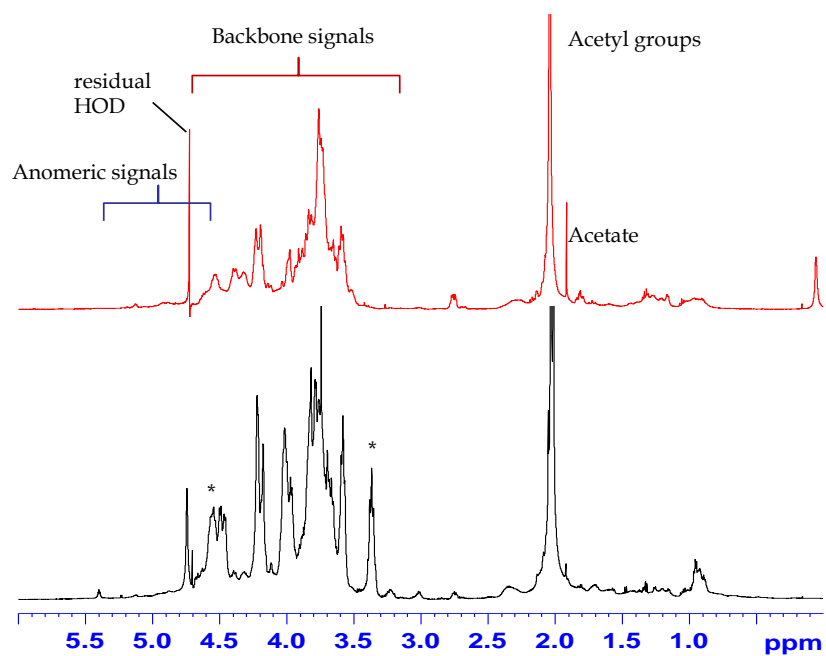


Figure A.II.3. ¹H-NMR spectra of GAGs from ART4-A (>10 kDa) before (black) and after (orange) the digestion with ChABC and hyaluronate lyase. * indicates GlcA signals that disappear after the enzymatic digestion.

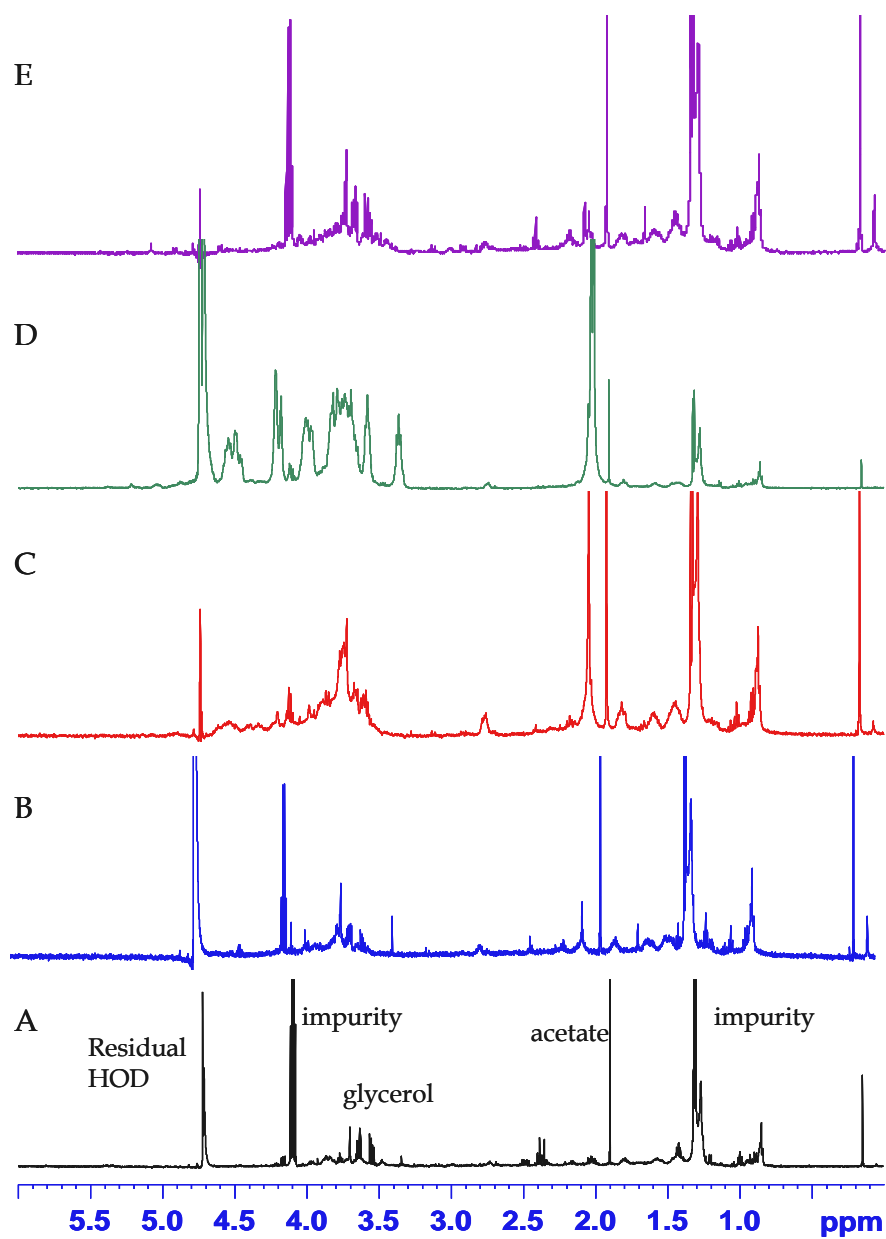


Figure A.II.4. ¹H-NMR spectra of the QAE-sephadex fractions of F5-A. A) 0M NaCl, B) 0.25M, C) 0.5M, D) 1M, E) 2.5M. Only fractions C, D and E (traces) contained GAGs.

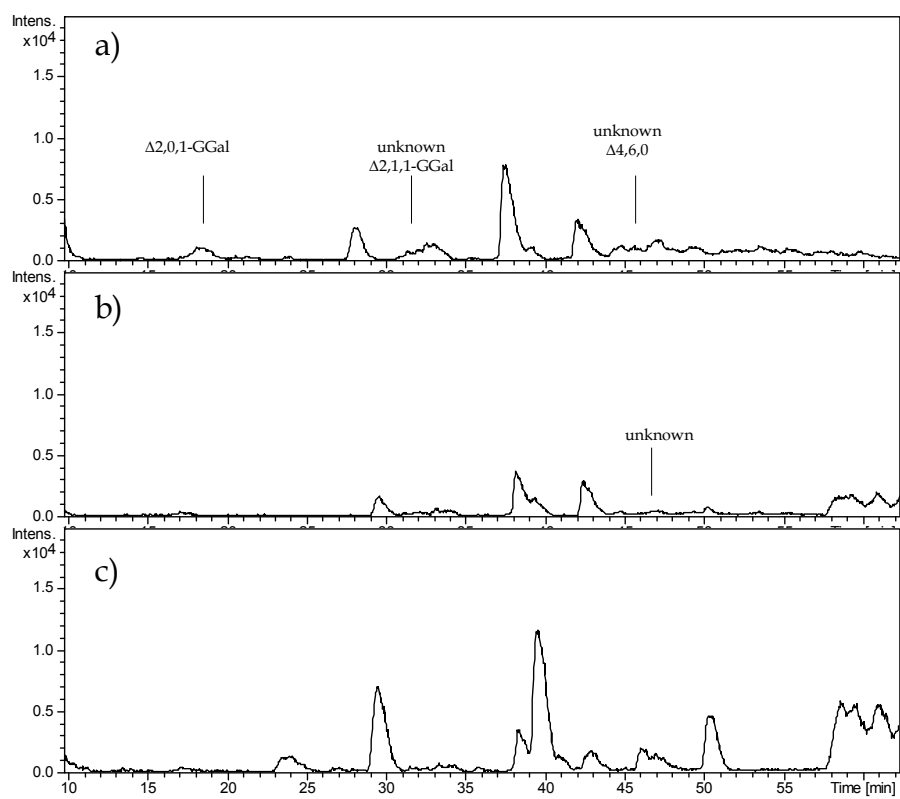


Figure A.II.5. HPLC-MS profiles of sequential digestions of ART2-A. a) products of the digestion with heparinase I, b) with heparinase III, c) with the broad heparinase II. Oligosaccharides for which a not precise interpretation is available were labeled as 'unknown'.

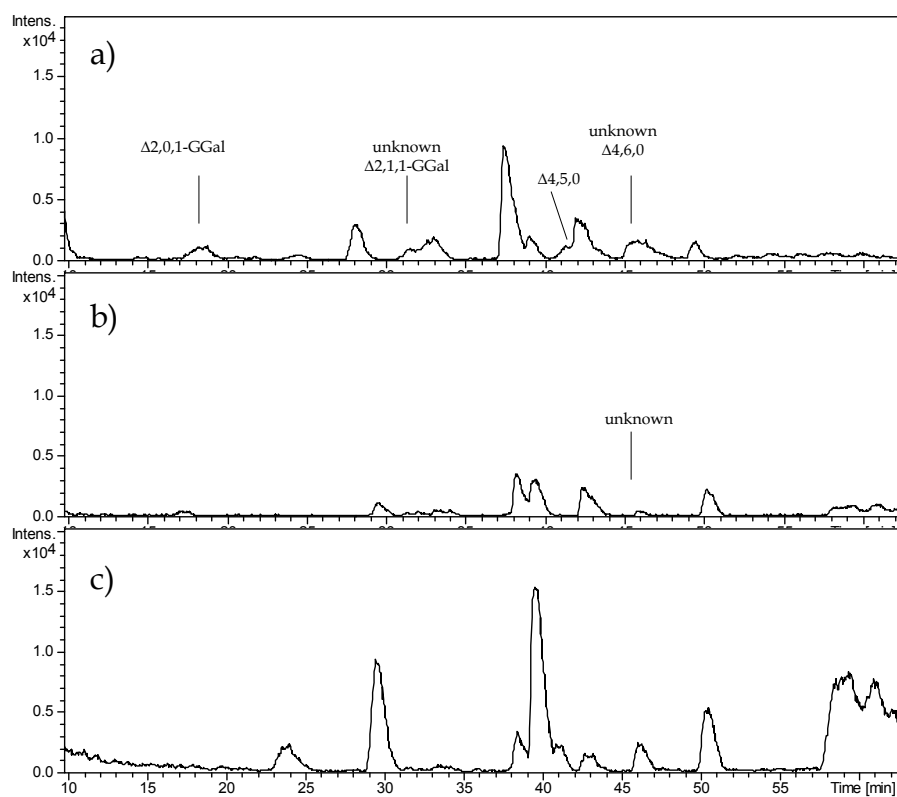


Figure A.II.6. HPLC-MS profiles of sequential digestions of GRP1-A. a) products of the digestion with heparinase I, b) with heparinase III, c) with the broad heparinase II.

Table A.II.1. LC-MS data for oligosaccharides detected from digested cartilaginous HS. When more interpretations are possible, alternatives are indicated. Oligosaccharides for which a not precise interpretation is available were labeled as 'unknown'.

<i>Monoisotopic m/z value</i>	<i>Corresponding mass value</i>	<i>Structure hypothesis</i>	<i>Prevalent ion form</i>
280.021	281	A1,1,0	[M-H] ¹⁻
300.035	301	A1,1,1	[M-H] ¹⁻
335.031	752	unknown	[M-2H-SO ₃] ²⁻
336.032	754	unknown	[M-2H-SO ₃] ²⁻
344.090	690	ΔLR (SerOx)	[M-2H] ²⁻
375.509	753	ΔU3,3,0	[M-2H] ²⁻
377.032	756	A3,3,0	[M-2H] ²⁻
378.094	379	Δ2,0,1	[M-H] ¹⁻
416.032	417	Δ2,1,0	[M-H] ¹⁻
437.032	876	Δ4,2,1	[M-2H] ²⁻

438.074	878	A3,4,1	[M-2H] ²⁻
456.077	914	Δ 4,3,0	[M-2H] ²⁻
456.977	916	A3,5,0 or A3,2,1-R	[M-2H-SO ₃] ²⁻
458.042	918	Δ 4,2,2	[M-2H] ²⁻
458.043	459	Δ 2,1,1	[M-H] ¹⁻
466.081	934	Δ U5,0,2	[M-2H] ²⁻
467.076	936	4,2,2	[M-2H] ²⁻
476.043	477	2,1,1	[M-H] ¹⁻
490.015	982	unknown	[M-2H] ²⁻
496.002	497	Δ 2,2,0	[M-H] ¹⁻
496.016	994	Δ 4,4,0	[M-2H] ²⁻
496.978	996	A3,6,0 or A3,3,1-R	[M-2H-SO ₃] ²⁻
504.647	1011	Δ 2,0,1-LR	[M-2H] ²⁻
506.108	1014	U5,1,2	[M-2H] ²⁻
507.042	1016	4,3,2	[M-2H] ²⁻
518.027	1038	unknown	[M-2H-SO ₃] ²⁻
526.662	1056	unknown	[M-2H] ²⁻
528.593	1059	A5,1,3	[M-2H] ²⁻
533.647	1069	Δ 2,0,1-LR (SerOx)	[M-2H] ²⁻
535.972	1074	Δ 4,5,0	[M-2H] ²⁻
538.022	539	Δ 2,2,1	[M-H] ¹⁻
544.622	1091	Δ 2,1,1-LR	[M-2H] ²⁻
546.077	1094	Δ U5,2,2	[M-2H] ²⁻
548.068	1098	A3,2,2-GGal	[M-2H] ²⁻
554.083	1110	unknown	[M-2H] ²⁻
555.078	1112	U5,2,2	[M-2H] ²⁻
573.621	1149	Δ 2,1,1-LR (SerOx)	[M-2H] ²⁻
575.962	577	Δ 2,3,0	[M-H] ¹⁻
575.962	1154	Δ 4,6,0	[M-2H-2SO ₃] ²⁻
577.038	1156	Δ 4,6,0+2H	[M-2H] ²⁻
584.589	1171	Δ 2,2,1-LR or Δ 6,2,0	[M-2H] ²⁻
596.009	1194	unknown	[M-2H] ²⁻
608.588	1219	A5,3,3 or Δ U5,3,0+DBA	[M-2H] ²⁻
611.598	1255	4,4,2+DBA	[M-2H] ²⁻
634.094	635	Δ U3,1,1	[M-H] ¹⁻
655.161	1312	A3,1,2-LR	[M-2H] ²⁻
655.662	1313	Δ U7,0,3	[M-2H] ²⁻
669.059	2009	Δ U7,6,2+3DBA or Δ 6,3,3-LR	[M-3H+DBA] ³⁻
669.682	2012	Δ U9,4,4	[M-3H+2DBA] ³⁻
674.061	675	U3,1,1+Na	[M-H+Na] ¹⁻
693.978	695	Δ 2,3,0-R	[M-2H] ²⁻
694.189	1390	Δ 4,0,2-LR	[M-2H] ²⁻
695.137	1392	unknown	[M-2H] ²⁻
696.590	1395	6,3,3	[M-2H] ²⁻
715.121	716	Δ 4,0,1	[M-H] ¹⁻
727.555	1457	Δ 6,4,3	[M-2H] ²⁻
734.169	1470	Δ 8,1,1 or Δ 4,1,2-LR or Δ U5,4,1+2DBA	[M-2H] ²⁻
744.657	1491	U7,2,3	[M-2H] ²⁻
751.012	752	unknown	[M-H] ¹⁻

753.037	754	unknown	[M-H] ¹⁻
753.121	2262	A9,6,3+DBA	[M-3H+DBA] ³⁻
758.522	1519	ΔU5,3,1+3DBA	[M-2H] ²⁻
766.120	1534	unknown	[M-2H] ²⁻
774.148	1550	Δ8,2,1 or Δ4,2,2-LR or ΔU5,5,1+2DBA	[M-2H] ²⁻
775.570	1553	ΔU7,3,3	[M-2H] ²⁻
778.766	1159	unknown	[M-2H] ²⁻
784.550	1571	U7,3,3	[M-2H] ²⁻
787.233	1576	A7,4,2-H ₂ O	[M-2H] ²⁻
814.125	1630	Δ8,3,1 or Δ4,3,2-LR or ΔU5,6,1+2DBA	[M-2H+DBA] ²⁻
821.799	2468	ΔU9,7,3+2DBA	[M-3H+DBA] ³⁻
825.138	1652	unknown	[M-2H] ²⁻
827.214	1656	unknown	[M-2H] ²⁻
833.713	1769	unknown	[M-2H] ²⁻
835.687	2510	ΔU9,7,4+2DBA	[M-3H+DBA] ³⁻
846.165	1694	8,2,4	[M-2H] ²⁻
851.571	1704	Δ6,6,2	[M-2H+DBA] ²⁻
863.082	1728	Δ8,1,4	[M-2H] ²⁻
875.081	876	Δ4,2,1	[M-H] ¹⁻
886.085	1774	8,3,4	[M-2H] ²⁻
900.673	1803	A7,5,2+DBA	[M-2H+DBA] ²⁻
902.717	1807	ΔU7,4,1	[M-2H+2DBA] ²⁻
910.692	1827	unknown	[M-2H] ²⁻
923.712	1849	unknown	[M-2H] ²⁻
927.323	1856.6	8,4,1+DBA or Δ6,0,3-LR(Ser)	[M-2H] ²⁻
939.834	2821	12,5,6+DBA	[M-3H+DBA] ³⁻
956.683	1915	unknown	[M-2H] ²⁻
957.891	1918	A7,7,4	[M-2H] ²⁻
960.207	1922	ΔU7,6,3+DBA	[M-2H+DBA] ²⁻
963.696	1929	ΔU7,5,2+2DBA or Δ6,2,3-LR	[M-2H+2DBA] ²⁻
965.213	1932	ΔU9,3,4	[M-2H+DBA] ²⁻
974.785	2927	Δ14,5,4	[M-3H+DBA] ³⁻
979.681	1961	Δ8,5,2+DBA	[M-2H+DBA] ²⁻
990.676	1983	8,4,4	[M-2H+DBA] ²⁻
1009.531	2901	12,6,6+DBA	[M-3H+DBA] ³⁻
1016.774	2035	8,3,1+3DBA	[M-2H] ²⁻
1055.263	2112	Δ8,4,4+2DBA	[M-2H+2DBA] ²⁻
1057.903	2118	unknown	[M-2H] ²⁻
1062.125	3189	14,7,6	[M-3H+DBA] ³⁻
1068.232	2138	ΔU7,6,2+3DBA or Δ6,3,3-LR	[M-2H+DBA] ²⁻
1108.177	3327	16,5,2+DBA	[M-3H+DBA] ³⁻
1153.715	2309	Δ10,6,3 or A7,4,2-LR	[M-2H] ²⁻
1205.252	3618	Δ16,11,1	[M-3H+DBA] ³⁻
1215.142	3648	16,8,7	[M-3H+DBA] ³⁻
1301.690	3908	Δ18,4,4+3DBA	[M-3H+DBA] ³⁻
1401.321	4209	16,16,2+DBA	[M-3H+DBA] ³⁻

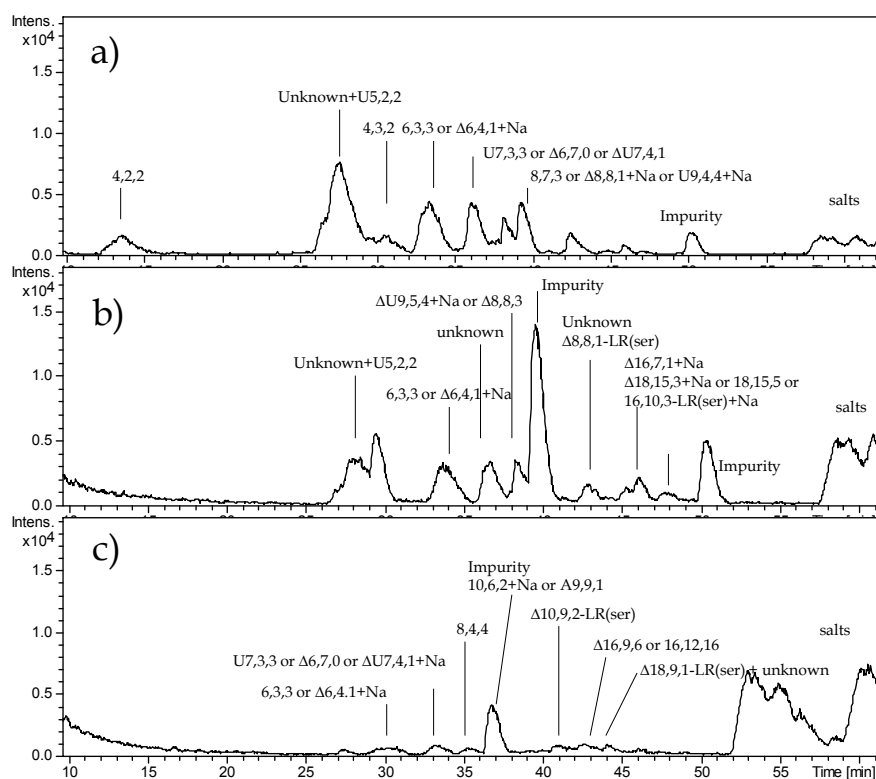


Figure A.II.7 HPLC-MS profiles of sequential digestions of GRP1-B. a) products of the digestion with heparinase I, b) with heparinase III, c) with the broad heparinase II. Oligosaccharides for which a not precise interpretation is available were labeled as ‘unknown’. An estimation of the monosaccharide units is also reported. Fragments bearing the intact linkage region and the serine residue of the proteoglycan are indicated by LR(ser). Many sodium adducts were found and are indicated.

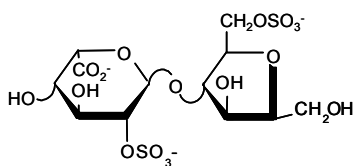


Figure A.II.8 Structure of the disaccharide IdoA2S-aM6S used as standard.

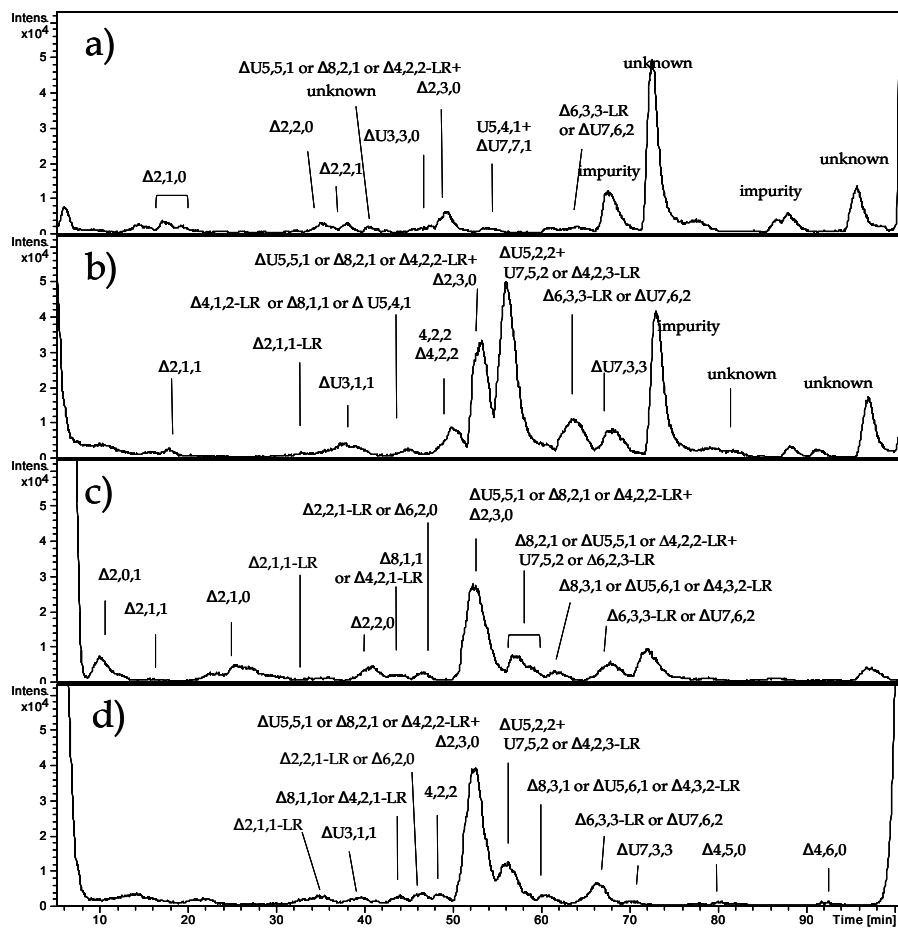


Figure A.II.9. HPLC-profiles of heparinases digestion products from fractions A and B of GRP3 and ART4. a) GRP3-A (>10 kDa), b) GRP3-B (<10 kDa), c) ART4-A (>10 kDa), d) ART4-B (<10 kDa). Oligosaccharides were identified by their mass/charge ratio (m/z) and labeled as follow. The unsaturated bond of the terminal uronic acid is indicated by Δ , and the number of monomers, the number of sulfates and the number of acetyls are reported. For some m/z ratios, more than one oligosaccharide structure is possible.

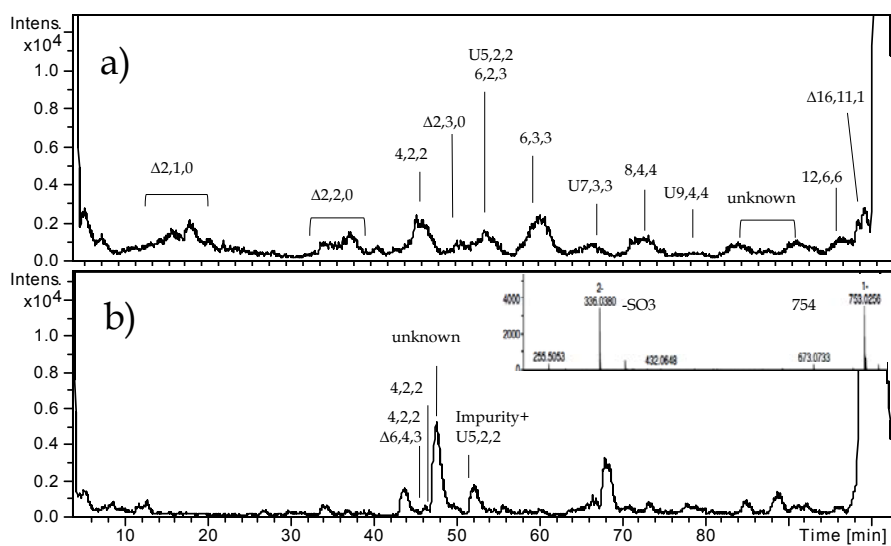


Figure A.II.10. HPLC-profiles of heparinases digestion products from fetal HS. a) F5-A (>10 kDa), b) F5-B (< 10 kDa). The unsaturated bond of the terminal uronic acid is indicated by Δ , and the number of monomers, the number of sulfates and the number of acetyls are reported. Oligosaccharides for which a not precise interpretation is available were labeled as 'unknown'. In the upper right corner of b) is reported the mass spectrum of the unknown peak eluted at 50 min.

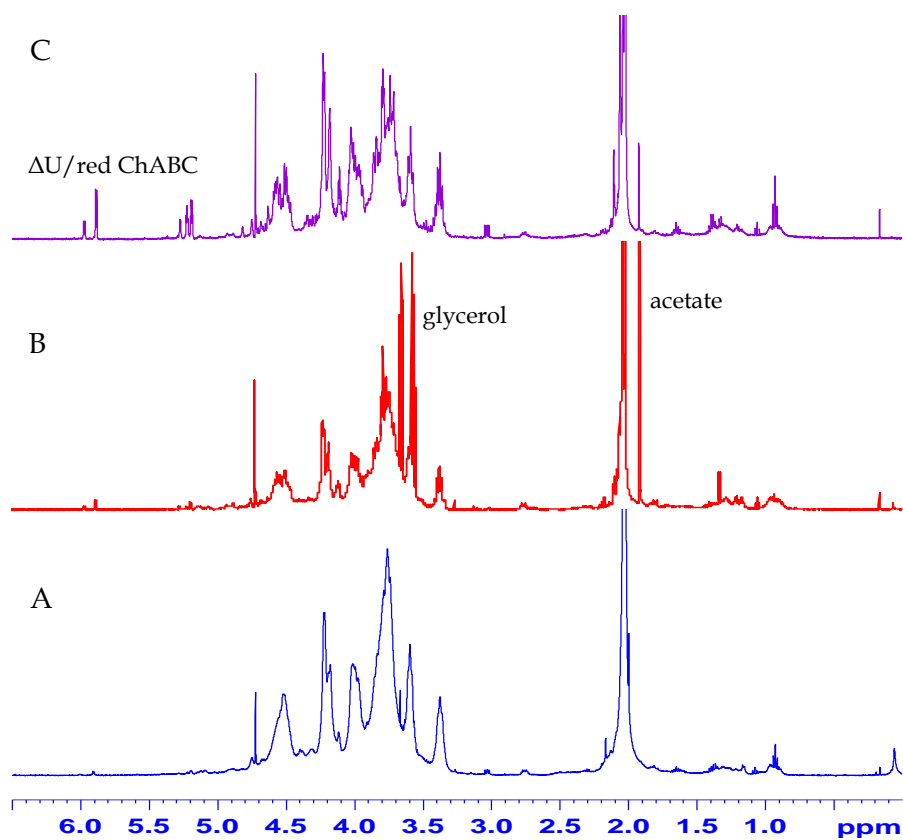


Figure A.II.11. $^1\text{H-NMR}$ spectra of the three fractions of MO2. After the digestion with ChABC and hyaluronate lyase, GAGs were fractionated by ultrafiltration and dialysis. A) > 10 kDa, B) < 10 kDa and > 3 kDa, C) < 3 kDa and > 1 kDa. The presence of digestion products is clearly observable in the smallest fraction and indicated by the signals of protons of unsaturated glucuronic acid (ΔU) and reducing ends (red).

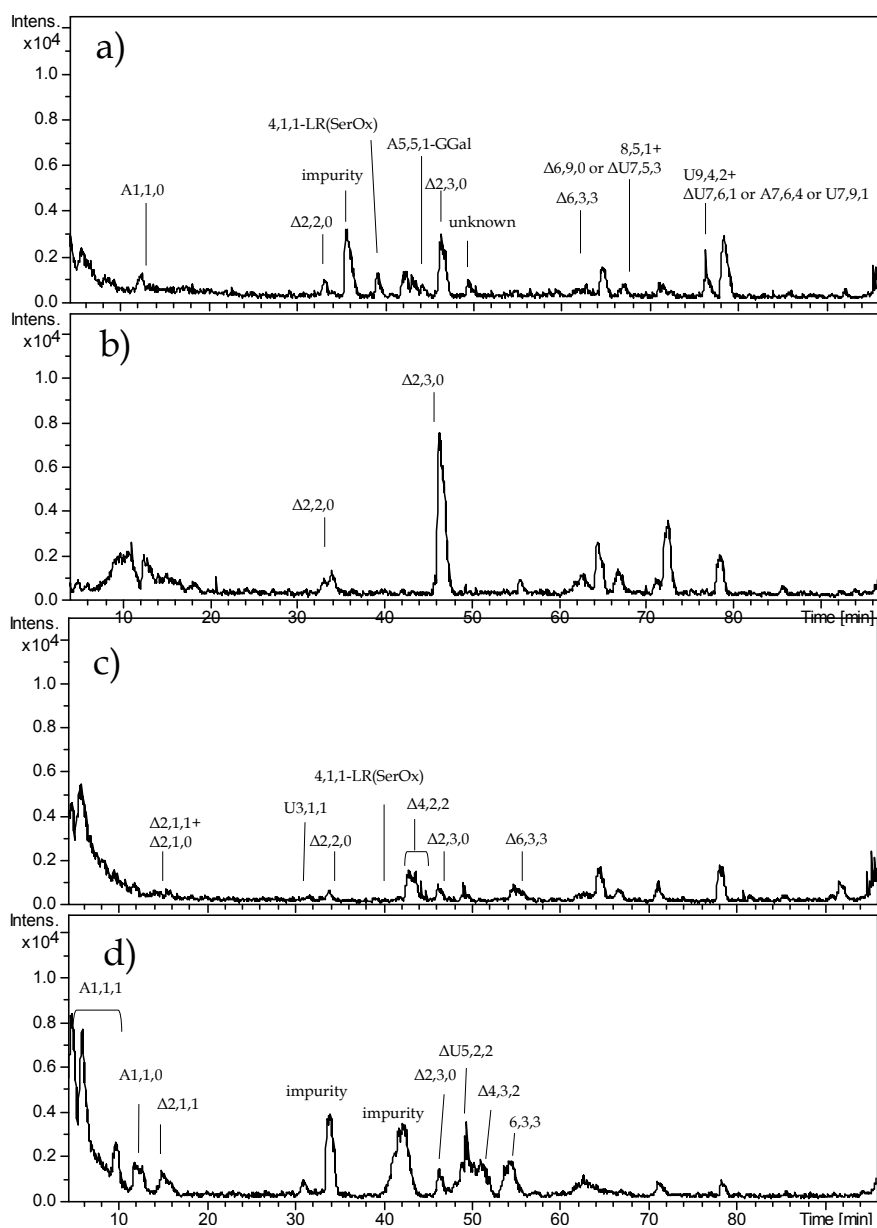


Figure A.II.12. HPLC-profiles of Heparinases digestion products from MO HS. a) MO1-A (>10 kDa), b) MO1-B (< 10kDa), c) C1-A (>10 kDa), d) C1-B (< 10kDa). The unsaturated bond of the terminal uronic acid is indicated by Δ , and the number of monomers, the number of sulfates and the number of acetyls are reported. Fragments bearing the oxidized serine residue of the proteoglycan linked to the linkage region are indicated by LR(SerOx).

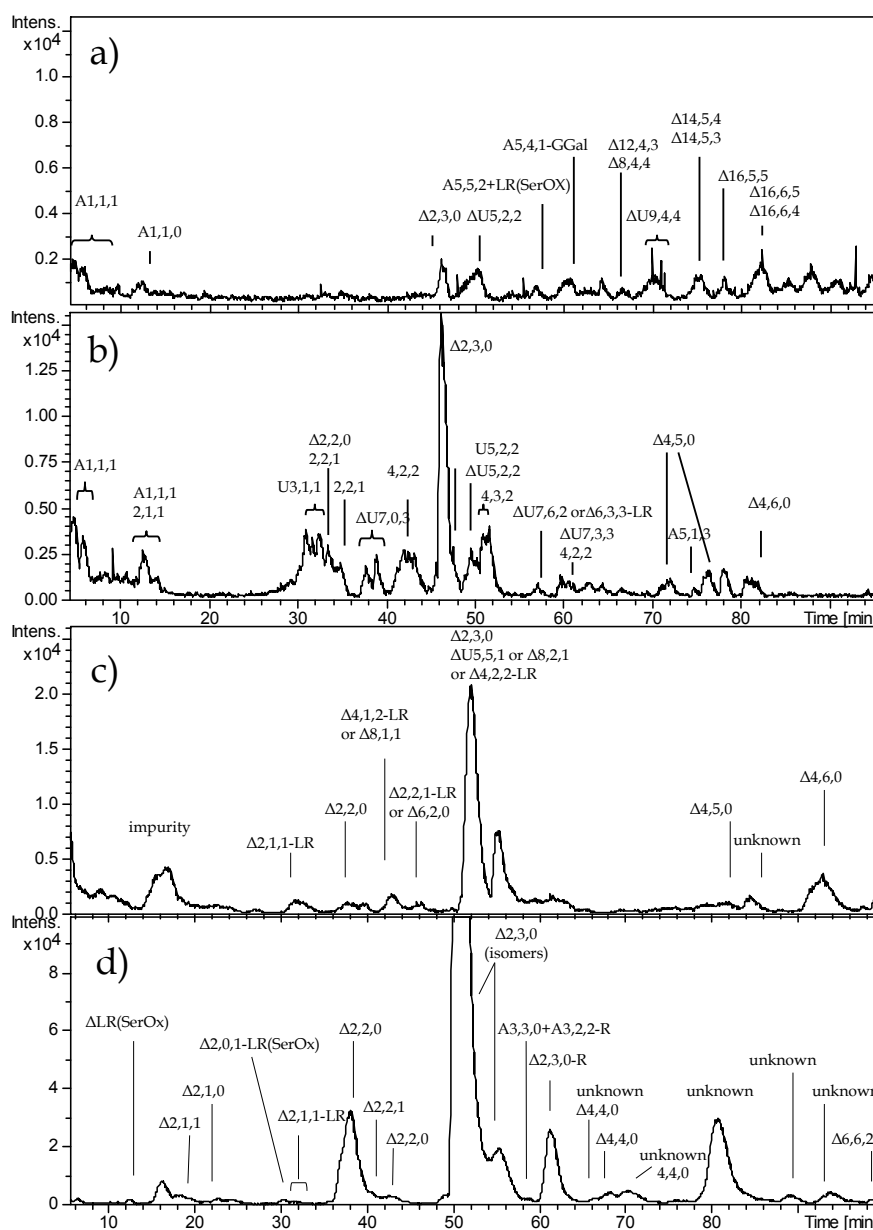


Figure A.II.13. Comparison between HPLC-profiles of heparinases digestion products from MO4 and MO4* HS. a) MO4-A (>10 kDa), b) MO4-B (<10 kDa), c) MO4*-A (>10 kDa), d) MO4*-B (<10 kDa). The spectrum of MO4*-B in which the trisulfated disaccharide reaches an intensity of 2×10^5 , has been cut to permit a better visualization of all the other peaks. Mass peaks identified as fragments bearing a remnant structure are indicated by the letter R.

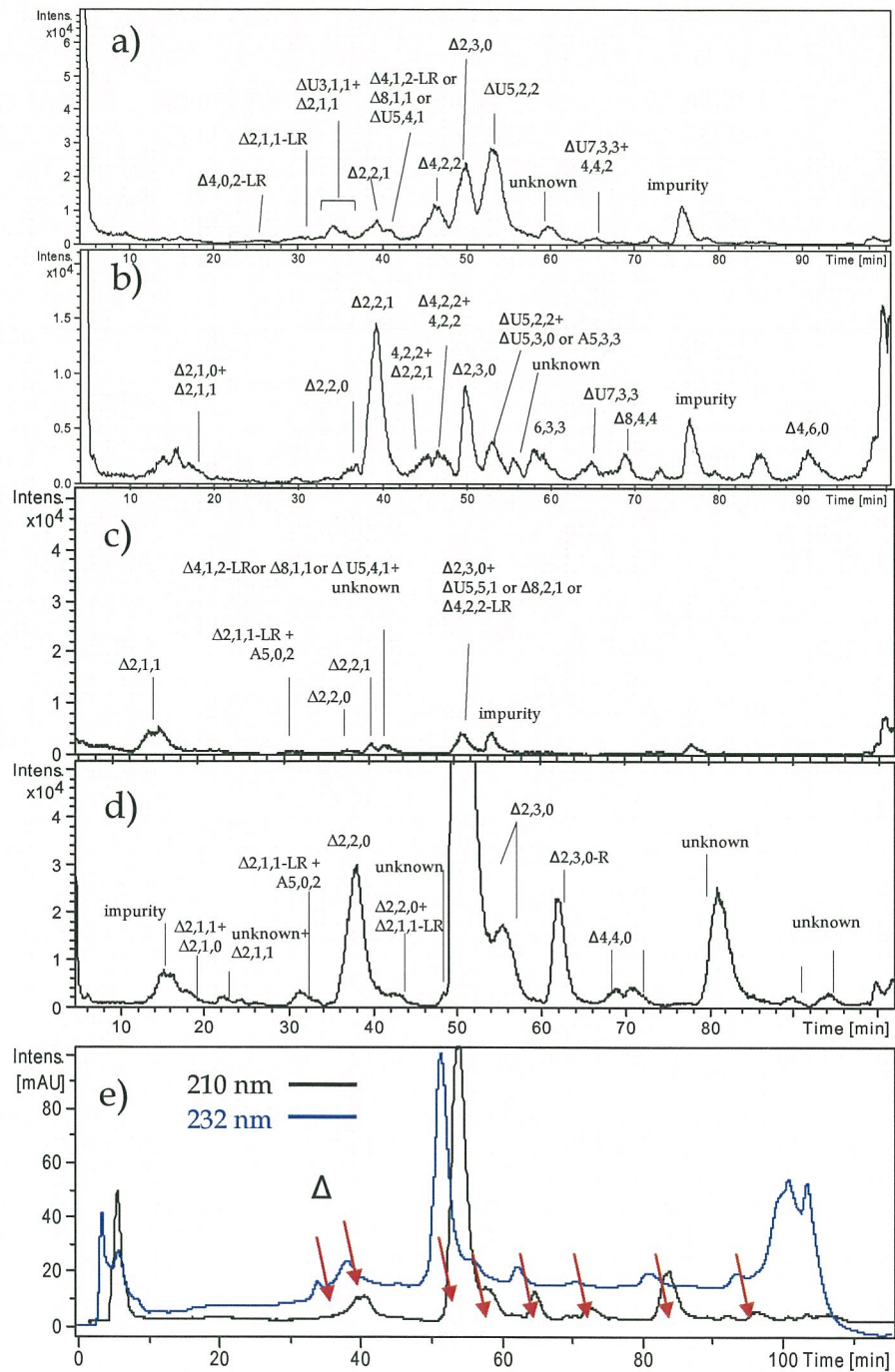


Figure A.II.14. HPLC-profiles of heparinases digestion products from MO HS. a) MO2-A (>10 kDa), b) MO2-B (< 10 kDa), c) MO5-A (>10 kDa), d) MO5-B (<10 kDa), e) profiles of MO5-B at

two different wavelengths. The unsaturated bond of the terminal uronic acid is indicated by Δ , and the number of monomers, the number of sulfates and the number of acetyls are reported. The spectrum of MO5-B in which the trisulfated disaccharide reaches an intensity of 2×10^5 , has been cut to permit a better visualization of all the other peaks. Mass peaks identified as fragments bearing a remnant structure are indicated by the letter R. The red arrows indicate the correspondence between peaks at 232 nm, specific for the unsaturation of the uronic residue, and 210 nm.

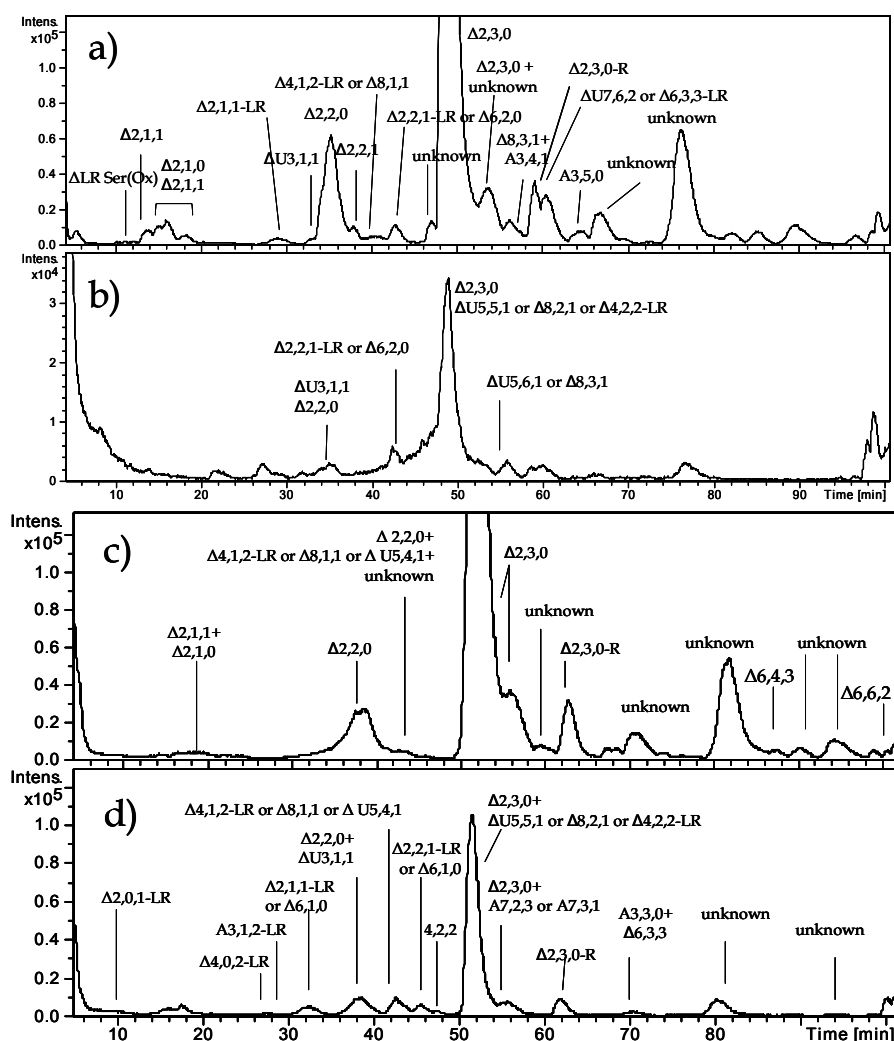


Figure A.II.15. HPLC-profiles of heparinase digestion products from C HS. a) C3-A (>10 kDa), b) C3-B (<10 kDa), c) C4-A (>10 kDa), d) C4-B (<10 kDa). The unsaturated bond of the terminal uronic acid is indicated by Δ , and the number of monomers, the number of sulfates

and the number of acetyls are reported. The spectrum of C3-A and C4-A in which the trisulfated disaccharide reaches an intensity of 3.5×10^5 , has been cut to permit a better visualization of all the other peaks. Mass peaks identified as fragments bearing a remnant structure are indicated by the letter R.

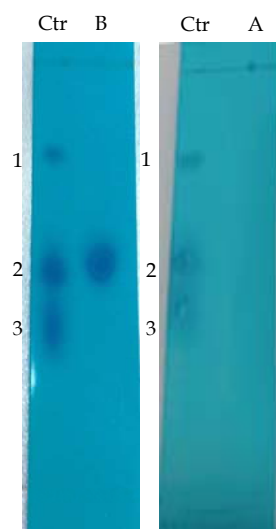


Figure A.II.16. Cellulose acetate electrophoresis of GAGs from pathologic cartilage. On the left of each strip were loaded $2 \mu\text{g}$ of a mixture of known GAGs: 1) HA, 2) CS, 3) HS. On the right was loaded $1 \mu\text{l}$ of a 8 mg/ml solution of GAGs from fractions A or B from ion exchange chromatography of MO-6.

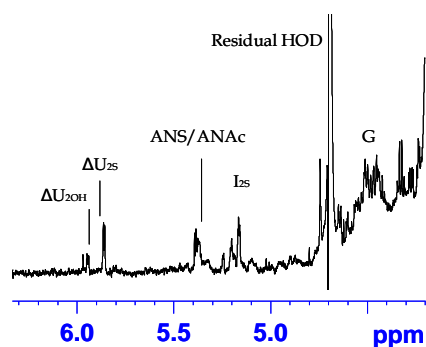


Figure A.II.17. 1D-NMR spectra of the mixture of the digestion products from HS of ART3 and GRP2. Signals of the anomer region are indicated in the spectrum. Δ is the insaturation on C4-C5 of the uronic residues (U) introduced by the enzymes. (A) glucosamine, (I) iduronic acid and (G) glucuronic acid.

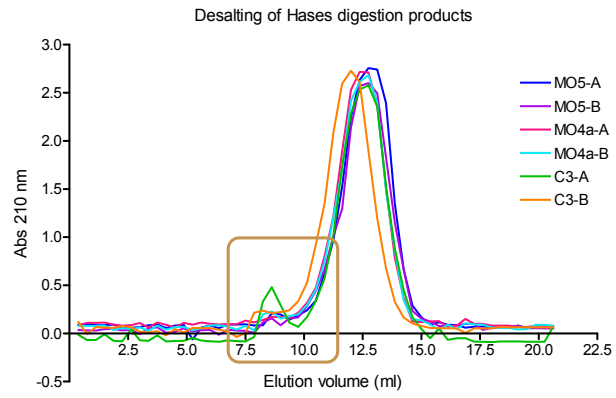


Figure A.II.18 First desalting of the products of HS digested with heparinases cocktail. The squared fraction contains the oligosaccharides of interest and was desalted a second time prior the last step of analysis by HPLC-MS.

CHAPTER III

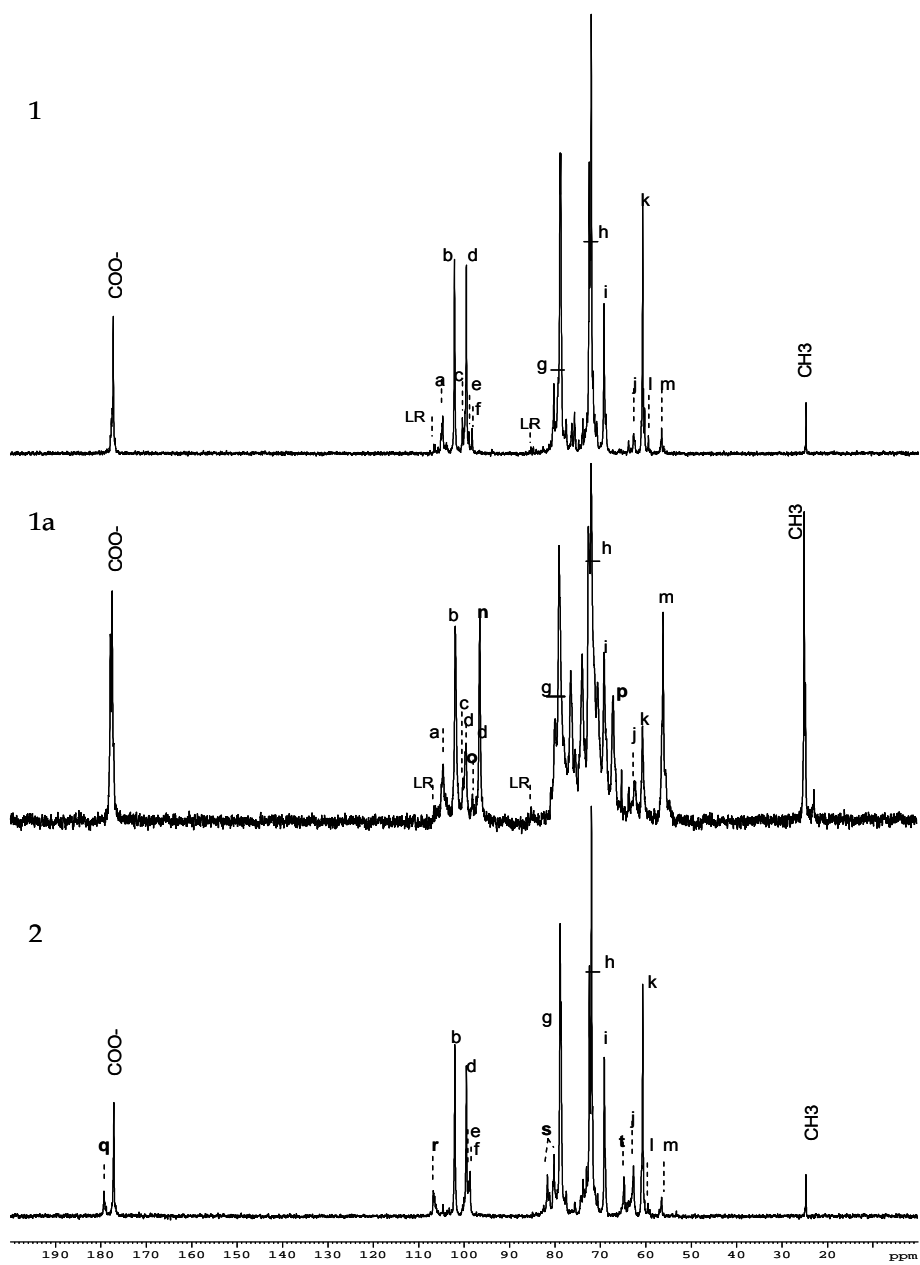


Figure A.III.1. ^{13}C NMR spectra of selected compounds: 1, 1a and 2. Labels on the groups of resonances correspond to the carbon of residues (see Scheme III.1) as follows: a, C-1 of GlcA and IdoA; b, C-1 of IdoA2S; c, C-1 of GlcNS linked to GlcA; d, C-1 of GlcNS linked to IdoA2S

and GlcNAc linked to GlcA; e, C-1 of GlcNS3S6S; f, C-1 of GlcNS linked to IdoA; g, C-4 of GlcN and IdoA2S, C-2 of IdoA2S; h, C-3 and C-5 of GlcN and IdoA2S; i, C-6 of GlcN6S; j, C-6 of GlcN6OH; k, C-2 of GlcNS; l, C-2 of GlcNS3S6S; m, C-2 of GlcNAc; LR indicates signals from the linkage region. Derivatives of series A present new groups of resonances the major signals of which correspond to the carbons of residues as follows: n, C-1 of GlcNAc linked to IdoA2S; o, C-1 of GlcNAc2S6S; p, C-6 of GlcNAc. Reference compound for series B present groups of resonances which find correspondence with the carbon of residues of (1) and new groups of resonances the major signals of which correspond to the carbons of residues as follows: q, carboxylic group of gsG and gsl; r, C-1of gsG and gsl; s, C-5 of gsG and gsl; t, C-2 and C-3 of gsG and gsl.

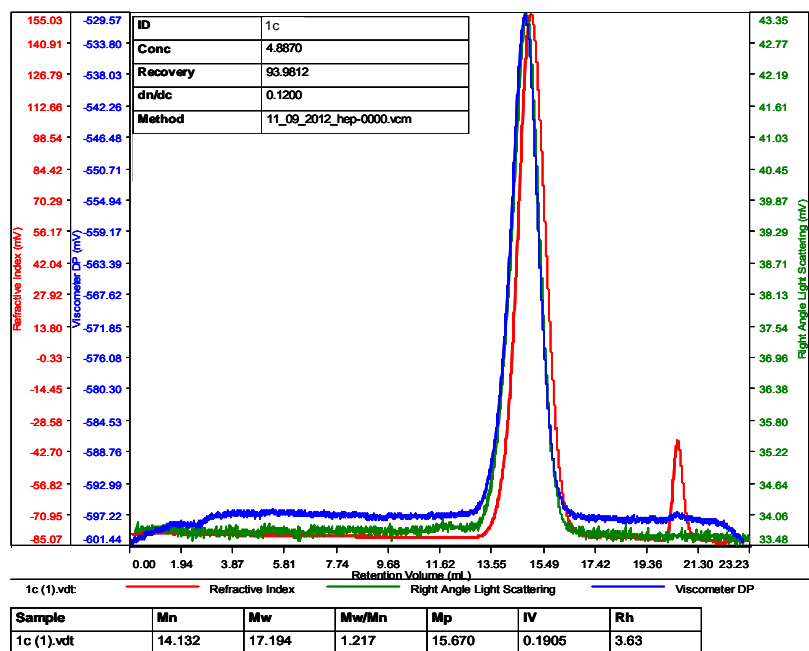


Figure A.III.2.TDA of compound (1c) and molecular weight distribution of an unfractionated heparin and Mark-Houwink plot (from [122]). The elaboration of LS and concentration RI detector responses gives molecular weight values: $RI = K \cdot dn/dc \cdot C$ and $LS = K' \cdot Mw \cdot (dn/dc)^2 \cdot C$, where RI and LS - refractometer and light-scattering response, K/K' - curve constants, dn/dc - differential index of refraction equal to 0.12 ml/g [122], C - concentration, Mw - weight average mean molecular weight. The dn/dc parameter is used to convert RI response to the concentration value that is then used to calculate Mw using LS data.

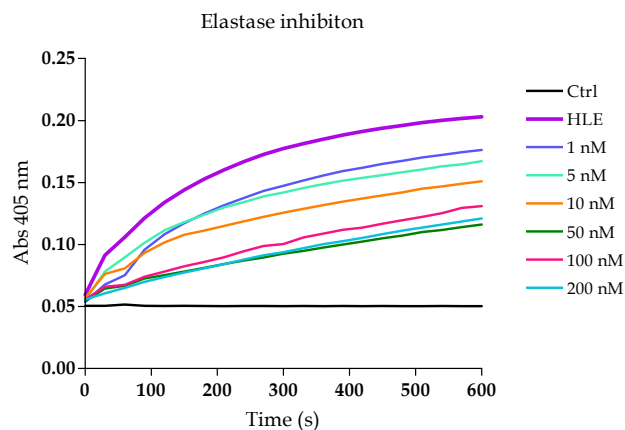


Figure A.III.3. Example of a dose-response curve of the inhibition of HLE. The increase in absorbance at 405 nm reports the inhibition of digestion of the chromogenic peptide by compound 2 (series B). Increasing the derivative concentration up to 200 nM, a maximum inhibition of 40% is observable. Data are the mean of three replicates.

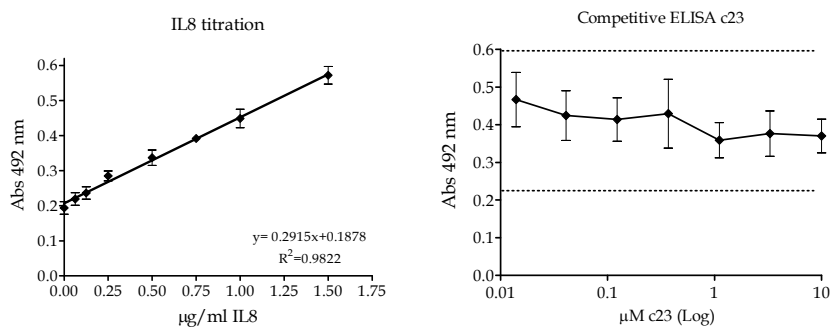


Figure A.III.4. Example of a titration curve of IL8 (left) and corresponding displacement by 1c (c23)(right). The dashed lines indicate the range of absorbance values of IL8 shown on the left.

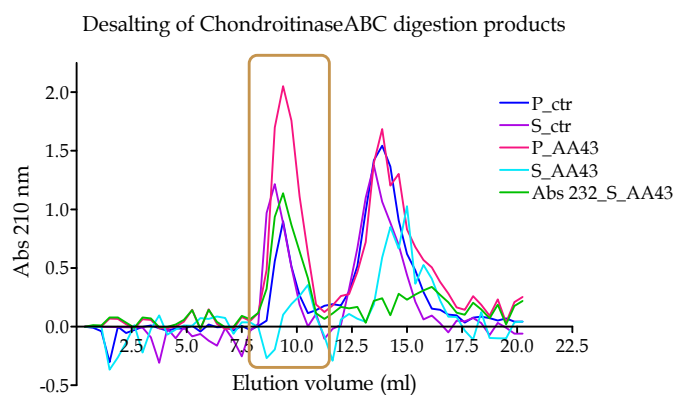


Figure A.III.5. Desalting of the products of digestion with chondroitinase ABC. The squared fraction contains the oligosaccharides of interest and was desalted a second time prior the last step of analysis by HPLC-MS. UV profile of S_AA43 at 232nm, which is the wavelength used to detect the unsaturation introduced by enzymatic cleavage, is also reported.

Table A.III.1. Summary of the relative percentages of disaccharides from digestion with heparinases. In the table is underlined the highest sum used as reference (100%). S) supernatant, P) pellet.

	S/P	Total Area	Relative %	% $\Delta 2,2,0$	% $\Delta 2,3,0$	% $\Delta 2,1,1 + \Delta 2,1,0$
Controls	S	92933,0	3,6	0,53	1,58	1,51
	S	148348,0	4,9	0,73	2,89	1,28
	S	61720,0	2,0	0,32	0,89	0,74
	P	1898687,0	48,1	16,81	8,21	23,10
	P	1211929,0	33,6	8,72	7,80	17,06
	P	2132851,0	52,9	14,75	13,52	24,65
AA43	S	299430,0	9,9	1,91	2,74	5,27
	S	78911,6	2,6	0,45	0,98	1,16
	S	63180,2	2,0	0,28	0,81	0,96
	P	3140823,6	<u>100,0</u>	24,98	13,63	61,39
	P	3095742,0	91,5	32,27	15,27	43,93
	P	2547399,0	77,1	21,91	12,33	42,81

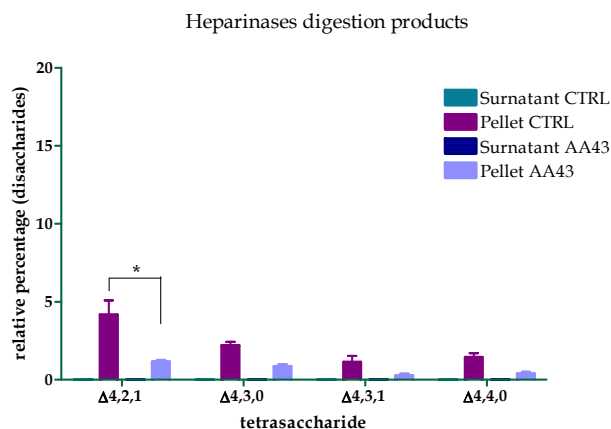


Figure A.III.6. Tetrasaccharide products of the digestion of HEP/HS from murine lungs. The graph shows the percentage of each tetrasaccharide species relative to the disaccharide moiety in each sample. 100% is considered the sum of integrals of disaccharides from AA43 pellet. Two-way ANOVA with Bonferroni's post-test was used to statistically analyze results. Data are the mean of three samples per type which have been processed independently.

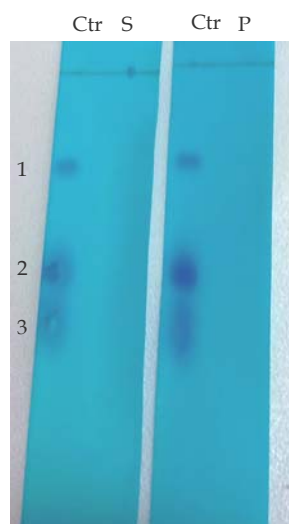


Figure A.III.7. Cellulose acetate electrophoresis of GAGs from healthy mouse lungs. The standard mix (2 ug) was loaded on the left of the strip, while samples (8 ug) are on the right. 1) HA, 2) CS, 3) HS+HEP. GAGs were stained with 1% Alcian Blue in pH 5.6 acetate buffer and EtOH. S) supernatant, P) pellet.